

| | | | | |
|---|----------------|--------------------|-----------------------------|----------------|
| Document ID 1399768 | Version 1.0 | Status Approved | Reg no | Page 1 (92) |
| Author Jan Hernelind 5T Engineering AB | | | Date 2013-06-24 | |
| Reviewed by Sabina Hammarberg (QA) | | | Reviewed date 2014-02-05 | |
| Approved by Jan Sarnet | | | Approved date 2014-02-05 | |

Analysis of creep in the KBS-3 copper canister due to internal and external loads

Abstract

Earlier simplified analyses indicate that internal pressure and different thermal expansion in copper shell and insert in combination with certain load cases could give rise to tensile stresses in the canister copper shell. This report is aimed to further investigate this effect. The presented analysis covers loads due to internal processes and external loads. Internal loads are due to thermal evolution and gas production whilst external loads are external pressure from swelling buffer and water pressure also including glaciations effects. The analyses are based on different assumptions for these factors.

All simulations are based on the BWR-design of the insert. The geometry of FSW (Friction Stir Welding) weld is modelled by an axial slit and a root defect in radial direction. Four axial-symmetric analyses have been performed using different histories for temperature and external pressure. In addition, a 3D model has been produced in order to verify that an axial symmetric approximation is sufficiently accurate. The 3D model also gives information about the stresses in the BWR insert.

Sammanfattning

Tidigare förenklade analyser indikerar att inre tryck och olika termisk expansion i kopparhölje och insats kombinerat med vissa lastfall orsakar dragspänningar i kapselns kopparhölje. Denna analys syftar till att undersöka denna effekt vidare. Analysen omfattar både laster orsakade av inre processer hos kapseln och yttre laster. Inre laster orsakas av termisk utveckling och gasbildning medan yttre laster utgörs av trycket från svällande buffert och vatten samt glaciationseffekter. Analyserna baseras på olika antaganden för dessa faktorer.

Alla simuleringar är baserade på BWR-design av insatsen. Geometrin av FSW-svetsen (Friction Stir Welding) modelleras som en axiell slits och en rotdefekt i radiell riktning. Fyra axial-symmetriska analyser har utförts med olika tidsförlopp av temperatur och extern tryckutveckling. Dessutom har en 3D-modell gjorts för att verifiera att en axial-symmetrisk approximation är tillräckligt noggrann för studie av kopparhöljets påverkan. 3D-modellen ger också en uppfattning om spänningarna i en BWR insats.

Contents

| | | |
|-----------|---|-----------|
| 1 | Introduction | 4 |
| 1.1 | Context for this report | 4 |
| 1.2 | Background | 4 |
| 2 | Simulation considerations | 5 |
| 2.1 | Factors considered in the simulation | 5 |
| 2.2 | Parameters used in the simulations | 5 |
| 2.2.1 | Canister geometry | 5 |
| 2.2.2 | Thermal evolution | 5 |
| 2.2.3 | Thermal expansion effects | 7 |
| 2.2.4 | Load evolution | 7 |
| 2.2.5 | Internal gas pressure effects | 8 |
| 3 | Simulation strategy | 10 |
| 4 | Geometry definitions and meshes | 11 |
| 4.1 | General | 11 |
| 4.2 | Geometry of parts (3D-model) | 12 |
| 4.2.1 | Insert | 12 |
| 4.2.2 | Insert lid | 13 |
| 4.2.3 | Copper shell | 14 |
| 5 | Material models | 15 |
| 5.1 | Nodular cast iron (insert) | 15 |
| 5.2 | Steel (channel tubes in the insert) | 16 |
| 5.3 | Steel (insert lid) | 17 |
| 5.4 | Copper model | 17 |
| 6 | Contact definitions | 19 |
| 7 | Initial conditions | 20 |
| 8 | Boundary conditions | 20 |
| 9 | Calculations | 20 |
| 9.1 | General | 20 |
| 9.1.1 | Creep analysis until glaciations | 20 |
| 9.1.2 | Analysis approach | 21 |
| 9.2 | Long term analyses | 21 |
| 10 | Results | 21 |
| 11 | Uncertainties | 26 |
| 12 | Evaluation and conclusions | 26 |
| | References | 28 |
| | Appendix 1 – Isostat_JLH_creep_red_dim | 29 |
| | Appendix 2 – Isostat_JLH_creep_red_mean | 43 |
| | Appendix 3 – Isostat_JLH_creep_blue_dim | 57 |
| | Appendix 4 – Isostat_JLH_creep_blue_mean | 71 |

Appendix 5 – Storage of files

85

1 Introduction

To investigate how the thermal and gas expansion effects give loads on the copper, numeric calculations are carried out in "Inre övertyck i kapseln" (SKBdoc 133208) and "Svar på begäran om kompletteringar angående kapselfrågor" (SKBdoc 133256). The conclusion was that the combined effect of creep deformation, when the axial gap between copper lid and insert closes due to buffer swelling, and contraction effects during the subsequent cooling process must be analyzed with FEM-based creep calculations.

Since there are some uncertainties regarding the assumptions, two temperature histories and two swelling pressure histories were studied (four cases) in this analysis.

1.1 Context for this report

The insert (nodular cast iron) material properties are based on experimental results. The steel lid and the steel cassette material properties are based on supplier's available information. The copper shell material model includes creep and is developed by Rolf Sandström (Sandström and Andersson 2008, Jin and Sandström 2008, Sandström et al. 2009).

This report summarizes the results for analyses performed by using an axi-symmetric approach based on:

- Temperature history
- Buffer condition (wet or dry)
- Pressure history (inside and outside)
- Creep material model for the copper shell

1.2 Background

The canister reference design takes into account the difference in the operational temperature and the associated thermal expansion between the cast iron insert and the copper shell. This is done by providing an axial gap between the insert and the copper shell. The gap is sufficient to prevent any contact between the insert lid and the copper lid under unloaded conditions according to "Svar på begäran om kompletteringar angående kapselfrågor" (SKBdoc 133256). In order to examine if external loads in combination with thermal expansion effects could create harmful effects, it is necessary to take into account both the thermal and the swelling load evolution and their interaction.

2 Simulation considerations

2.1 Factors considered in the simulation

The following factors are taken into account in the simulations.

Canister geometry

- Tolerances for the nominal gap between insert and copper lid.
- The weld is modelled by the nominal axial slit but also with a circumferential root defect with a radial extension of 3 mm.

Thermal evolution

- Differences in wet and dry deposition holes under mean and dimensioning temperature evolution.

Thermal expansion effects

- Thermal expansion coefficients for nodular cast iron and copper.

Load evolution

- Hypothetic local swelling effects due to uneven water saturation.
- Isostatic pressure from buffer swelling, water and glaciations.

Internal gas pressure effects

- The expected pressure evolution due to gas production and thermal expansion of the gas in the canister has been calculated in "Inre övertyck i kapseln" (SKBdoc 133208). This pressure is included in the simulations.

2.2 Parameters used in the simulations

2.2.1 Canister geometry

The dimensions of the reference design are specified in TR-10-14 (SKB 2010).

- nominal length of the insert is 4573 (+0/-0.5) mm (at 20°C).
- nominal internal length of the copper shell is 4575 (+0.6/-0.1) mm (at 20°C).
- nominal axial gap can be calculated to 2 (+1.1/-0.3) mm, on account of steel lid tolerances.

The maximum strain increases with the size of the initial gap between copper lid and steel lid, which is set to 3.1 mm according to the tolerances above.

All other dimensions are nominal.

2.2.2 Thermal evolution

The temperature evolution in different bedrock domains in the planned repository at Forsmark have been modelled by Hökmark et al. (2011).

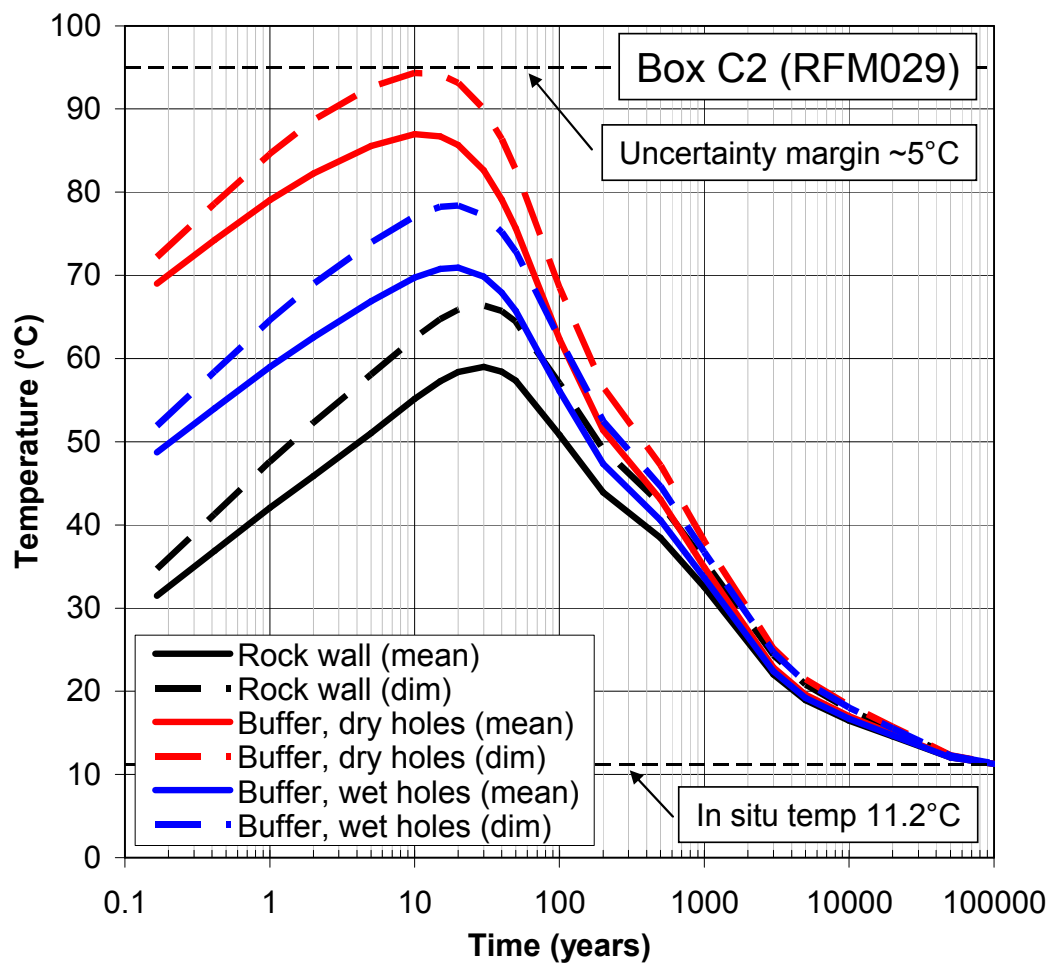


Figure 2-1. The temperature evolution in bedrock with different thermal properties at the Forsmark site according to Hökmark et al. (2011, chapter 5.3). Curves denoted “mean” represent the normal case and “dim” the highest expected temperature.

The simulation presented in figure 2-1 shows the evolution of the buffer temperature with an installed canister for different thermal conditions.

The blue curves correspond to wet deposition holes. A wet hole is an idealization assuming that the wetting and the corresponding swelling of the buffer starts directly. In a wet hole, contact is established between the copper shell and the buffer due to the swelling forces, and the buffer temperature presented is given at the axial midpoint of the canister. It is assumed that the copper shell and the bentonite have the same temperature.

The red curves correspond to dry holes meaning that no wetting will take place. Consequently, no overall contact is assumed to exist between insert, copper shell and the dry buffer, except in the contact point at the base and top. The presented temperature is the peak temperature of the bentonite in the contact point in the top. The thermal conductivity of a wet buffer is higher compared to a dry buffer which also is reflected in diagram 2-1.

In the following analysis some assumptions are made:

- No temperature gradients exist in the canister. It is, however, likely that the temperature in reality is somewhat higher in the insert compared to the copper. The coefficient of thermal expansion is higher for copper than for nodular iron, which implies that the maximum gap of

interest is overestimated. The external pressure will close the gap followed by a temperature decrease. The resulting creep strain will thus be overestimated with the assumption made.

- The outside pressure, corresponding to buffer swelling, is treated as an independent parameter to the temperature. This is further commented in "2.2.4 Load evolution".

2.2.3 Thermal expansion effects

The thermal expansion effects are included using the following expansion coefficients for (oxygen free) copper and ductile iron, see "Inre övertyck i kapseln" (SKBdoc 133208).

$$\alpha_{Cu} = 1.77 \cdot 10^{-5} \text{ m/m,K}$$

$$\alpha_{Fe} = 1.18 \cdot 10^{-5} \text{ m/m,K}$$

2.2.4 Load evolution

The loads are chosen in a conservative way in order to provide limit-setting load cases. Hence, the assumed glacial load of 60 MPa is higher than the design pressure of 45 MPa for the canister. Figures 2-2 and 2-3 show the evolution of temperature and pressure for wet and dry holes, respectively, followed by definitions of the simulation cases.

Wet holes

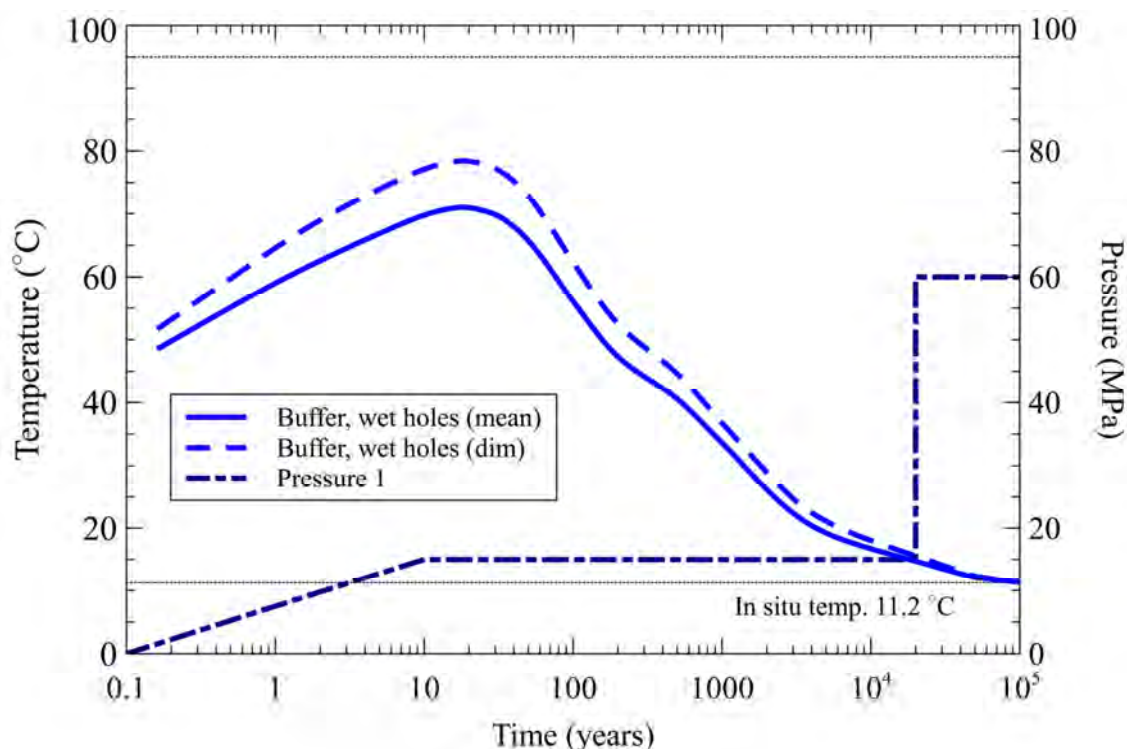


Figure 2-2. Pressure and temperature development in wet holes, case a) and b).

Case a). The water saturation process is assumed to start immediately and full swelling- and water pressure is reached after 10 years (blue dotted line, Pressure 1). The canister temperature is following the blue solid line (normal). The case is chosen to examine a normal evolution in a wet area. A hypothetical glacial load is applied after 20,000 years (Pressure 1).

Case b). Same as case a) except that the canister temperature is following the blue dashed line (upper limit). This case is chosen to examine the influence of elevated temperature in a wet hole.

Dry holes

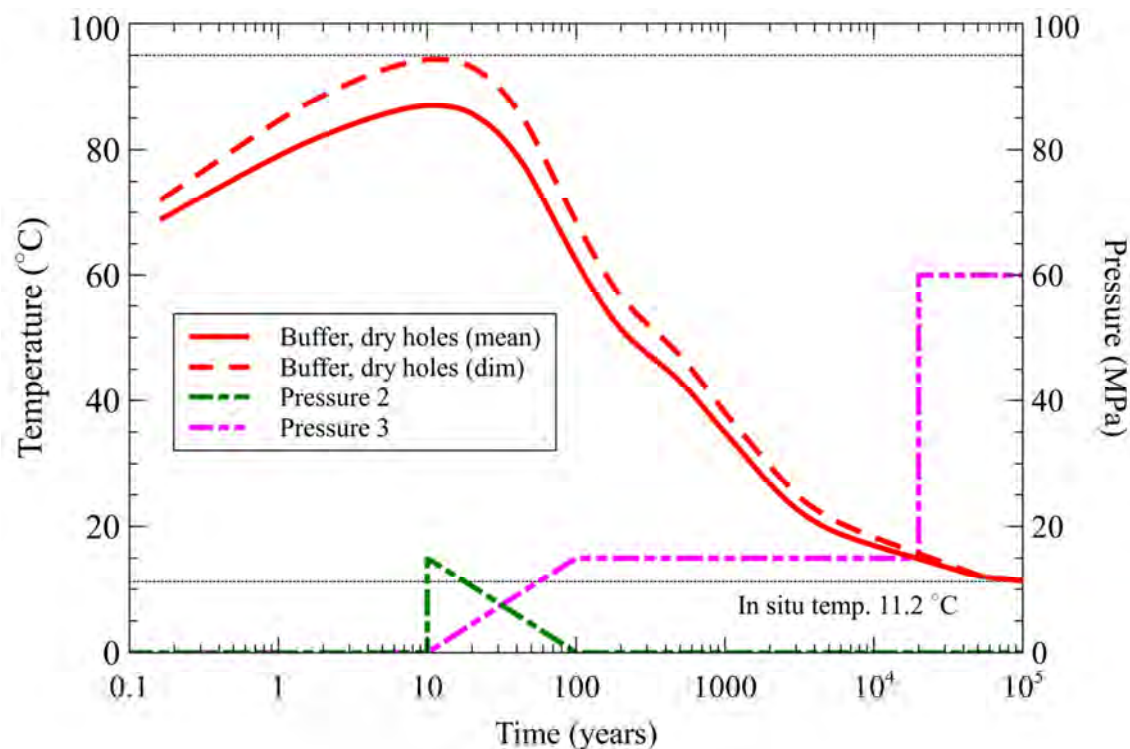


Figure 2-3. Pressure and temperature development in dry holes, case c) and d).

Case c). The water saturation process is assumed to start after ten years and full pressure is reached after 100 years (magenta dotted line, Pressure 3). The load component in axial direction (green dotted line, Pressure 2) is assumed to develop quickly at the canister top and will gradually be replaced by the isostatic pressure (magenta dotted line) assumed to gradually develop under 100 years and a hypothetical glacial load is applied after 20,000 years (Pressure 3). The canister temperature is following the red solid line (normal case).

It should be emphasised for this case that the temperature in reality will drop when the swelling takes place and merge to wet hole conditions. Maintaining the temperature evolution in the analysis is a pessimistic assumption as both the creep rate and the temperature dependent gap is overestimated.

Case d). Same as case c) except that the canister temperature is following the red dashed line (upper limit).

2.2.5 Internal gas pressure effects

SKB has presented the expected pressure evolution due to gas production and thermal expansion of the gas in the canister, "Inre övertyck i kapseln" (SKBdoc 133208), see Figure 2-4. Taken into account that the steel lid initially is tested to be leak tight it is assumed in this analysis that the pressure acting on the copper shell will gradually build up during the first ten years to mimic a minor leakage (under the detection limit in the leak test). The time variation used in the analyses is given in Figure 2.5.

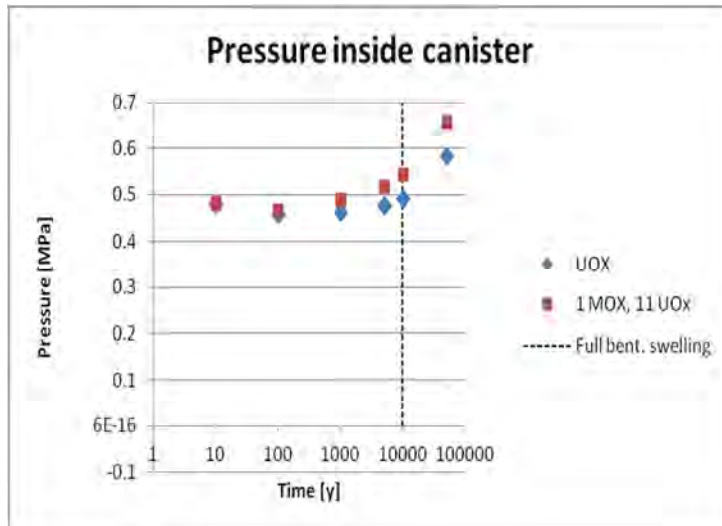


Figure 2-4. Evolution of the internal pressure in the canister. Argon, water/hydrogen and helium from pre pressure treatment of the fuel rods are included, see "Inre övertyck i kapseln" (SKBdoc 133208). Full bentonite swelling is there assumed at 10,000 years as a pessimistic assumption.

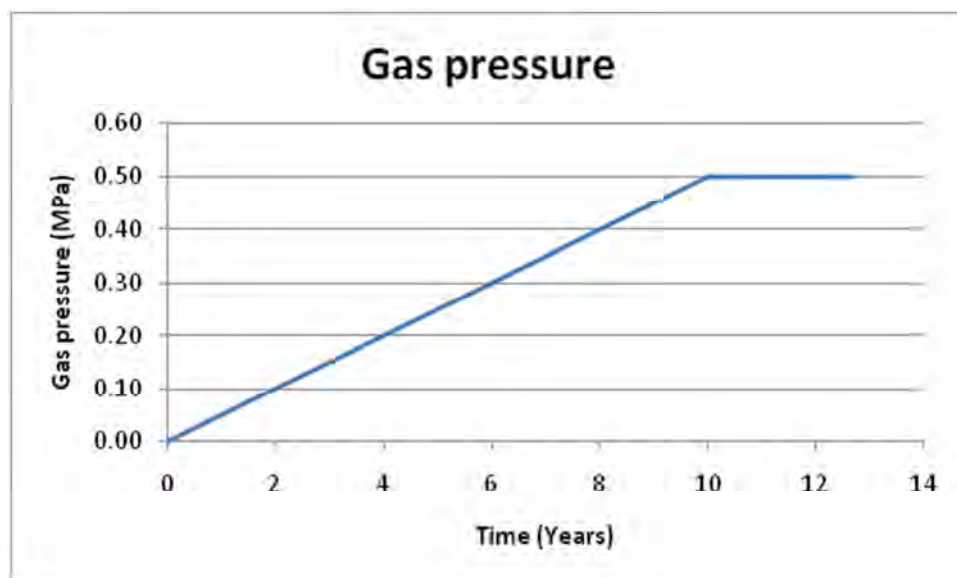


Figure 2-5. Gas overpressure variation used in the analyses. The initial phase is not accounted for in Figure 2-4.

3 Simulation strategy

The performed simulations are all based on the same geometry which consists of a copper shell, canister (iron), lid (steel) and insert (steel) and is defined through a 3-dimensional model that are used for verification of a simplified axi-symmetric model.

The insert is assumed to completely consist of cast iron when defined by the axi-symmetric model. All analyses are performed using the ‘*visco’-procedure in Abaqus which will consider creep effects. The procedure works as a static analysis with special attention to creep material definition.

4 Geometry definitions and meshes

4.1 General

The geometry consists of the insert, the insert lid and the surrounding copper shell. The geometry is based on CAD-geometries received from SKB “Ritningförteckning för kapselkomponenter” (SKBdoc 1203875) and should therefore correspond to the current design.

Due to symmetry only one half has been modelled. The mesh is then generated by 3-dimensional solid elements, mainly 8-noded hexahedral (most of them using full integration technique) and a few 6-noded wedge elements, see Figure 4-1. The model size is defined by about 140,000 elements and 170,000 nodes (total number of variables about 800,000).

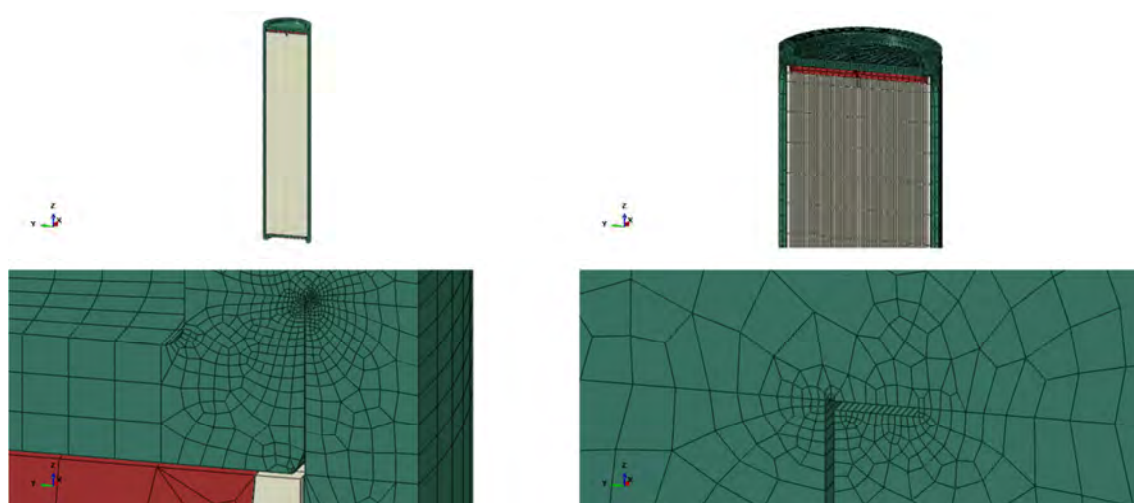


Figure 4-1. Top left figure shows the 3D- model with mesh. Top right shows detail of the mesh, bottom left figure show details of the mesh (green – copper shell, red – steel lid, grey – insert) and bottom right details of the weld and the circumferential 3 mm root defect.

The 3-dimensional model consists of the insert (made of nodular cast iron), the steel tubes (made of steel and welded to the insert), the insert lid (made of steel) and the surrounding copper shell. The model is only used to verify the simplified axi-symmetric model which is used for detailed analysis of how the copper shell is affected by creep caused by the temperature and pressure history until glaciations occurs.

An axi-symmetric approach is used since the main focus in this study is on the copper shell and the insert stiffness could be approximated by an axi-symmetric geometry based on previous analyses.

The axi-symmetric model neglects the steel cassettes and thus only consists of the insert, the insert lid and the surrounding copper shell; see Figures 4-2 – 4-3. The mesh is then generated by 2-dimensional solid elements, mainly 4-noded quads and a few 3-noded elements. The axi-symmetric model size is defined by about 13,000 elements and 14,000 nodes (total number of variables about 36,000).



Figure 4-2. Axi-symmetric mesh (green – copper shell, red – steel lid, grey – insert).

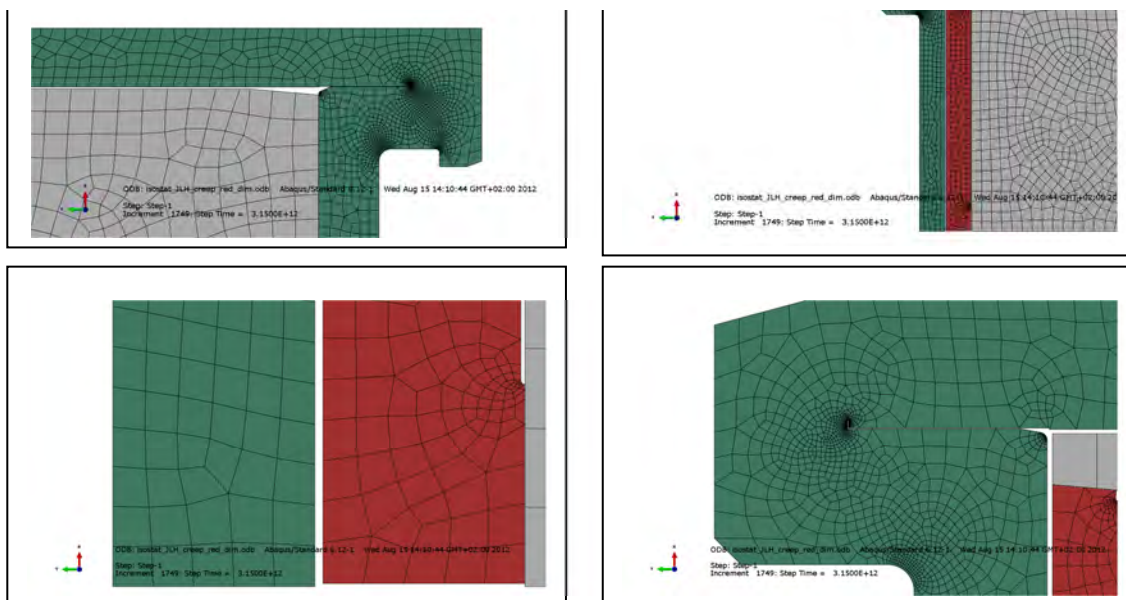


Figure 4-3. Plot of details in the axi-symmetric model (green – copper shell, red – steel lid, grey – insert).

4.2 Geometry of parts (3D-model)

4.2.1 Insert

The insert is made of nodular cast iron and has been simplified regarding the square tubes which are assumed to be tied to the nodular cast iron insert and thus these contribute as added material to the insert. This simplification will probably overestimate stresses and strains in this region.

The insert is modelled as a homogeneous part with 3D solids, see Figure 4-4.

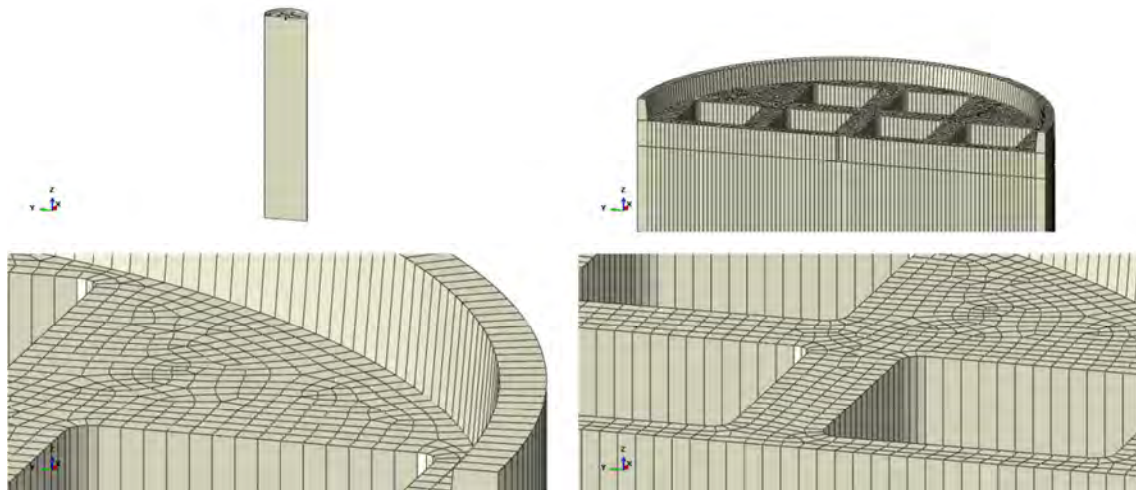


Figure 4-4. Insert BWR geometry (top left), mesh details (top right, bottom left and bottom right).

4.2.2 Insert lid

The insert lid is made of steel and is modelled with 3D solids, see Figure 4-5.

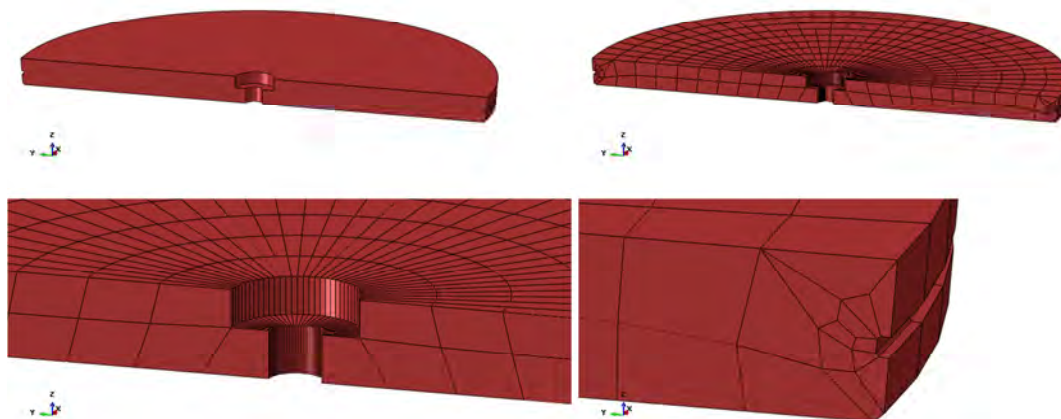


Figure 4-5. Insert lid geometry and mesh.

4.2.3 Copper shell

The copper shell surrounds the insert. The canister has been modelled rather accurately in order to catch “hot spots” where large strains are expected, e.g. the fillets at the bottom and top (the lid). The lid is welded to the flange (modelled by an axial slit and a root defect in radial direction with 3 mm in size) - the canister will thus act as one part, see Figure 4-6.

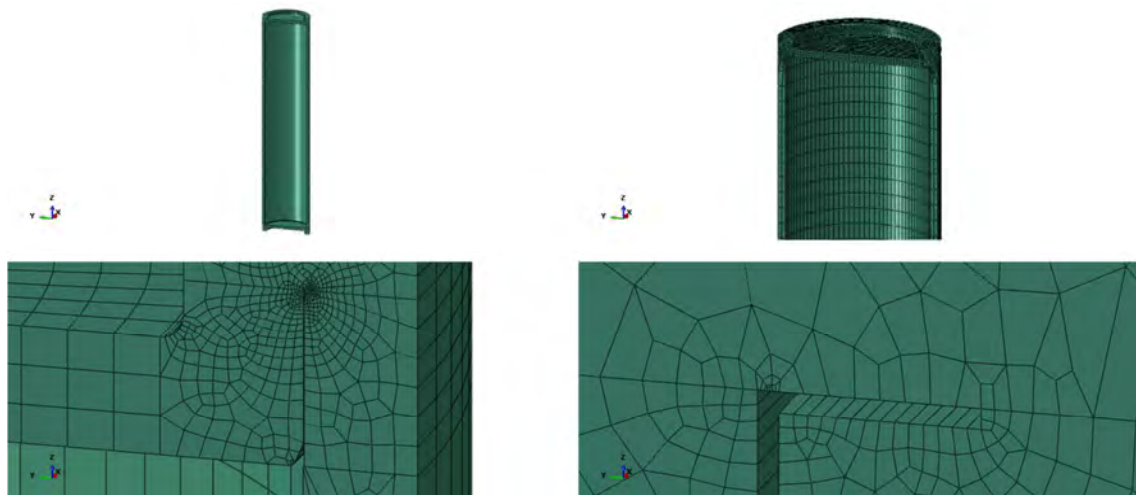


Figure 4-6. Copper shell geometry (top left), mesh (top right), weld mesh (bottom left) and weld root (bottom right).

5 Material models

The finite element code Abaqus (version 6.12, Dassault Systèmes Simulia Corp.) was used for the calculations. The materials have been modelled as elastic-plastic with stress-strain properties that correspond to each material and the applied shear load induced strain rate, when applicable.

5.1 Nodular cast iron (insert)

The material model for the insert is based on a von Mises' material model with elastic behaviour defined by Young's modulus and the Poisson's ratio and the plastic behaviour defined through yield surface (true stress) versus plastic strain (defined as logarithmic strain), see Table 5-1 and Figure 5-1 "Dragprovning av gjutjärn" (SKBdoc 1201865).

The experiments were performed at 0°C.

Table 5-1. Stress-strain definition for the insert.

| Plastic Strain (%) | Stress (MPa) | | | Strain rate factor at strain rate=0.5 /s |
|--------------------|------------------|-----------------------------------|--------------------|--|
| | Strain rate=0 /s | Strain rate=2·10 ⁻⁴ /s | Strain rate=0.5 /s | |
| 0 | 293 | 293 | 348 | 1.19 |
| 1 | 324 | 324 | 367 | 1.13 |
| 2 | 349 | 349 | 385 | 1.10 |
| 3 | 370 | 370 | 406 | 1.10 |
| 4 | 389 | 389 | 423 | 1.09 |
| 5 | 404 | 404 | 438 | 1.09 |
| 6 | 418 | 418 | 451 | 1.08 |
| 7 | 428 | 428 | 464 | 1.08 |
| 8 | 438 | 438 | 474 | 1.08 |
| 9 | 447 | 447 | 483 | 1.08 |
| 10 | 456 | 456 | 490 | 1.07 |
| 11 | 465 | 465 | 498 | 1.07 |
| 12 | 472 | 472 | 504 | 1.07 |
| 13 | 478 | 478 | 510 | 1.07 |
| 14 | 484 | 484 | 516 | 1.07 |
| 15 | 488 | 488 | 520 | 1.07 |
| 16 | 491 | 491 | 521 | 1.06 |

The strain rate dependency is defined by assuming that the yield surface is proportional to the strain rate factor (at the strain rate 0.5 /s the factor 1.08 has been chosen and at strain rate 0 /s the factor is 1.0). The instantaneous strain rate factor is then linearly interpolated between 1 and 1.08 using the instantaneous strain rate.

Furthermore, Young's modulus $E = 166$ GPa and Poisson's ratio $\nu = 0.32$ (Raiko et al. 2010).

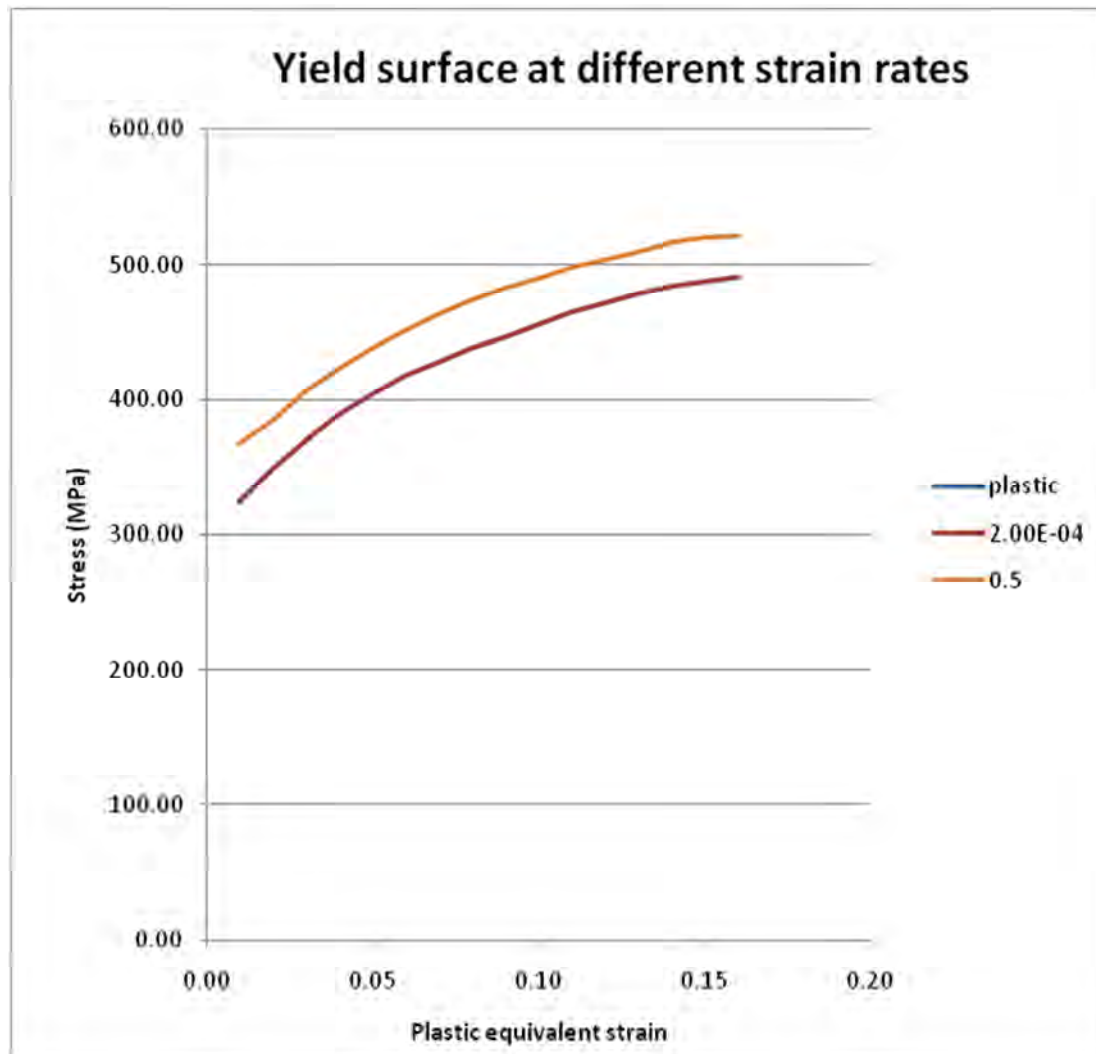


Figure 5-1. Yield surface versus plastic strain for different plastic strain rates. Note that the base (plastic) is defined to coincide with strain rate = $2 \cdot 10^{-4}$ /s.

5.2 Steel (channel tubes in the insert)

The material model for the channel tubes in the insert is based on a von Mises' material model with elastic behaviour defined by Young's modulus and the Poisson's ratio. The plastic behaviour is defined through yield surface (true stress) versus plastic strain (using logarithmic strain).

The steel cassette tubes are manufactured by steel S355J2H, for example Domex 355 MC B. SKB has earlier supplied test data for the yield point of their material, but no stress-strain data to be used in a plastic analysis. The stress-strain curve for Domex 355 MC B (SSABDirekt 2008) can be scaled using the yield stress and tensile ultimate strength measured by (JRC) $R_e = 412$ MPa (yield stress) and $R_m = 511$ MPa (ultimate stress). With this procedure a simplified stress-strain curve is obtained and described by Table 5-2, see Raiko et al. (2010, Table 4-2).

Table 5-2. Stress-strain definition for channel tubes used in the insert.

| Strain (%) | Stress (MPa) | Log Strain (%) | True Stress (MPa) |
|------------|--------------|----------------|-------------------|
| 0 | 0 | 0 | 0 |
| 0.196 | 412 | 0.196 | 412 |
| 15 | 511 | 14.3 | 587 |
| 20 | 511 | 18.5 | 613 |

Furthermore, Young's modulus $E = 210$ GPa and Poisson's ratio $\nu = 0.3$ according to Raiko et al. (2010, Table 4-3).

The data with lowest value from the experiment has been chosen for the yield surface. However, the plasticity definition for the steel channel tubes has minor influence on the overall results due to almost elastic behaviour.

5.3 Steel (insert lid)

The material model for the insert lid is based on a von Mises' material model with elastic behaviour defined by Young's modulus and the Poisson's ratio. The plastic behaviour is defined through yield surface (true stress) versus plastic strain (calculated as logarithmic strain).

Manufacturing drawings for the lid specify steel S355J2G3. Strain versus stress for steel Domex 355 MC B with $Re = 389$ MPa (yield stress) and $Rm = 484$ MPa (ultimate stress) can be found from SSABDirekt (2008). According to SS-EN 10025-2:2004, the material S355 with nominal thickness 40-63 mm has $Re = 335$ MPa (yield stress) and $Rm = 470-630$ MPa (ultimate stress). Scaling stress-strain curves for Domex 355 by the minimum values given in SS-EN 10025-2:2004 implies the simplified material definition (engineering data) shown in Table 5-3.

Table 5-3. Nominal stress-nominal strain definition for the insert lid.

| Strain (%) | Stress (MPa) | Log Strain (%) | True Stress (MPa) |
|------------|--------------|----------------|-------------------|
| 0 | 0 | 0 | 0 |
| 0.1595 | 335 | 0.1593 | 335 |
| 15 | 470 | 13.98 | 540 |
| 20 | 470 | 18.2 | 564 |

Furthermore, Young's modulus $E = 210$ GPa and Poisson's ratio $\nu = 0.3$ according to Raiko et al. (2010, Table 4-2)

The data with lowest value from the experiments (SS-EN 10025-2:2004) has been chosen for the yield surface. However, the plasticity definition for the insert lid has very minor influence on the overall results.

5.4 Copper model

The stress-strain properties of the copper in the copper shell were investigated by Swerea KIMAB, and the results were then represented by a creep material model developed by Rolf Sandström, see Sandström and Andersson (2008), Jin and Sandström (2008) and Sandström et al. (2009).

The material model for short duration analysis is based on a simplified elastic-plastic model, see Table 5-4, using data from the creep model assuming a strain rate of 5×10^{-3} /s which is considered as

pessimistic. This model thus illustrates the model used for long term duration for a fixed strain rate when the load suddenly is increased.

The flow curve data is based on Sandström et al. (2009) wherein eq. (17) has been used together with the parameter values defined in the corresponding table 4-2, as well as $m = 3.06$, $\alpha = 0.19$, $\omega = 14.66$.

The copper model data is shown in Figure 5-2.

Table 5-4. Elastic-plastic material data for the copper at strain rate 5×10^{-3} / s.

| Elastic part | | Plastic part: von Mises stress σ_j (MPa) at the following plastic strains (ϵ_p) | | | | | |
|------------------|-------|---|------|------|------|------|------|
| E (MPa) | ν | 0 | 0.10 | 0.20 | 0.30 | 0.40 | 0.50 |
| $1.2 \cdot 10^5$ | 0.308 | 72 | 178 | 235 | 269 | 288 | 300 |

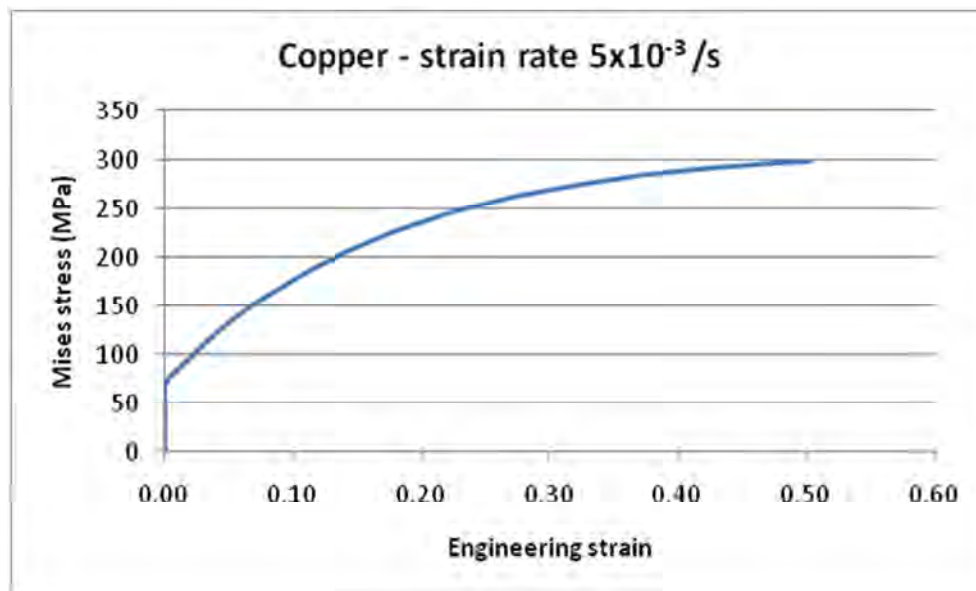


Figure 5-2. Copper shell material model gives the Mises stress as a function of the engineering strain at strain rate $5 \cdot 10^{-3}$ /s.

The long term duration has been simulated using the creep model implemented in Abaqus as a user supplied subroutine (CREEP) which is essentially based on eqn. 50 in Andersson-Östling and Sandström (2009).

6 Contact definitions

All the boundaries of the buffer, the copper shell, the insert and the insert lid interact through contact surfaces allowing finite sliding. All contact surfaces have friction at sliding with no cohesion and the friction coefficient 0.1, i.e. the friction angle (ϕ) is 5.7° and the cohesion (c) is 0 kPa.

The contact is released when the contact pressure is lost.

A few contact pairs are tied together (tied means that the surfaces are constrained together and will not allow for opening/closing or sliding). This is done in order to improve the numerical convergence rate. This applies at the contact pairs between the insert and insert lid and also at the bottom of insert and copper shell bottom.

7 Initial conditions

Initial conditions are defined as:

The temperature for all nodes in the model is 293 K. The temperature change during the analysis is specified through an amplitude definition (magnitude versus time).

8 Boundary conditions

Symmetry conditions have been specified for the symmetry plane (displacements in the normal direction to the symmetry plane prescribed to zero) and also the copper shell has prescribed zero displacements in the vertical direction at the base, see Figure 8-1.

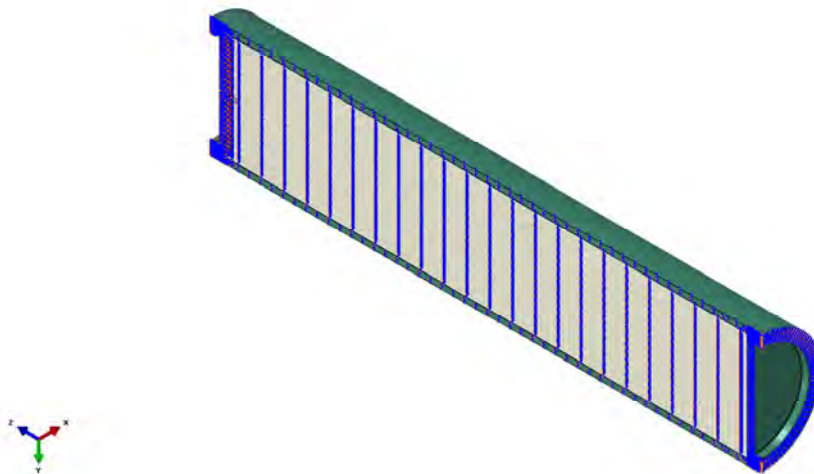


Figure 8-1. Prescribed boundary conditions.

9 Calculations

9.1 General

9.1.1 Creep analysis until glaciations

The reference case for BWR is based on buffer material consisting of Na-bentonite converted to Ca-bentonite with density 2050 kg/m³. The four cases a-d according to section 2.2.1 have been analyzed and are denoted as follows:

Dimensioning temperature history when buffer is placed in a dry hole (red_dim).

Jobnames are isostat_JLH_creep_red_dim and half_3d_JLH_red_dim (3D-analysis)

Mean temperature history when buffer is placed in a dry hole (red_mean).

Jobname is isostat_JLH_creep_red_mean

Dimensioning temperature when buffer is placed in a wet hole (blue_dim).

Jobname is isostat_JLH_creep_blue_dim

Mean temperature history when buffer is placed in a wet hole (blue_mean).

Jobname is isostat_JLH_creep_blue_mean

9.1.2 Analysis approach

The numerical calculations are performed using the FE-code Abaqus (version 6.12, Dassault Systèmes Simulia Corp.) assuming non-linear geometry and material definitions. This means that all non-linearities defined by the input will be considered such as large displacements, large deformations, non-linear interactions (contact) and non-linear materials. All non-linear contributions will be used when forming the equations to be solved for each equilibrium iteration. Long term analysis is based on static response, but the results will depend on the time used for the simulation since rate-dependent material data is used. The code will choose suitable time-increments for the loading based on (in most cases) default convergence tolerances.

9.2 Long term analyses

The long term analyses (100,000 years) consist of one step where the loading (temperature and pressure) is specified by amplitude definitions (magnitude versus time).

The results are shown in Appendix 1-4.

10 Results

For each analysis a large amount of results are available and to have an indication only a few values are reported for the most extreme case, isostat_JLH_creep_red_dim. Additional results can be found in appendices after 10 (helium gas pressure applied) and 100,000 years:

Appendix 1 shows results for isostat_JLH_creep_red_dim

Appendix 2 shows results for isostat_JLH_creep_red_mean

Appendix 3 shows results for isostat_JLH_creep_blue_dim

Appendix 4 shows results for isostat_JLH_creep_blue_mean

The creep strain in the copper shell after 10,000 years from the 3D-analysis is presented in Figure 10-1.

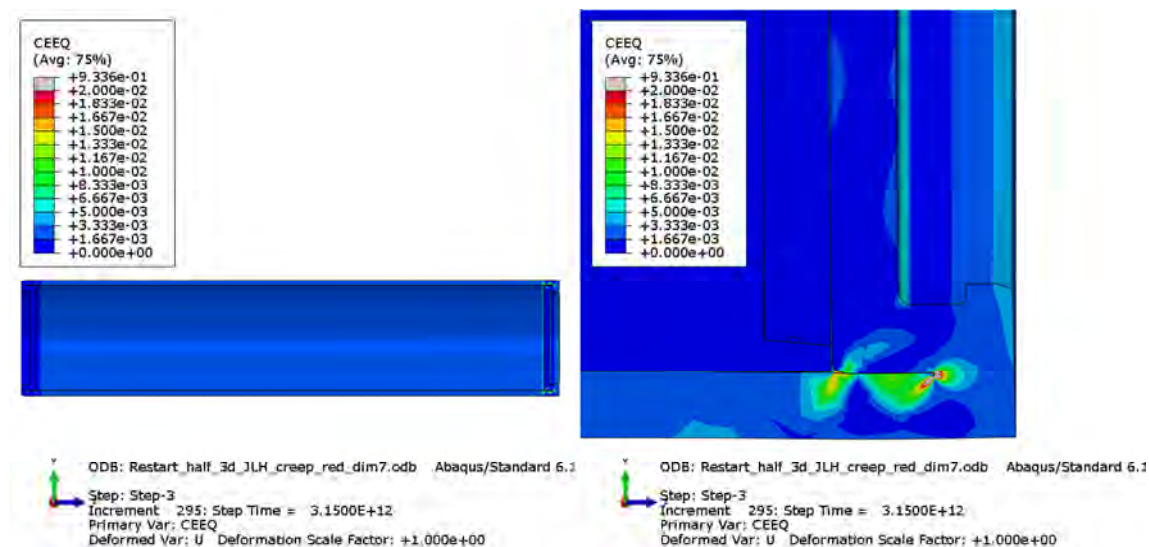


Figure 10-1. Equivalent creep strain (CEEQ) after 10,000 years in the copper shell, 3D-analysis. This represents the situation before glaciations.

The corresponding creep strain after 10,000 years in the copper shell from the axi-symmetric analysis is presented in Figure 10-2. The axi-symmetric model shows similar results as the 3-D model but gives

somewhat higher strain levels and also larger affected areas except for a local area in the root of the lid weld. Hence the use of the axi-symmetric model is pessimistic.

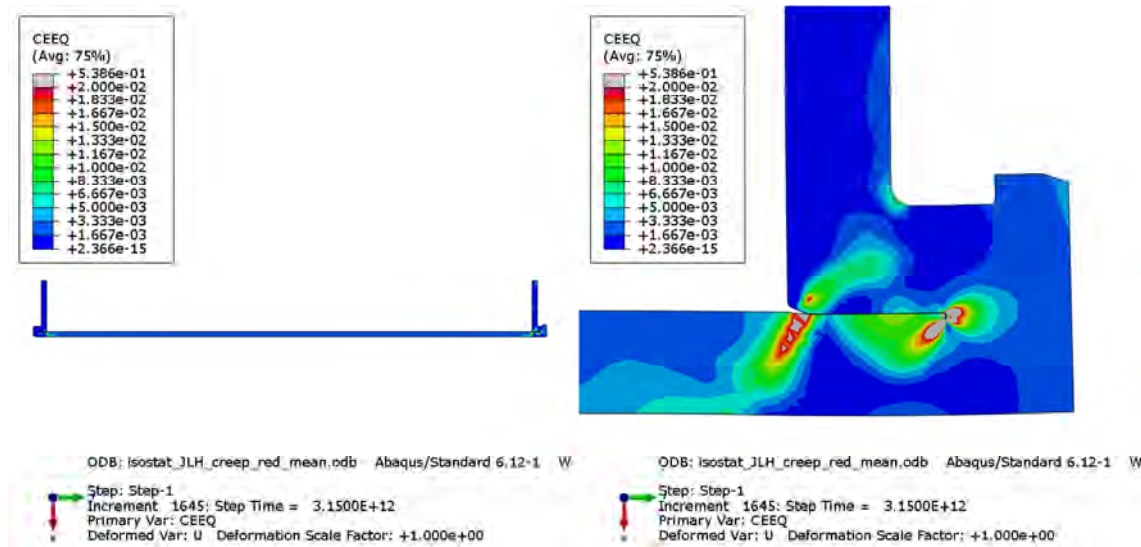


Figure 10-2. Equivalent creep strain (CEEQ) in the copper shell after 10,000 years, axi-symmetric analysis.

The visco-plastic strains include normal plasticity and Figure 10-3 shows how the equivalent creep strain (CEEQ) develops for all axi-symmetric cases and also for the 3D-analysis. The figure shows the history response for that node having the maximum equivalent creep strain. The node position is at the root of the weld. As can be seen from the figure, the traditional creep effect is rather small compared to the plastic response when the external load is changed. The plot indicates that the 3D-analysis gives the highest magnitude but that is only for one specific node (compare also Figure 10-1 and 10-2).

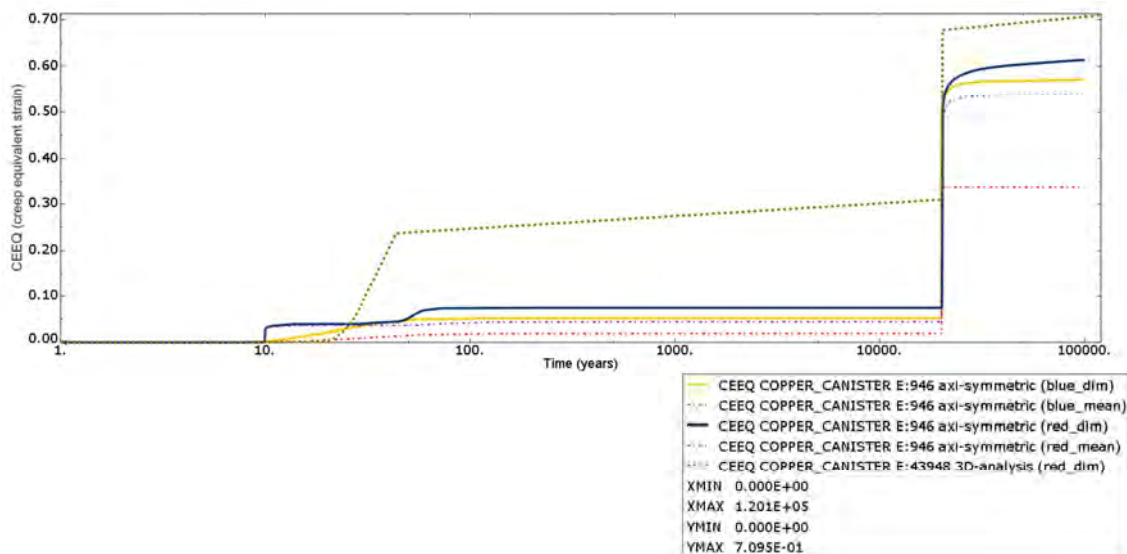


Figure 10- 3. Equivalent creep strain (CEEQ) for all cases. Highest value, about 70%, is achieved for case half_3d_JLH_creep_red_dim7. Most of the increase in magnitude occurs instantaneously when the load is increased and only a few percent is traditional creep strain.

The copper shell and the cast iron insert have different coefficient of thermal expansion which means that the copper shell will expand more when the temperature is increasing. The external pressure will compress the copper shell until it gets in contact with the insert. A subsequent temperature decrease will then eventually increase the creep strain in the copper shell.

However, the difference in the coefficient of thermal expansion for copper and iron ($1.7 \cdot 10^{-5}$ and $1.18 \cdot 10^{-5}$, respectively) is rather small and will only contribute with additional thermal strains of about $50 \cdot (1.7 - 1.18) \cdot 10^{-5} = 2.6 \cdot 10^{-4}$ for 50°C temperature increase.

Figure 10-4 shows how all creep strain components change when the external pressure is increased to 60 MPa and from the figure it is obvious that the shear strain (CE12) is the component most affected. The component CE11 is in the radial direction, CE22 is in the axial direction, CE33 is in the hoop direction and CE12 is shearing in the radial/axial plane.

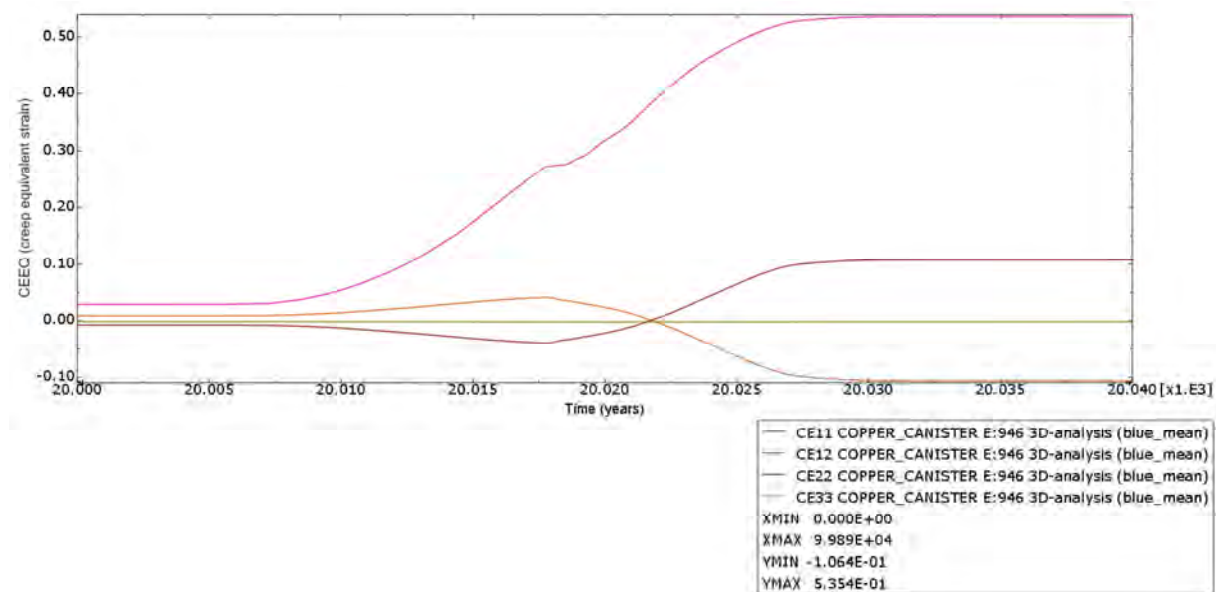


Figure 10-4. Creep strain components in the time window close to when the external pressure is increased to 60 MPa. Maximum creep strain is about 50% and occurs for CE12 for the 3D-case.

Figure 10-5 shows displacements at the outer corner for the insert and copper shell. Also the gap between these nodes is plotted. The temperature is increased for 10 years implying a gap increase. After 10 years the axial pressure is applied implying a gap decrease. Increasing the outer pressure (15 MPa is reached after 100 years) results in a gap increase because only the radial component is increasing which forces the copper shell to move upward. The temperature is then slowly decreased to about 10°C which causes the gap to slightly decrease. Increasing the external pressure (axial and radial) to 60 MPa implies further decrease of the gap and at the end of the process the gap is almost closed.

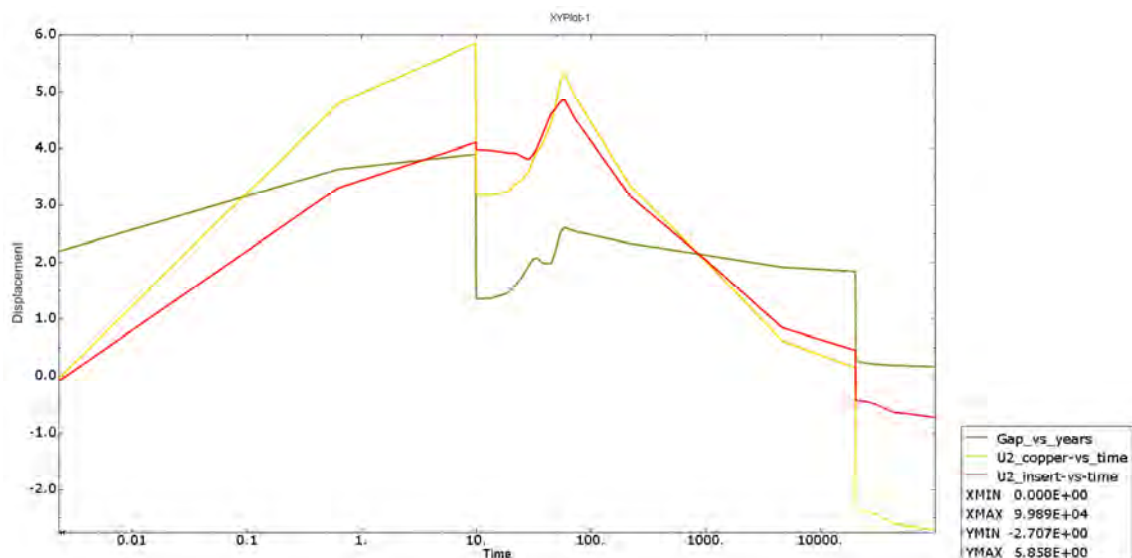


Figure 10-5. Axial displacement for the outer corner of the insert and corresponding coordinate for the copper shell. The gap is represented by the green line. Time is in years and displacement is in mm.

Figure 10-6 shows the hydrostatic pressure for the copper shell close to where the maximum equivalent creep strain occurs at 60 MPa. The figure shows that the stresses are compressive in this region.

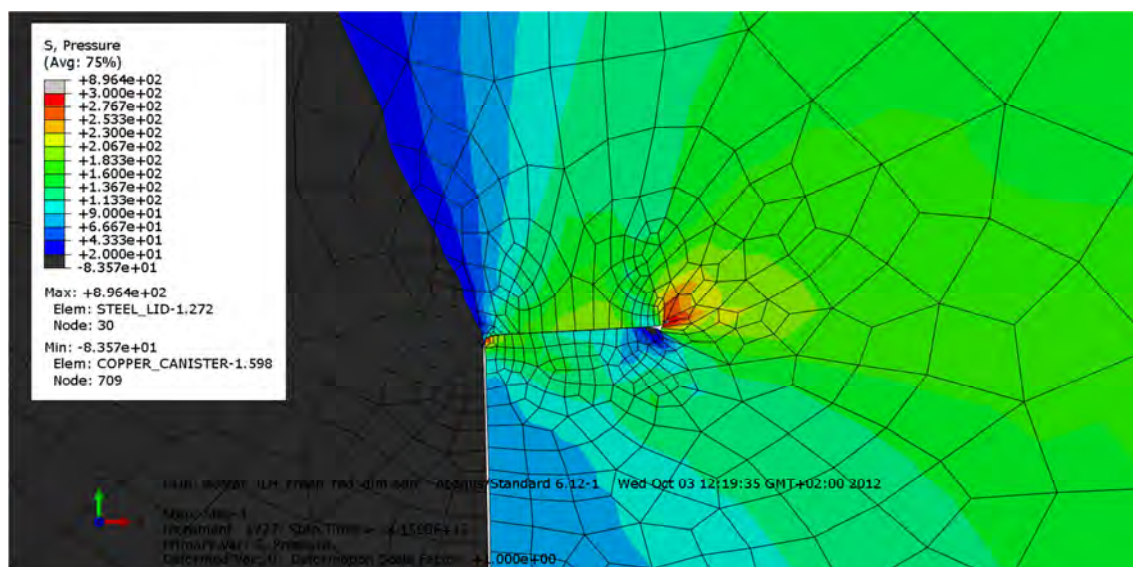


Figure 10-6. Plot of hydrostatic pressure close to the weld for the copper shell at the end of the process.

Cast iron insert

The highest value for Mises stress, 550 MPa, occurs in the fillets, see Figure 10-7.

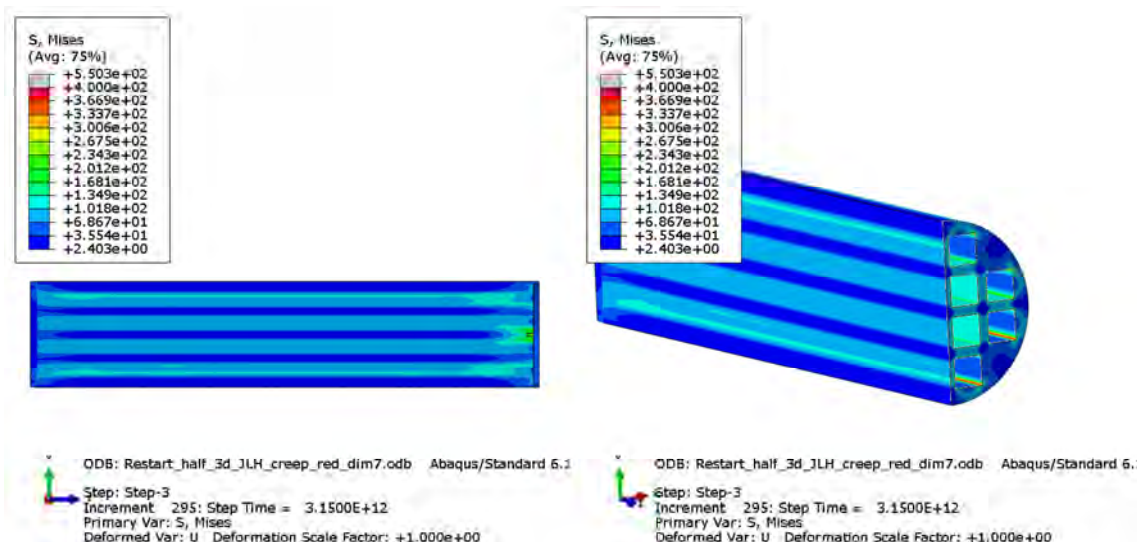


Figure 10-7. Plot of Mises stress in the insert at the end of the process.

Steel lid

The steel lid has a large equivalent plastic strain (PEEQ) at the geometric discontinuity, 21.5%; see Figure A1-25, but also in this region the dominating pressure is in compression, see Figure A1-28.

Steel channels (only 3D-analysis)

The steel channels show mainly an elastic response and the highest Mises stress occurs at the fillets and at the connection to the steel lid, se Figure 10-8.

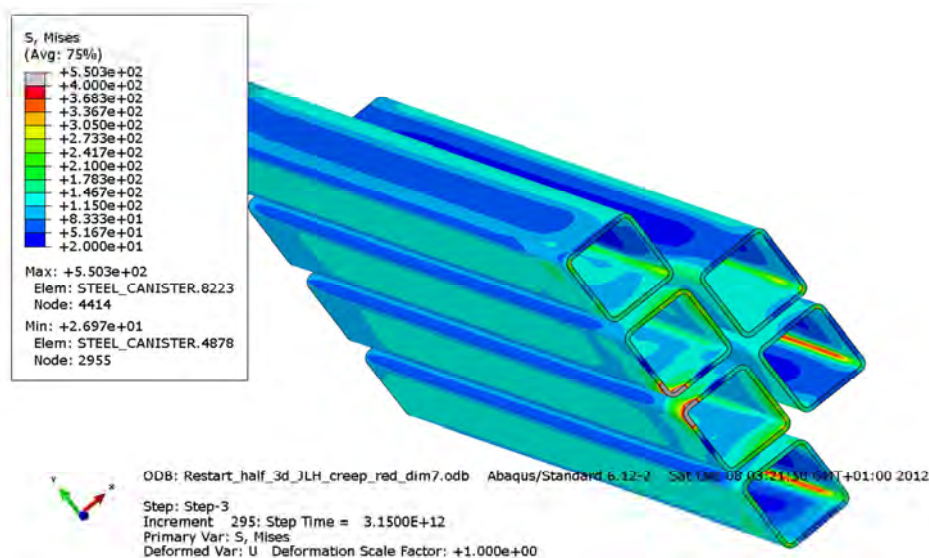


Figure 10-8. Plot of Mises stress for the steel channels at the end of the process.

Copper shell

The maximum equivalent creep strain (CEEQ) is shown in Figures A1-8 and A1-10. The maximum magnitude, 61.4%, occurs for case isostat_JLH_creep_red_dim at the top weld, Figure A1-10. Figure A1-20 shows that the pressure is positive for the corresponding element. Comparing Figure A1-19 (showing results after applying the helium gas pressure) with A1-20 implies that the hydrostatic pressure at the weld corner changes from -159 MPa to almost zero. However, the equivalent creep strain is small after applying the helium gas pressure, see Figure A1-9.

11 Uncertainties

The obtained results are based on several assumptions regarding loads and material properties. Also the discretization in the computer model will affect the results. Some of these influencing factors are addressed below.

- Strain rate effects in the copper and iron will affect the results. For the copper shell the strain rate effect has been included for all reported analyses.
- All experimental data used for material calibration have a spread which will imply a range for the properties defining each material model.
- The element mesh is rather fine but nevertheless too coarse in some regions, especially at the welds and in regions with geometric discontinuities. A more refined mesh will probably increase the maximum stress and strain levels. Fortunately, the use of non-linear material properties (such as plasticity and creep) will decrease the sensitivity to the used mesh. The used mesh has been judged to be accurate enough considering also the required computer resources to obtain the results. Since several models have been executed with different mesh densities it has been possible to make comparisons and the conclusion is that the mesh in a global sense is accurate.

12 Evaluation and conclusions

The study aimed to simulate the complete time history of stresses and strains in the canister due to external and internal loads such as helium gas pressure, swelling pressure from the saturation phase and overburden from glaciations based on assumed evolutions of these loads. A few general conclusions from the performed simulations are listed below.

- The temperature is assumed to increase for 20-30 years due to heat generation in the spent fuel and then the temperature declines. At the same time interval (20-50 years) the swelling pressure is also assumed to increase and at the glaciations, which is assumed to occur after about 20,000 years, the external pressure increases significantly. The external pressure will increase the pressure between the copper shell and the insert, while the temperature decreases the pressure since copper expands more than iron. When the temperature drops, the pressure between the copper shell and the insert increases.
- The different models behave in a very similar way where an axi-symmetric approach represents the stress/strain distribution accurately. The axi-symmetric approach allows a much finer mesh without requiring extremely long computer time.
- The stiffness for the insert could be approximated with an axi-symmetric approach but stress and strain distribution in the insert requires a 3D approach.

The results obtained from the creep analyses could be summarized as:

- The magnitude of the external pressure has the highest impact on the results but also increased temperature is important to consider since the yield surface depends on the temperature.
- Despite the differences in the assumptions regarding temperature and pressure development, the dominant factor for the creep strain is the high external pressure under glaciations.
- The creep from the internal processes, before external loads are applied, case c) and d), is very small and of minor importance.
- High creep strains occur locally in the weld roots due to external pressure. The maximum equivalent creep strain in the copper shell occurs at the top weld and is very local. The magnitude will depend on the mesh, but the current mesh at least shows that very high magnitudes are reached. It should be noted that strain is caused by compressive stresses. The maximum plastic strains in the insert occur at the lid where the geometry has a discontinuity.
- The total creep effect seems to be small during the whole process time and show small variations despite differences in the temperature evolution.
- Comparing obtained results after applying the helium gas pressure with long term results show that the long term results imply the highest stress and strain levels, see e.g. Figures A1-9, A1-10, A1-20 and A1-21. Another observation is that the hydrostatic negative pressure (corresponds to tension) is greater after applying the gas pressure than after long time but the corresponding equivalent creep strain is still low for this case.

References

Andersson-Östling H C M, Sandström R, 2009. Survey of creep properties of copper intended for nuclear waste disposal. SKB TR-09-32, Svensk Kärnbränslehantering AB.

Hökmark H, Lönnqvist M, Fälth B, 2011. THM-issues in repository rock. Thermal, mechanical, thermo-mechanical and hydro-mechanical evolution of the rock at the Forsmark and Laxemar sites. SKB TR-10-23, Svensk Kärnbränslehantering AB.

Jin L-Z, Sandström R, 2008. Creep of copper canisters in power-law breakdown. Computational Materials Science 43, 403–416.

Raiko H, Sandström R, Rydén H, Johansson M, 2010. Design analysis report for the canister. SKB TR-10-28, Svensk Kärnbränslehantering AB.

Sandström R, Andersson H C M, 2008. Creep in phosphorus alloyed copper during power-law breakdown. Journal of Nuclear Materials 372, 76–88.

Sandström R, Hallgren J, Burman G, 2009. Stress strain flow curves for Cu-OFP. SKB R-09-14, Svensk Kärnbränslehantering AB.

SKB, 2010. Design, production and initial state of the canister. SKB TR-10-14, Svensk Kärnbränslehantering AB.

SSABDirekt, 2008. Steelfacts Domex 355 MC. Available at: <http://www.ssabdirect.com>. [19 September 2008].

SS-EN 10025-2:2004. Hot rolled products of structural steels – Part 2: Technical delivery conditions for non-alloy structural steels. Stockholm: Swedish Standards Institute.

Unpublished documents

| SKBdoc id, version | Title | Issuer, year |
|--------------------|---|--------------|
| 1201865 ver 1.0 | Dragprovning av gjutjärn. (In Swedish.) | KTH, 2009 |
| 1203875 ver 1.0 | Ritningsförteckning för kapselkomponenter. (In Swedish.) | SKB, 2009 |
| 1333208 ver 2.0 | Inre övertryck i kapseln. (In Swedish.) | SKB, 2012 |
| 1333256 ver 2.0 | Svar på begäran om kompletteringar angående kapselfrågor. (In Swedish.) | SKB, 2012 |

Appendix 1 – Isostat_JLH_creep_red_dim

Plots showing temperature and pressure contours and history.

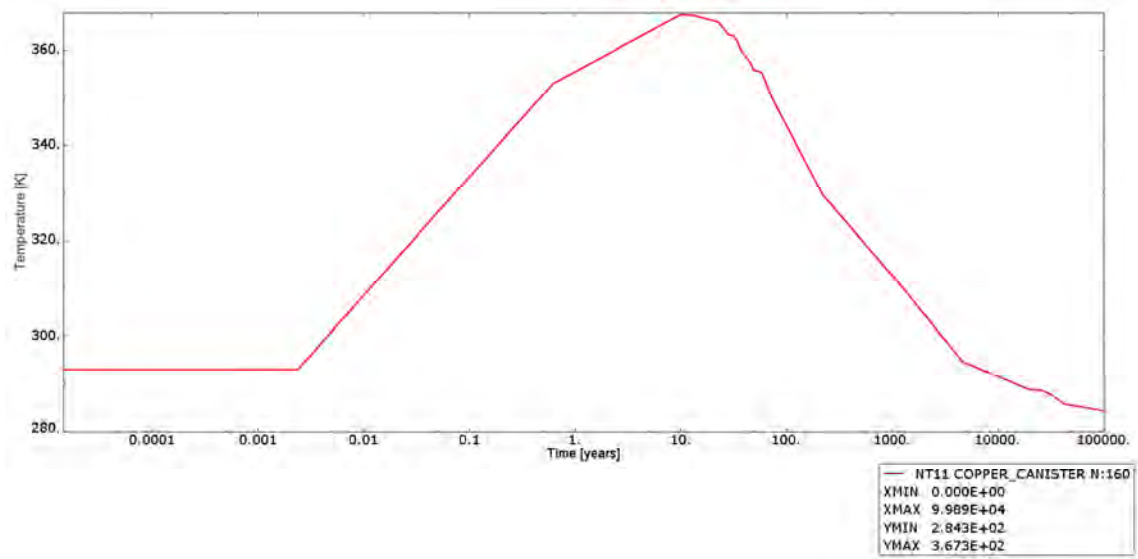


Figure A1-1. Plot showing temperature history. Time is in years, temperature is in Kelvin.

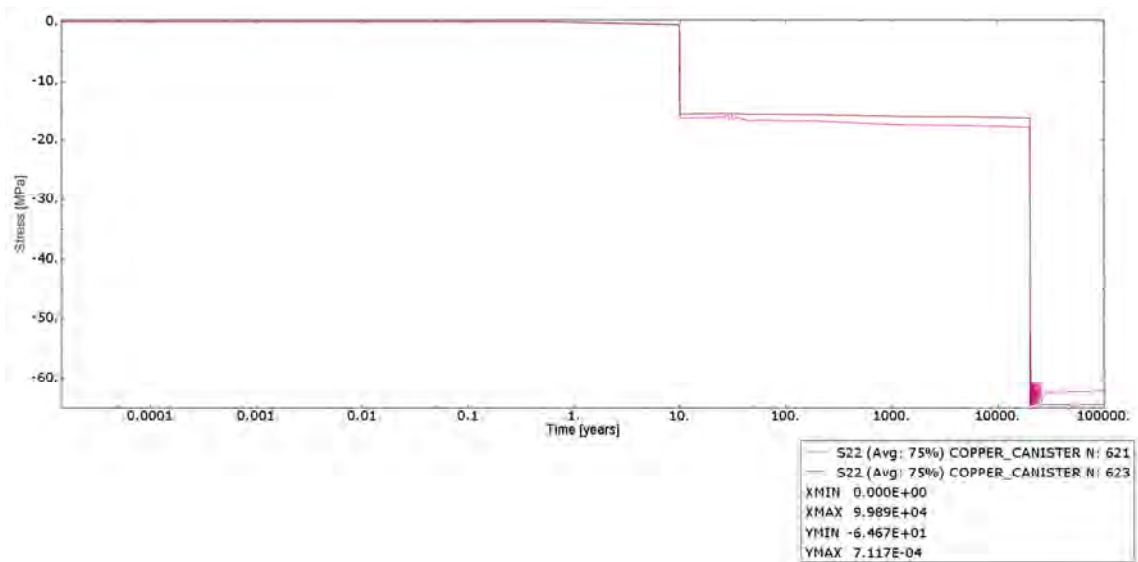


Figure A1-2. Plot showing applied pressure at the top lid of the copper shell. Time is in years and stress is in MPa.

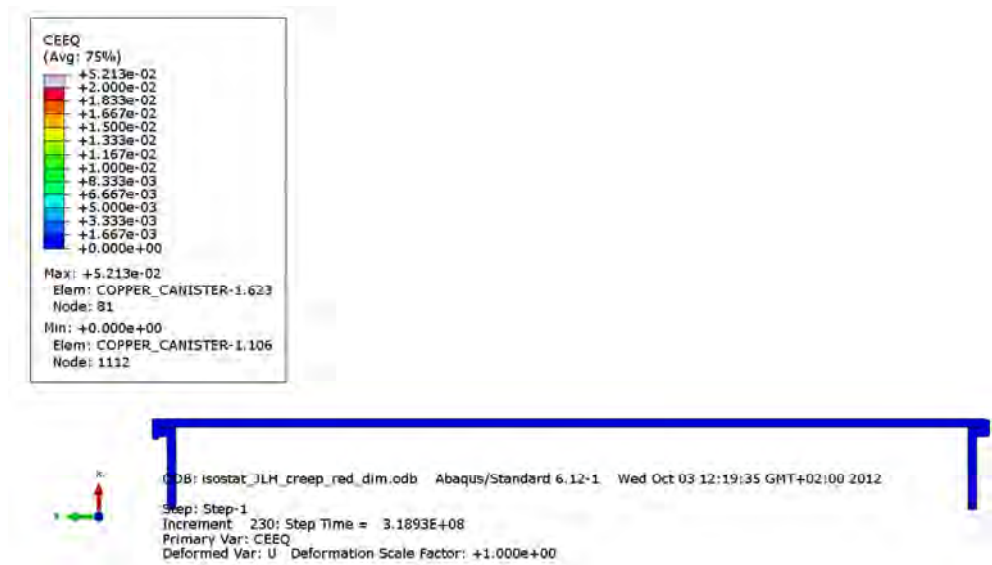


Figure A1-3. Plot showing equivalent creep strain after 10 years. Gas pressure is applied.



Figure A1-4. Plot showing equivalent creep strain after 100,000 years.

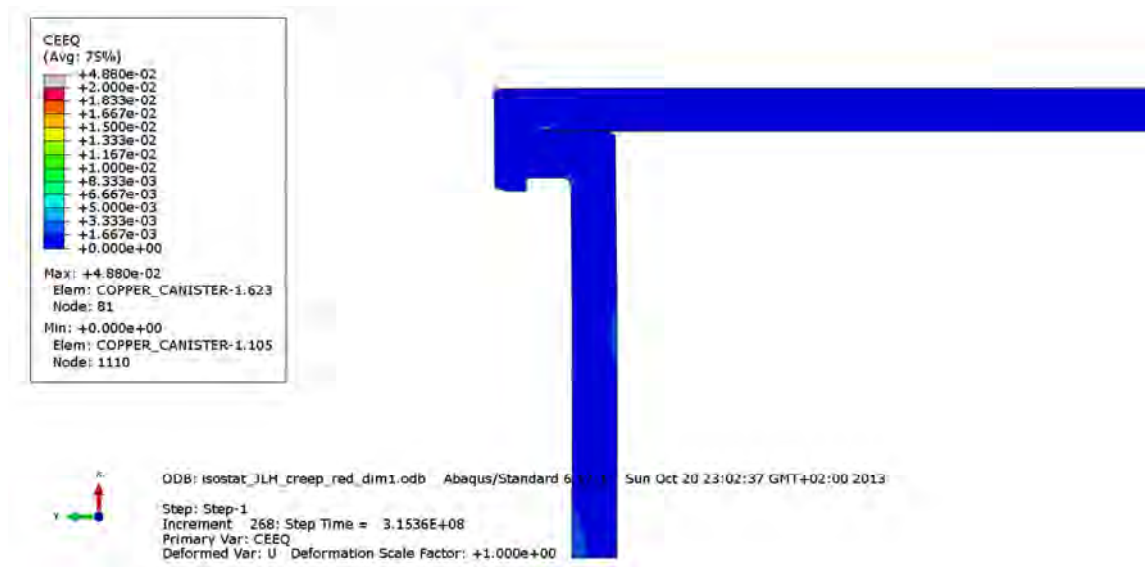


Figure A1-5. Plot showing equivalent creep strain at the top weld of the copper shell after 10 years. Gas pressure is applied.

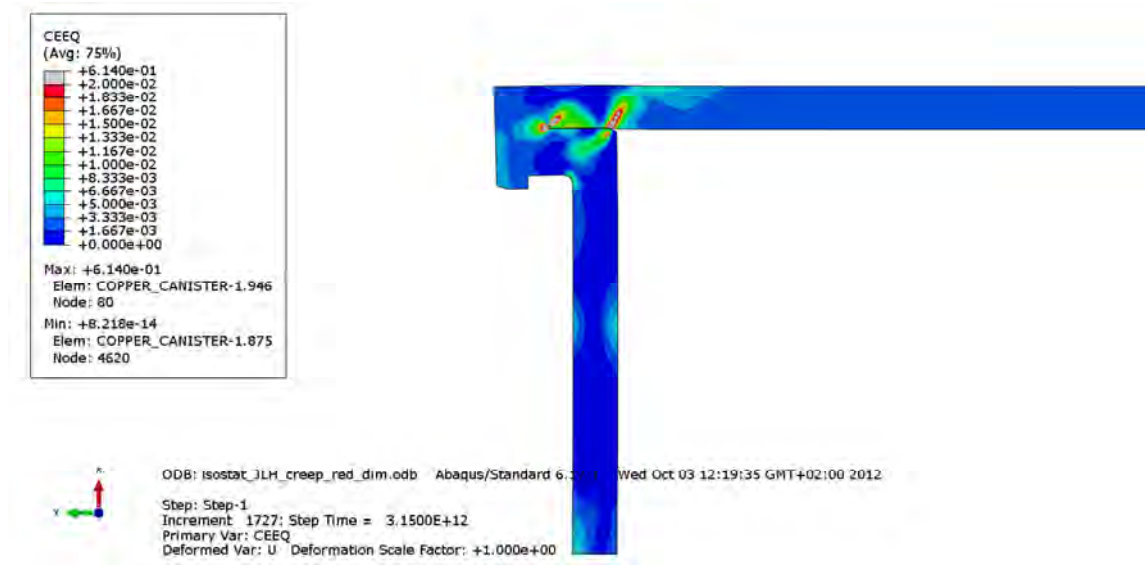


Figure A1-6. Plot showing equivalent creep strain at the top weld of the copper shell after 100,000 years.

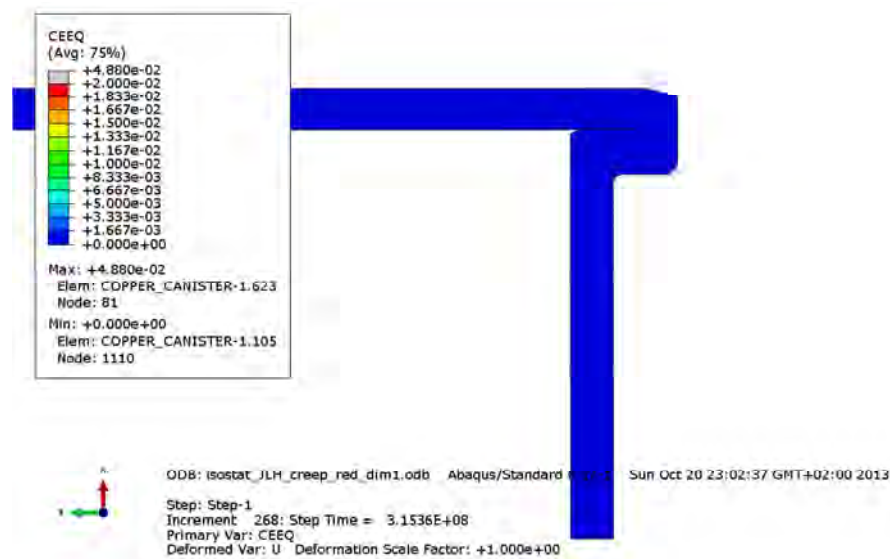


Figure A1-7. Plot showing equivalent creep strain at the bottom weld of the copper shell after 10 years. Gas pressure is applied.

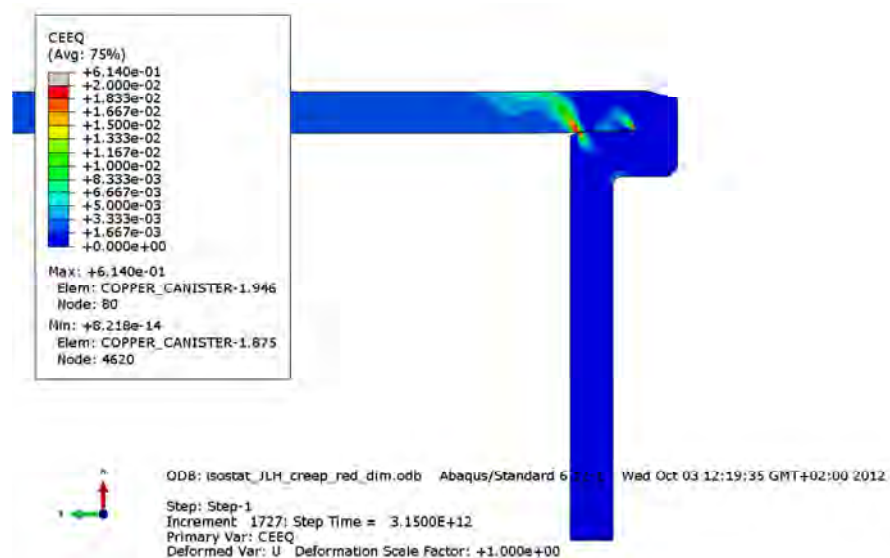


Figure A1-8. Plot showing equivalent creep strain at the bottom weld of the copper shell after 100,000 years.

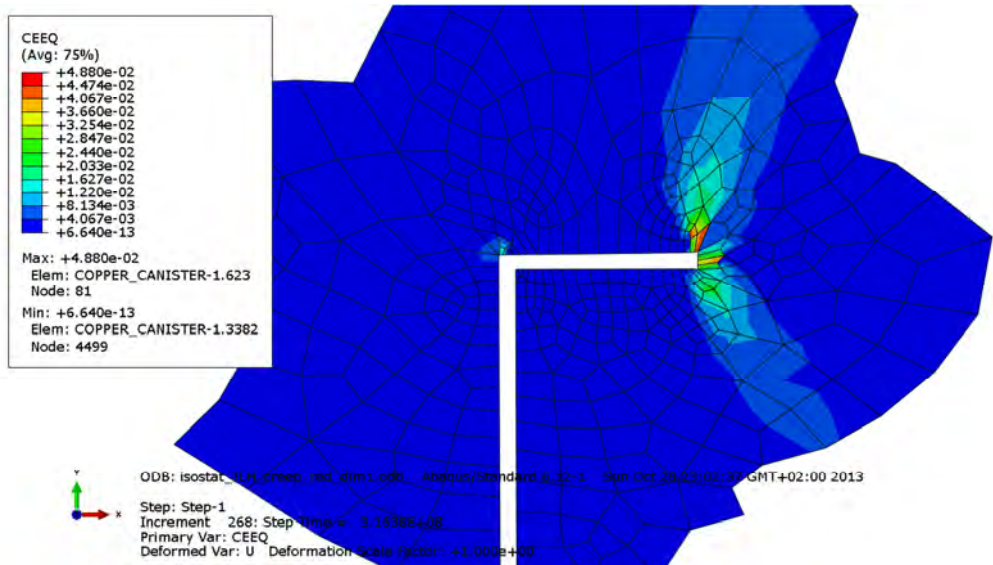


Figure A1-9. Plot showing equivalent creep strain at the copper shell top weld after 10 years. Gas pressure is applied.

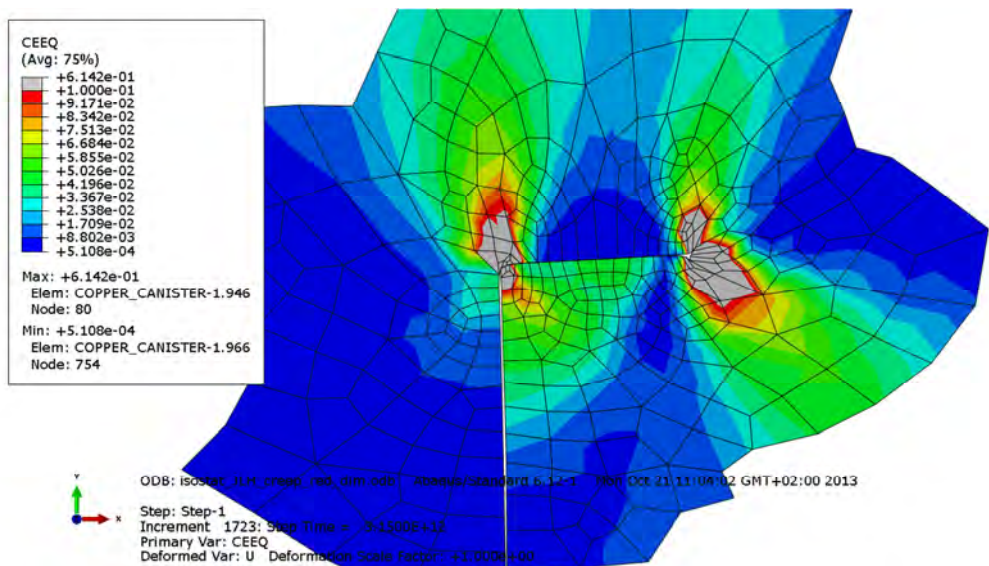


Figure A1-10. Plot showing equivalent creep strain at the copper shell top weld after 100,000 years.

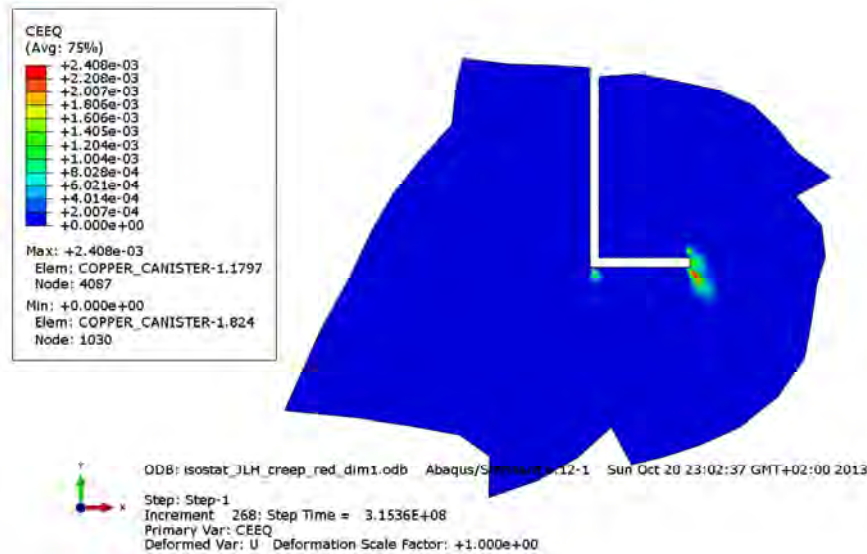


Figure A1-11. Plot showing equivalent creep strain at the copper shell bottom weld after 10 years. Gas pressure is applied.

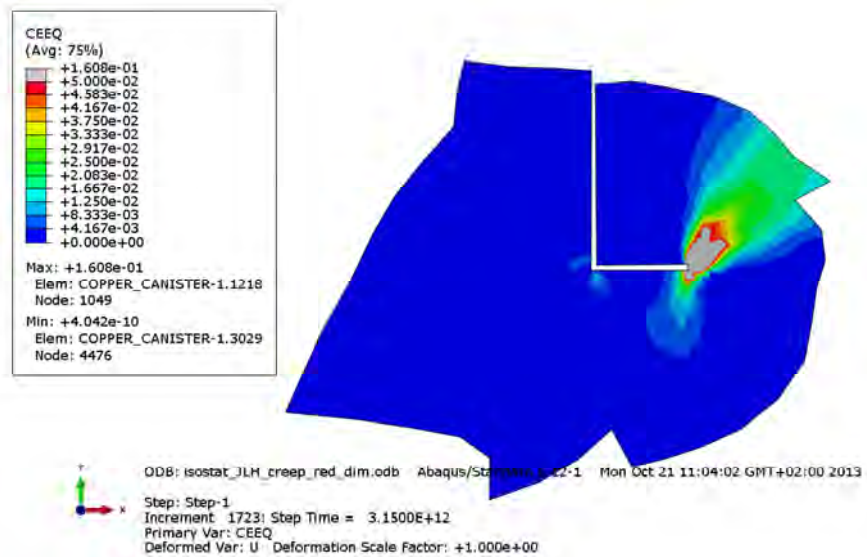


Figure A1-12. Plot showing equivalent creep strain at the copper shell bottom weld after 100,000 years.

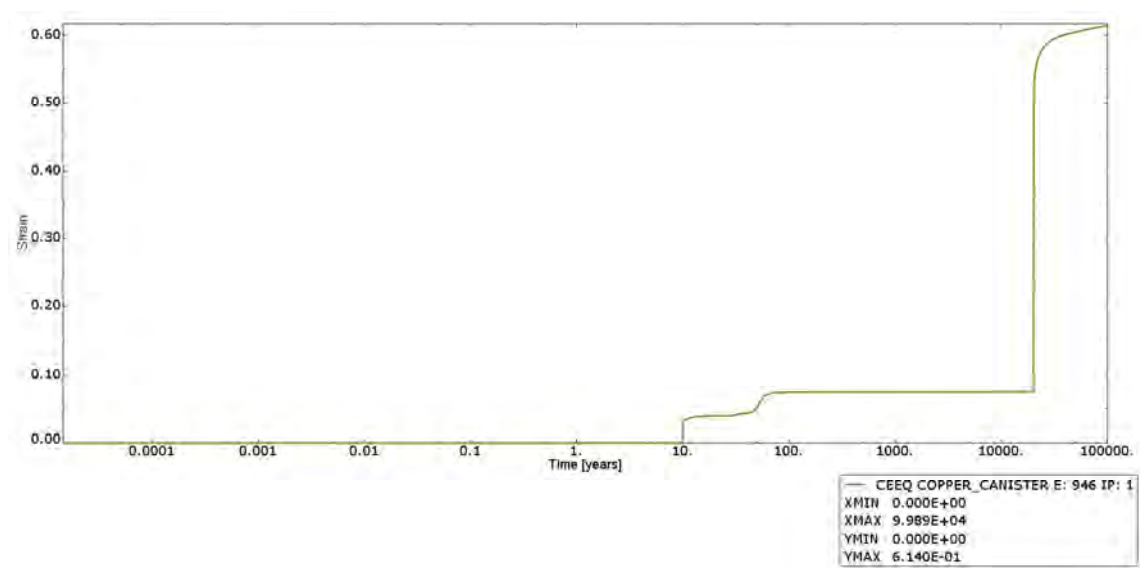


Figure A1-13. Plot showing history of equivalent creep strain in the element having the maximum magnitude. Time is in years and strain is dimensionless.

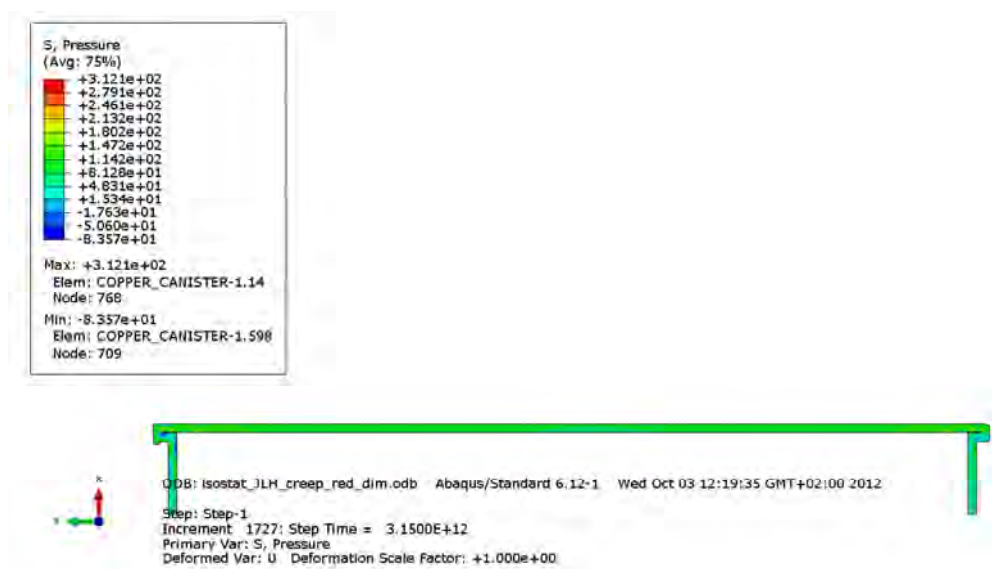


Figure A1-14. Plot showing pressure stress in the copper shell after 10 years. Gas pressure is applied.



Figure A1-15. Plot showing pressure stress in the copper shell after 100,000 years.

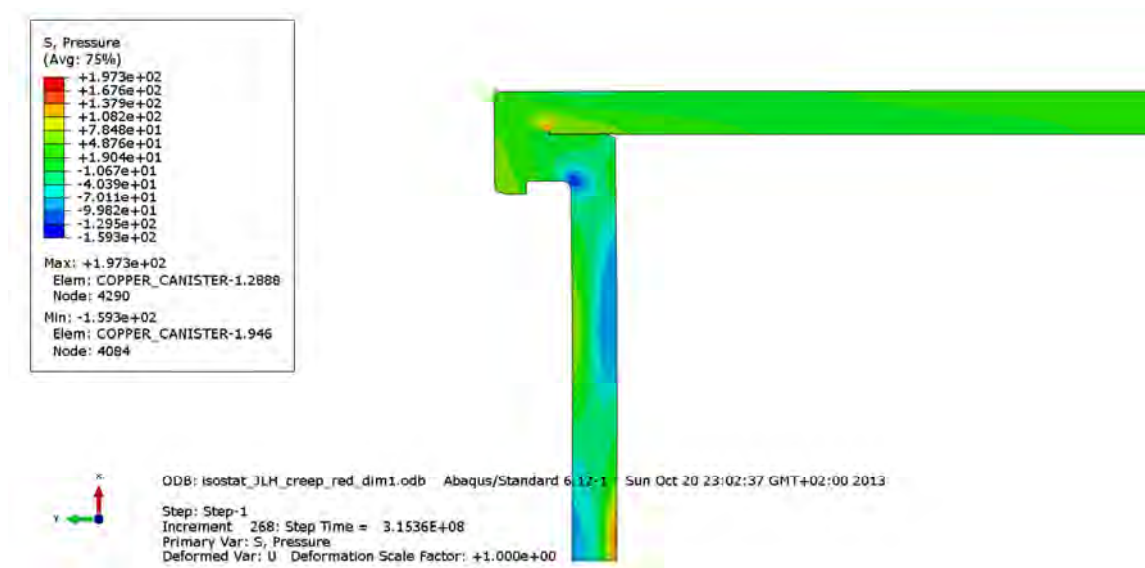


Figure A1-16. Plot showing pressure stress at the copper shell top weld after 10 years. Gas pressure is applied.

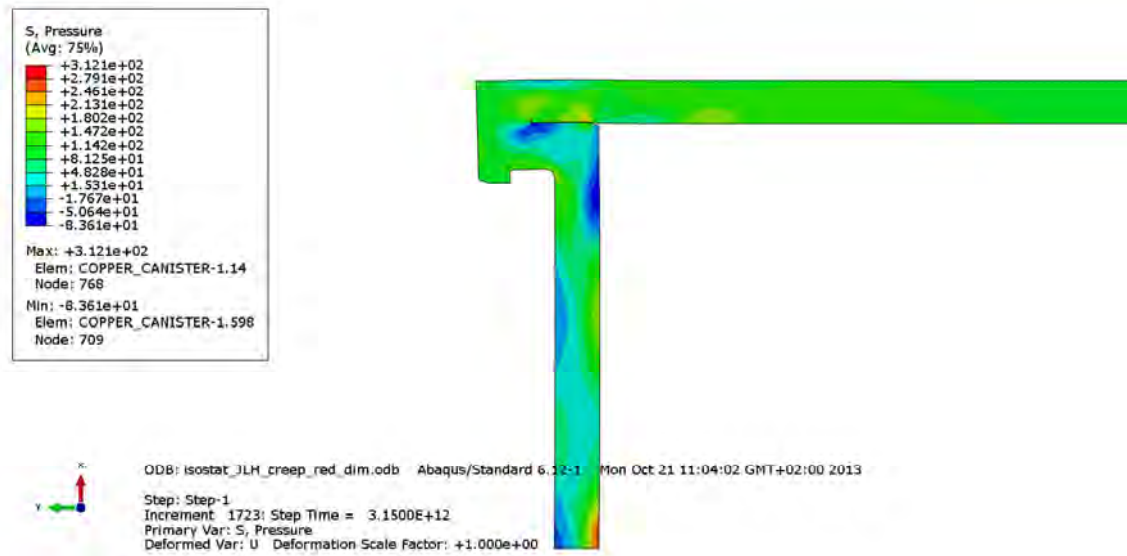


Figure A1-17. Plot showing pressure stress at the copper shell top weld after 100,000 years.

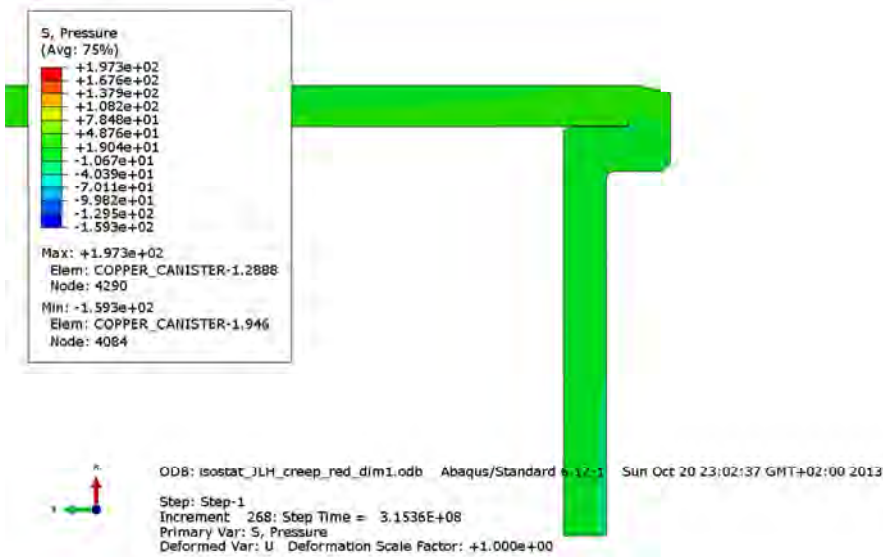


Figure A1-18. Plot showing pressure stress at the copper shell bottom weld after 10 years. Gas pressure is applied.

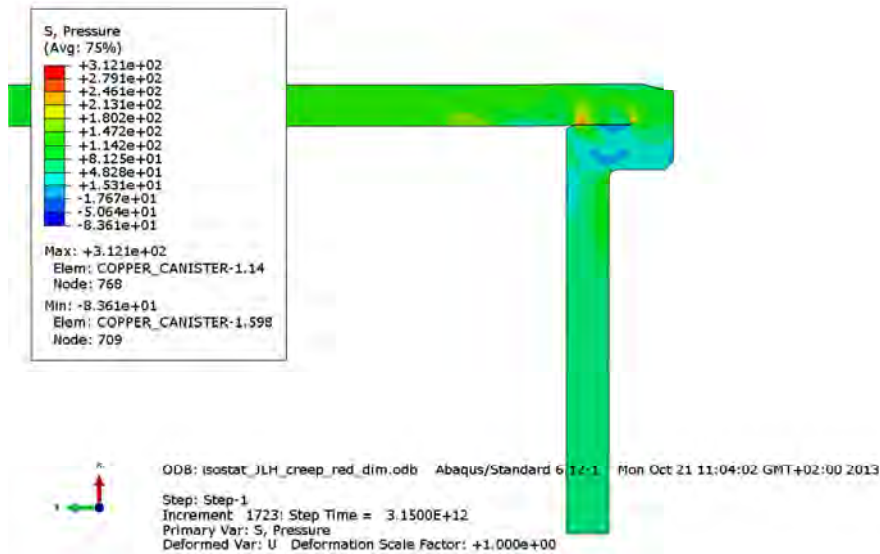


Figure A1-19. Plot showing pressure stress at the copper shell bottom weld after 100,000 years.

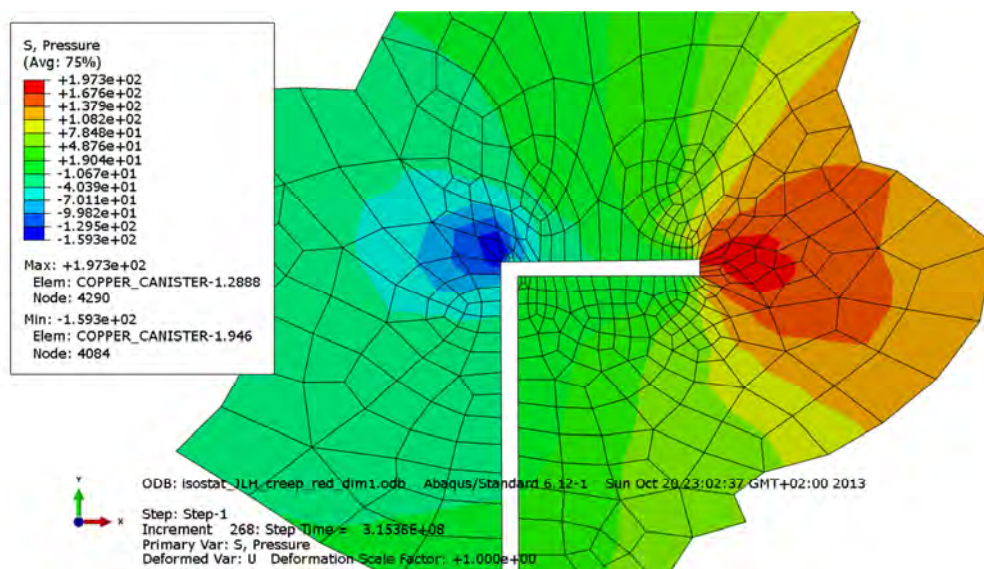


Figure A1-20. Plot showing pressure stress at the copper shell top weld after 10 years. Gas pressure is applied.

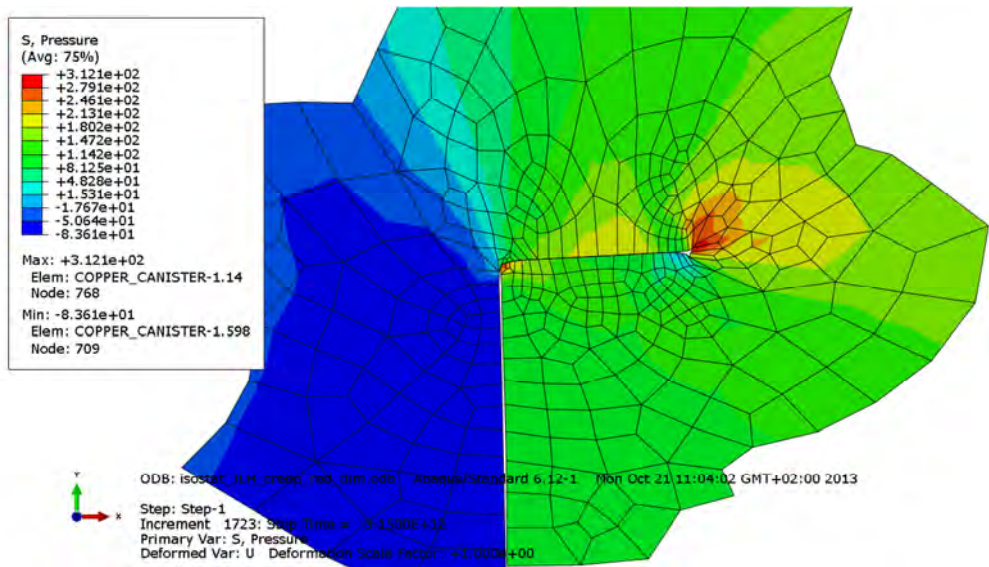


Figure A1-21. Plot showing pressure stress at the copper shell top weld after 10,000 years.

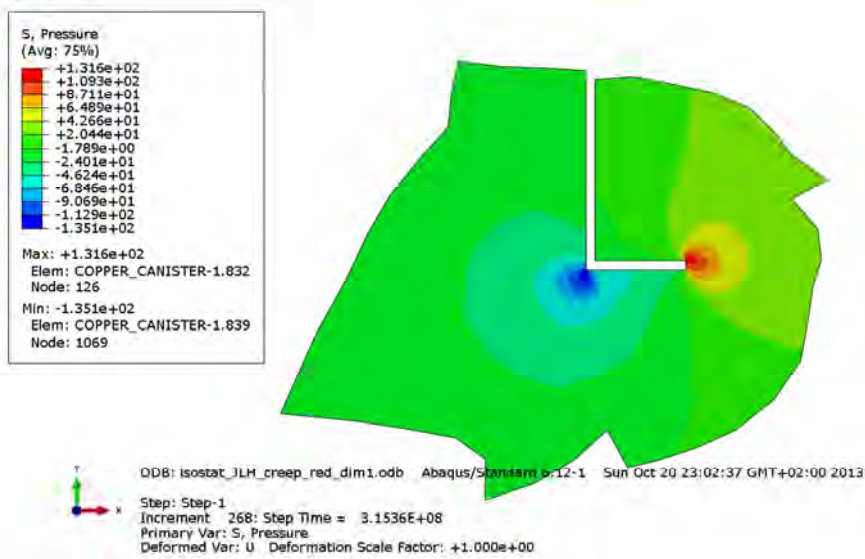


Figure A1-22. Plot showing pressure stress at the copper shell bottom weld after 10 years. Gas pressure is applied.

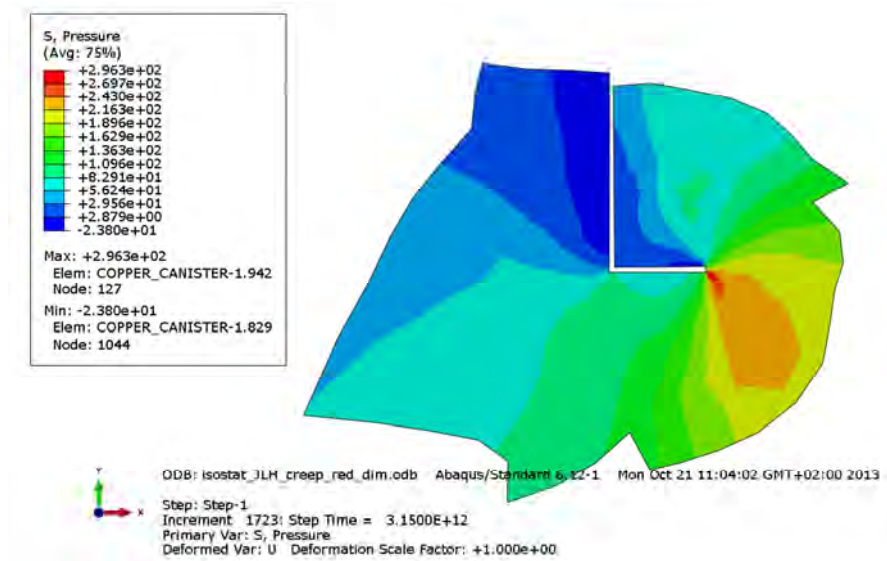


Figure A1-23. Plot showing pressure stress at the copper shell bottom weld after 100,000 years.

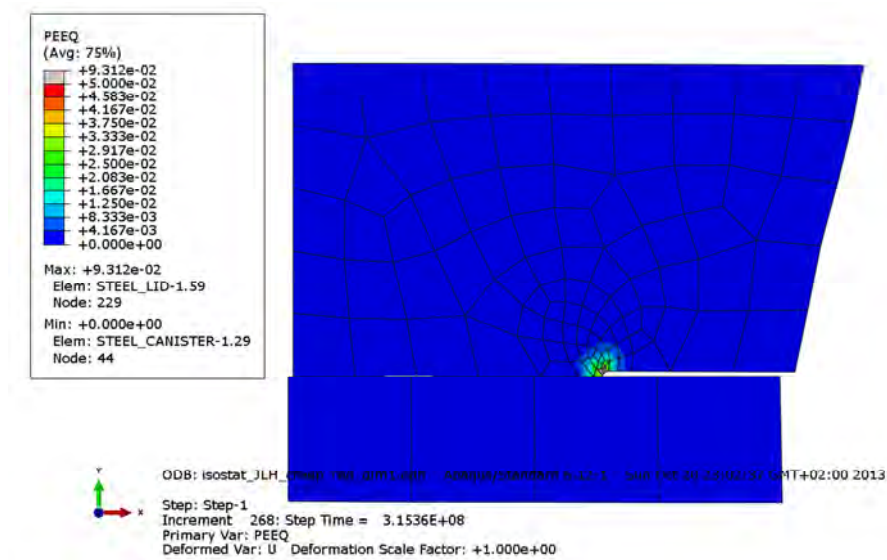


Figure A1-24. Plot showing equivalent plastic strain at the steel lid after 10 years; see also Figure 4-3 for explanation of the details. Gas pressure is applied.

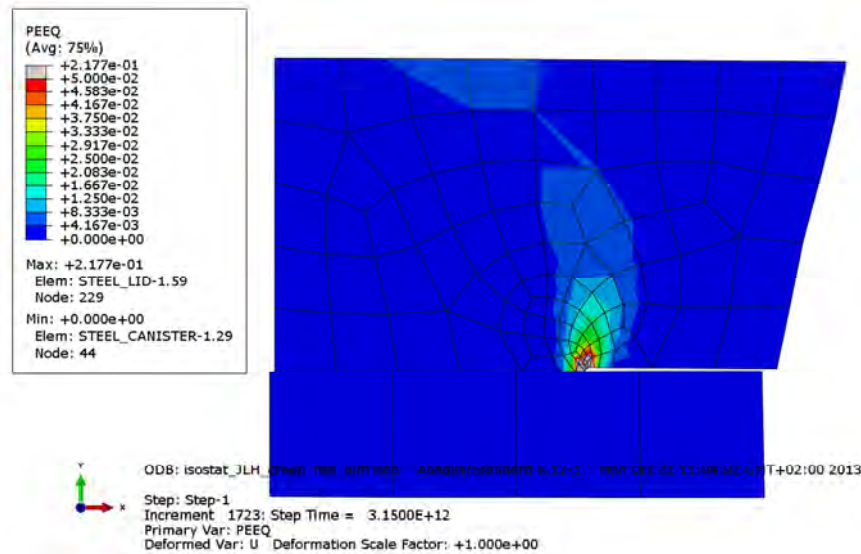


Figure A1-25. Plot showing equivalent plastic strain at the steel lid after 100,000 years; see also Figure 4-3 for explanation of the details.

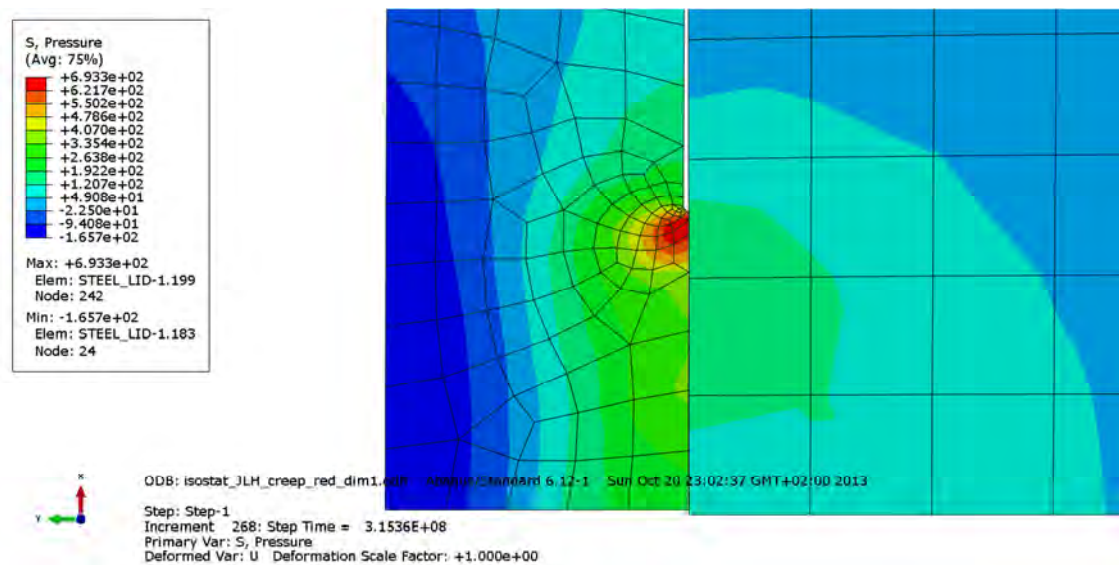


Figure A1-26. Plot showing pressure stress at the discontinuity of the insert after 10 years. Gas pressure is applied.

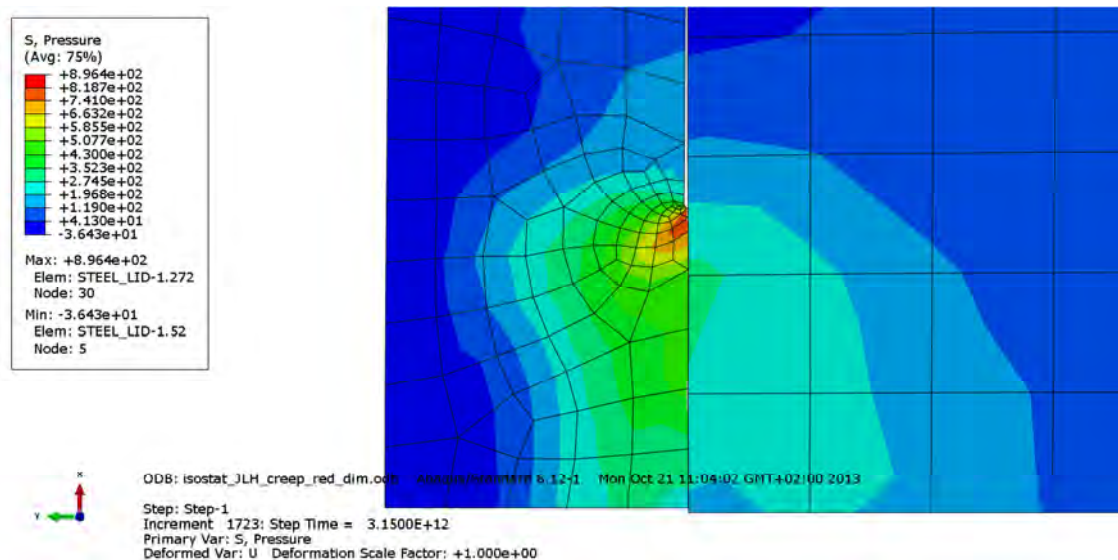


Figure A1-27. Plot showing pressure stress at the discontinuity of the insert after 100,000 years.

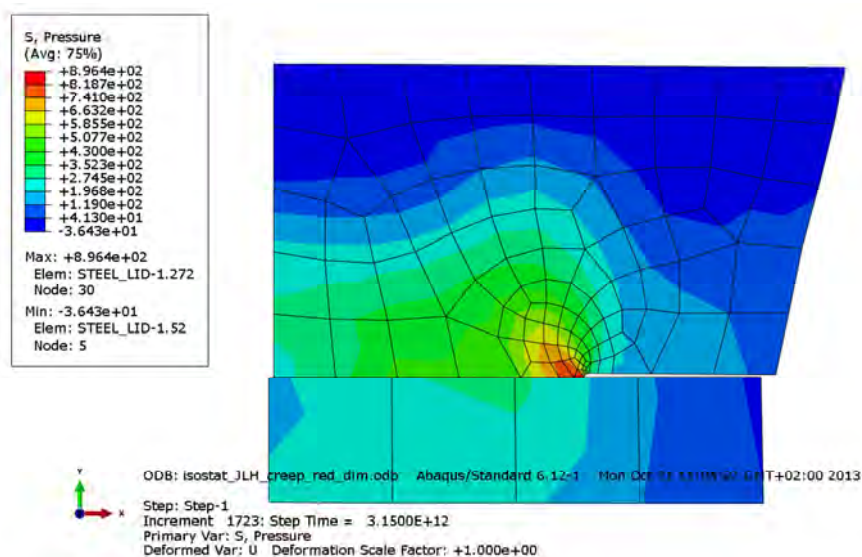


Figure A1-28. Plot showing pressure stress at the steel lid after 100,000 years; see also Figure 4-3 for explanation of the details.

Appendix 2 – Isostat_JLH_creep_red_mean

Plots showing temperature and pressure contours and history.

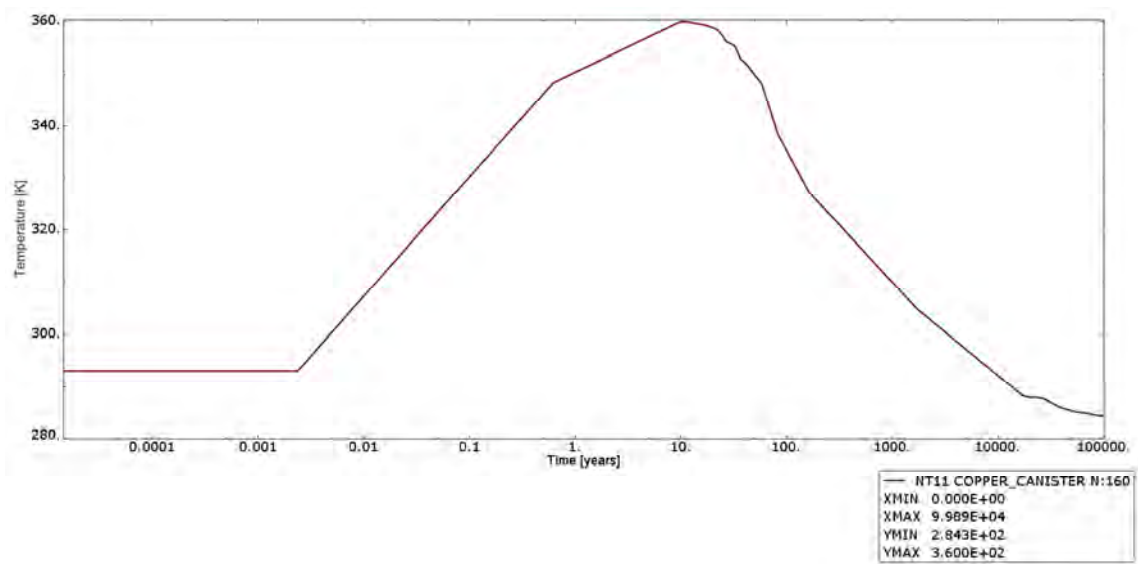


Figure A2-1. Plot showing temperature history. Time is in years, temperature is in Kelvin.

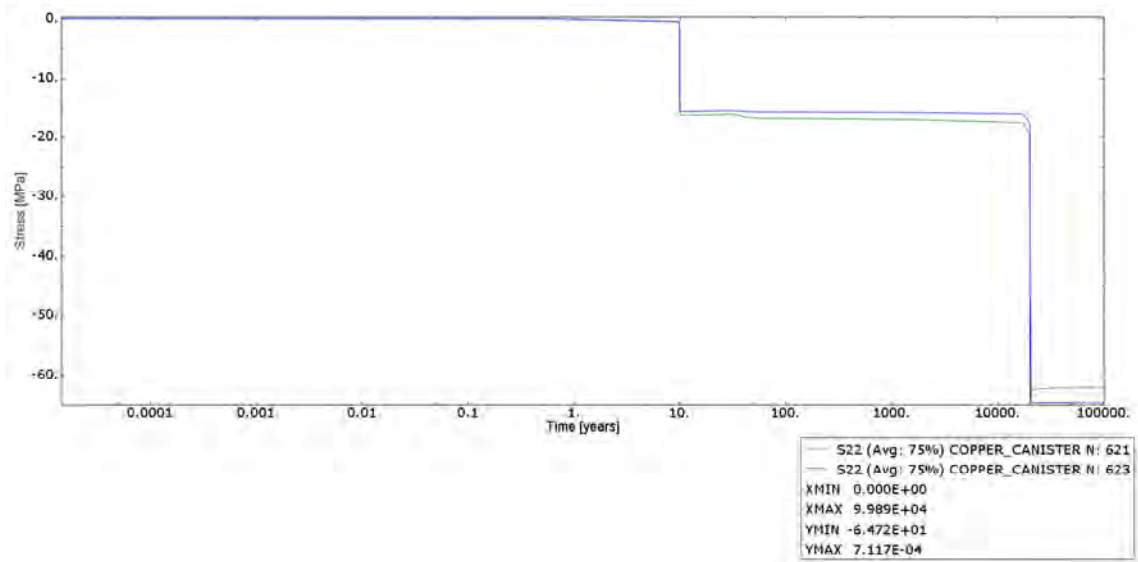


Figure A2-2. Plot showing applied pressure at the top lid of the copper shell. Time is in years and stress is in MPa.

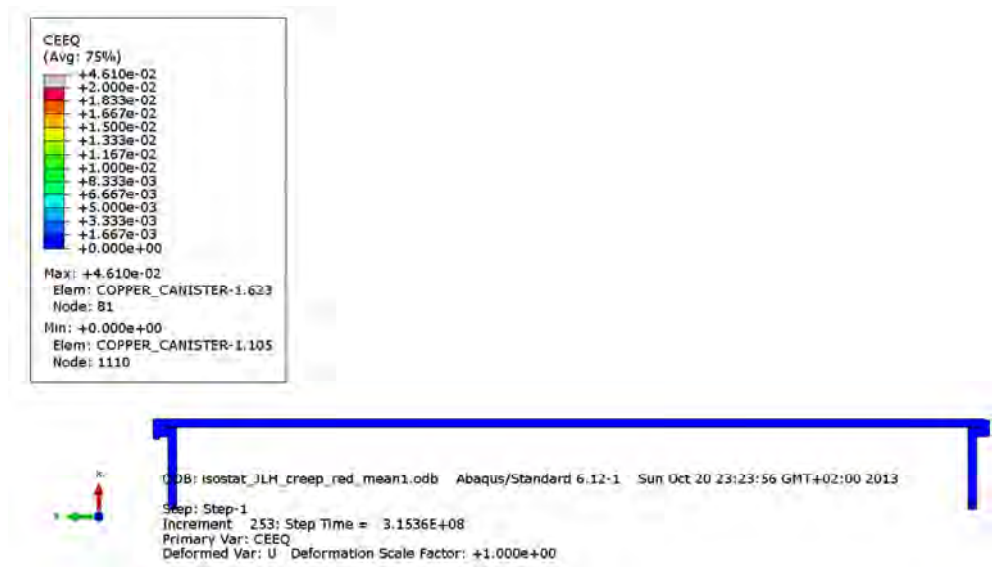


Figure A2-3. Plot showing equivalent creep strain after 10 years. Gas pressure is applied.

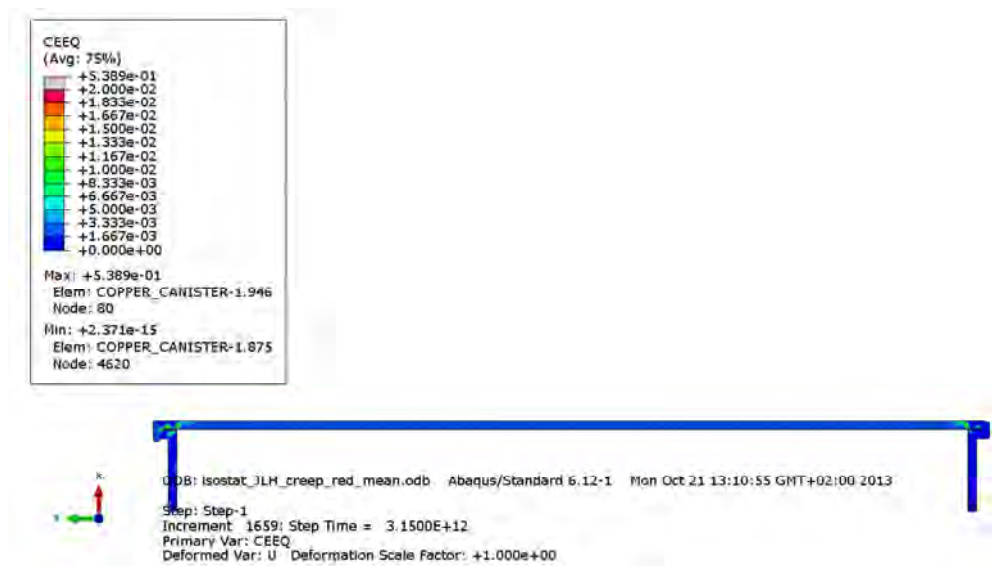


Figure A2-4. Plot showing equivalent creep strain after 100,000 years.

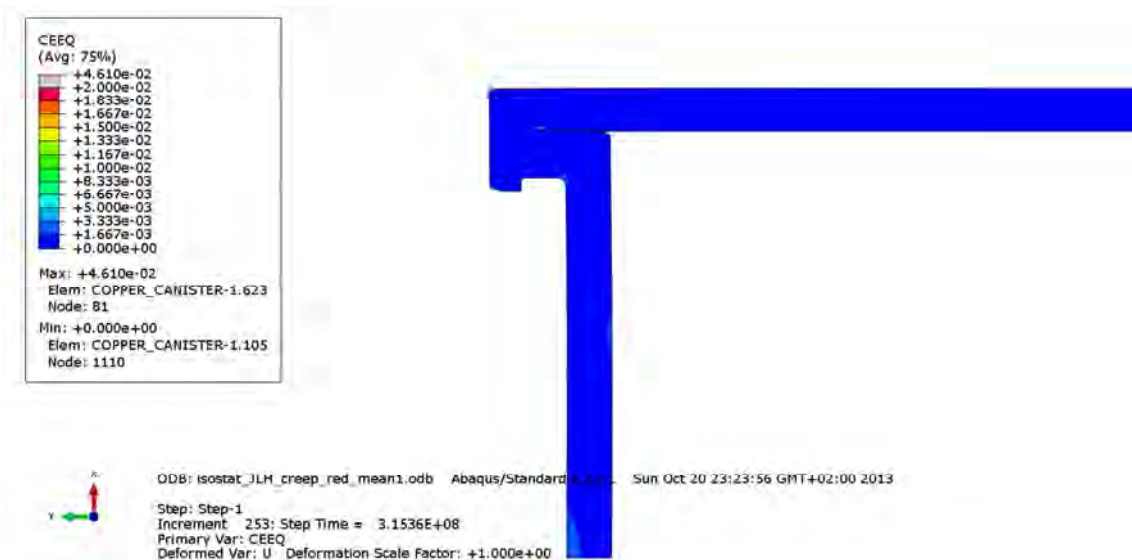


Figure A2-5. Plot showing equivalent creep strain at the top weld of the copper shell after 10 years. Gas pressure is applied.

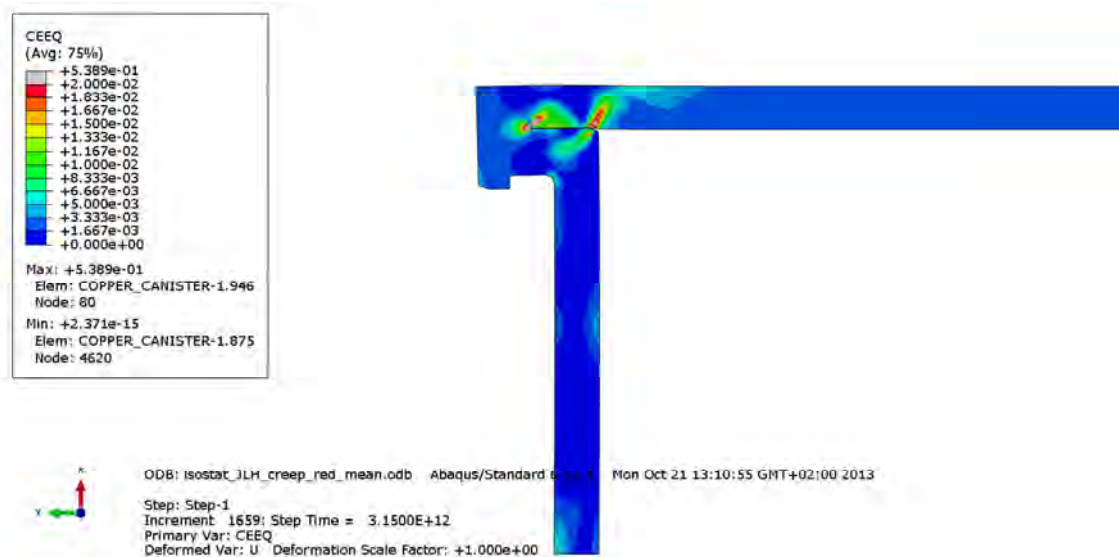


Figure A2-6. Plot showing equivalent creep strain at the top weld of the copper shell after 100,000 years.

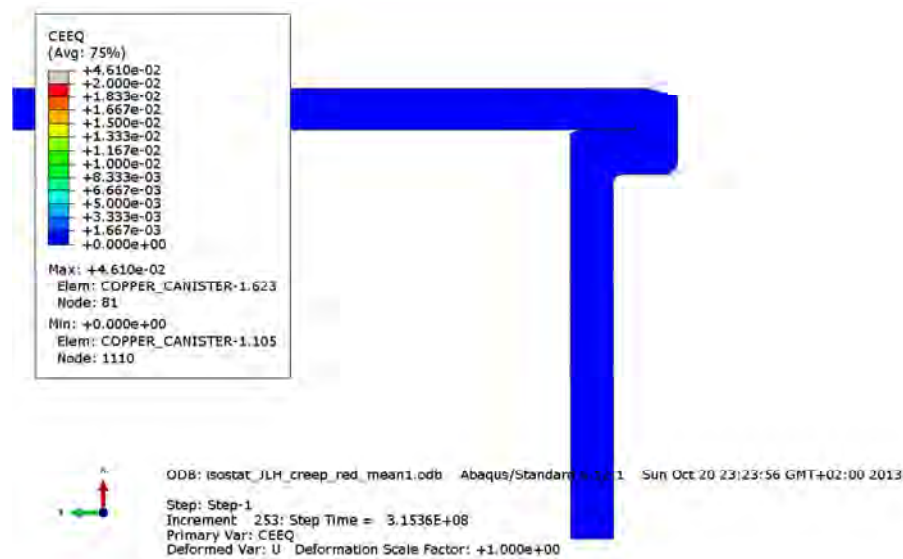


Figure A2-7. Plot showing equivalent creep strain at the bottom weld of the copper shell after 10 years. Gas pressure is applied.

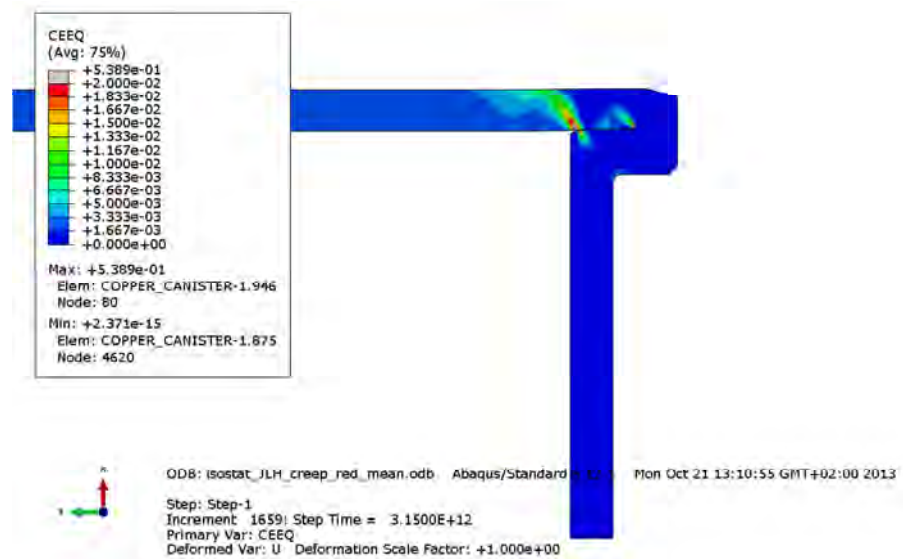


Figure A2-8. Plot showing equivalent creep strain at the bottom weld of the copper shell after 100,000 years.

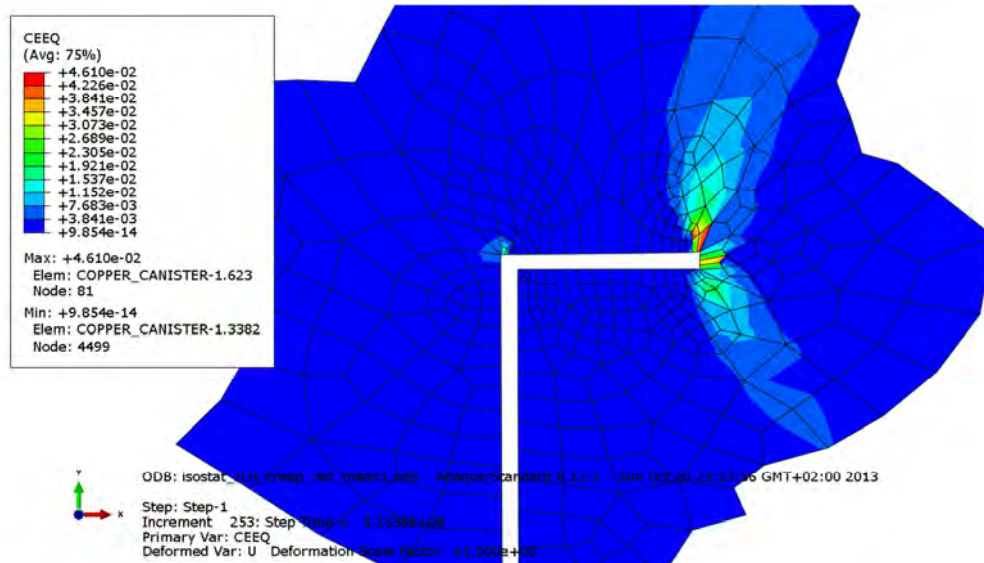


Figure A2-9. Plot showing equivalent creep strain at the copper shell top weld after 10 years. Gas pressure is applied.

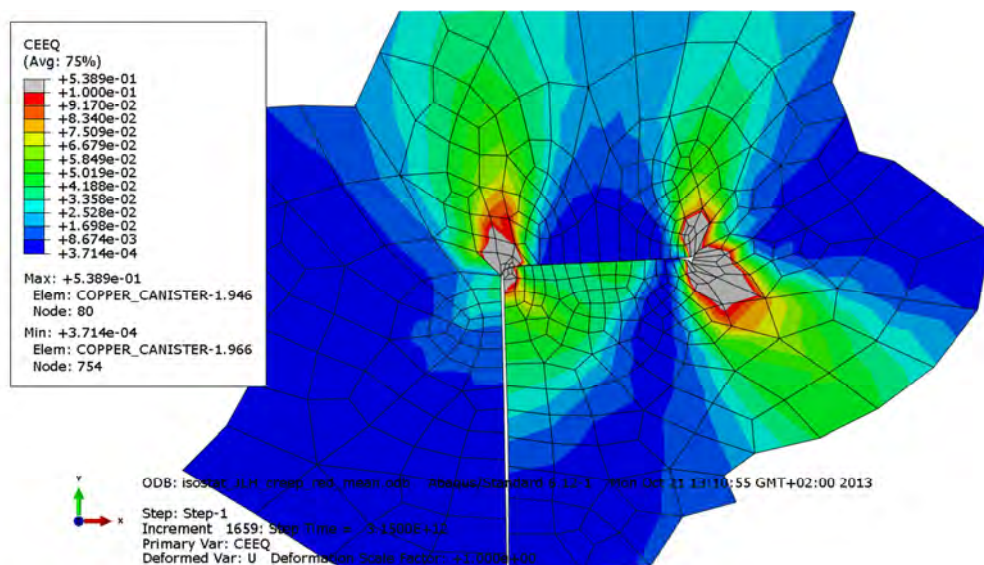


Figure A2-10. Plot showing equivalent creep strain at the copper shell top weld after 100,000 years.

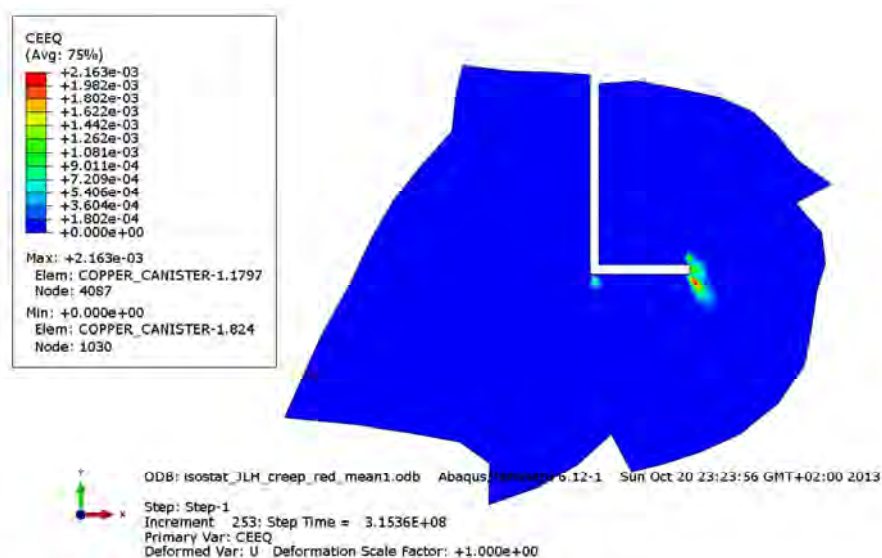


Figure A2-11. Plot showing equivalent creep strain at the copper shell bottom weld after 10 years. Gas pressure is applied.

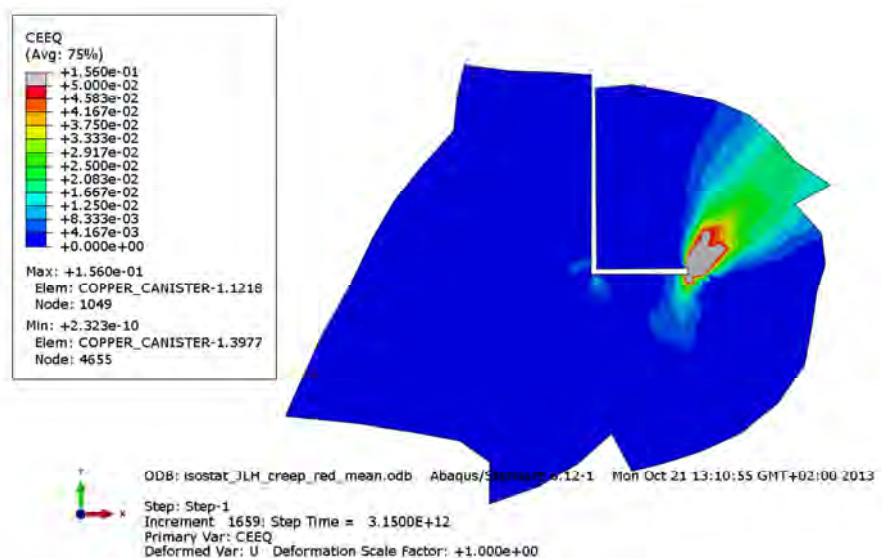


Figure A2-12. Plot showing equivalent creep strain at the copper shell bottom weld after 100,000 years.

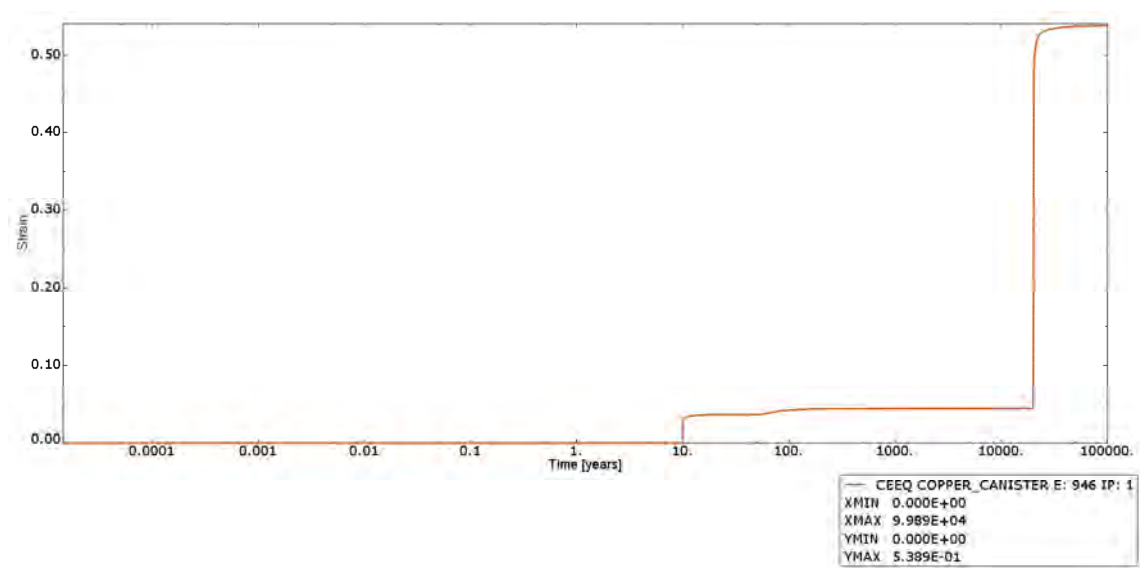


Figure A2-13. Plot showing history of equivalent creep strain in the element having the maximum magnitude. Time is in years and strain is dimensionless.

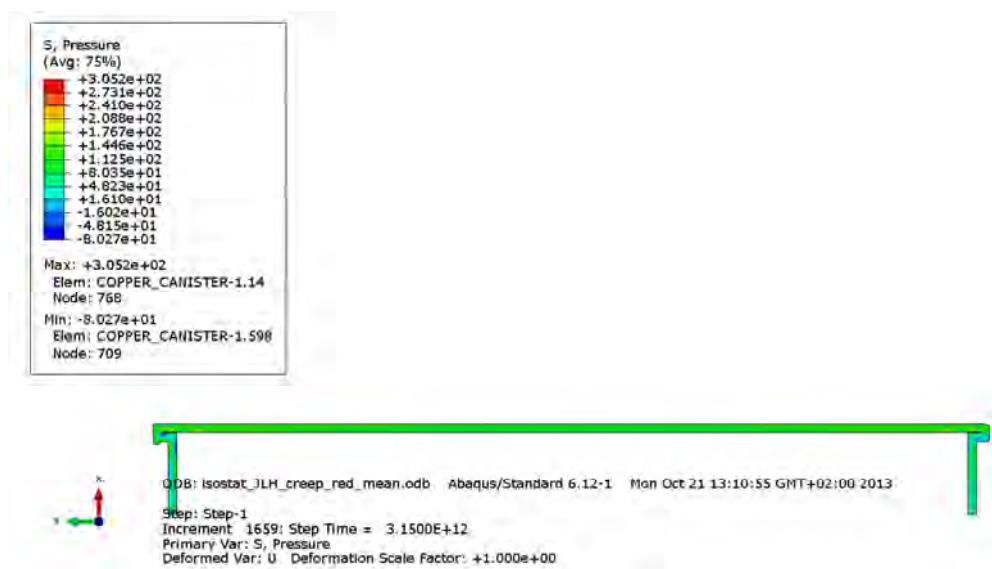


Figure A2-14. Plot showing pressure stress in the copper shell after 10 years. Gas pressure is applied.

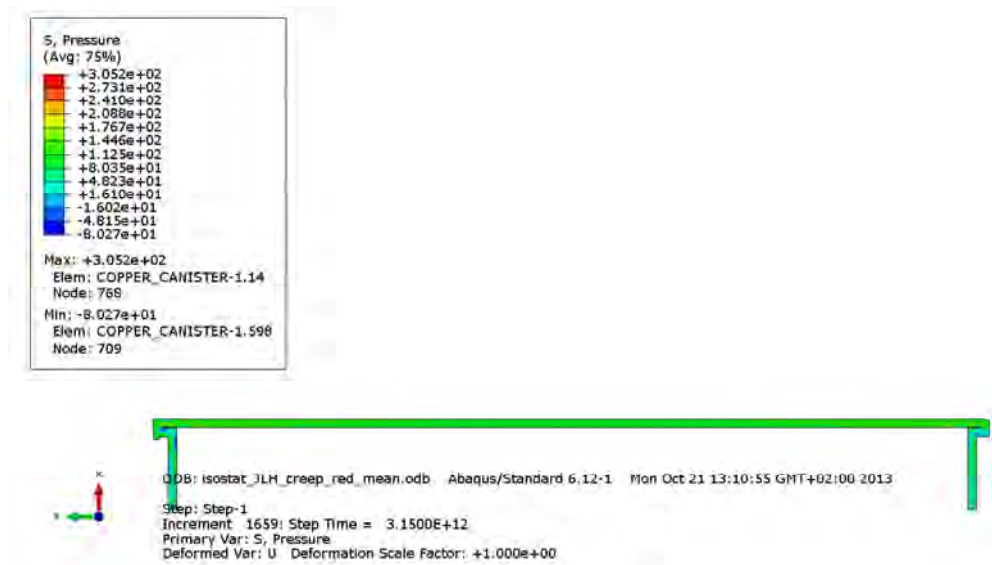


Figure A2-15. Plot showing pressure stress in the copper shell after 100,000 years.

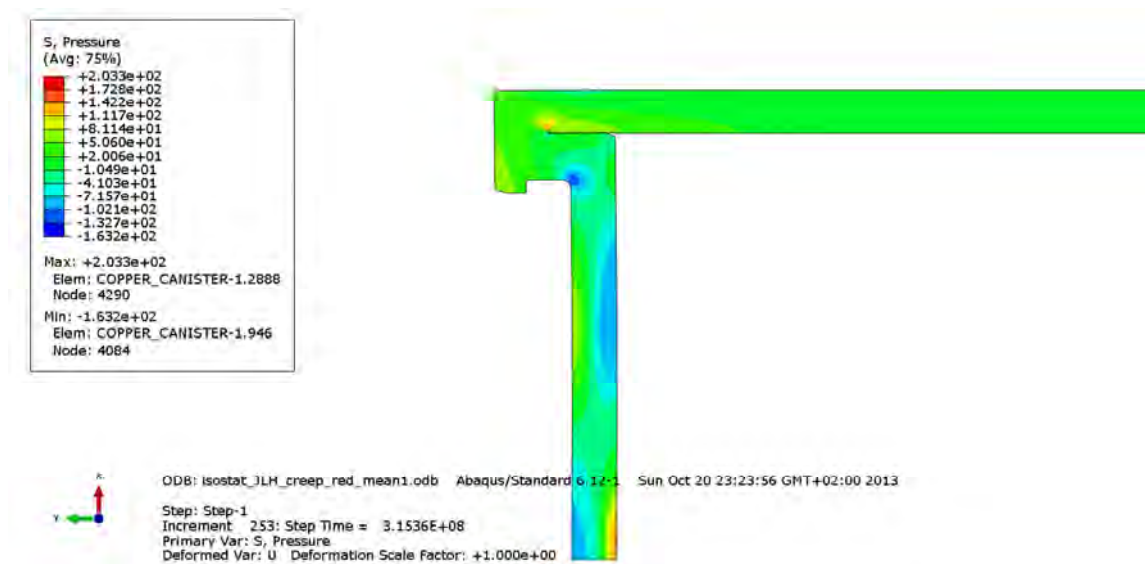


Figure A2-16. Plot showing pressure stress at the copper shell top weld after 10 years. Gas pressure is applied.

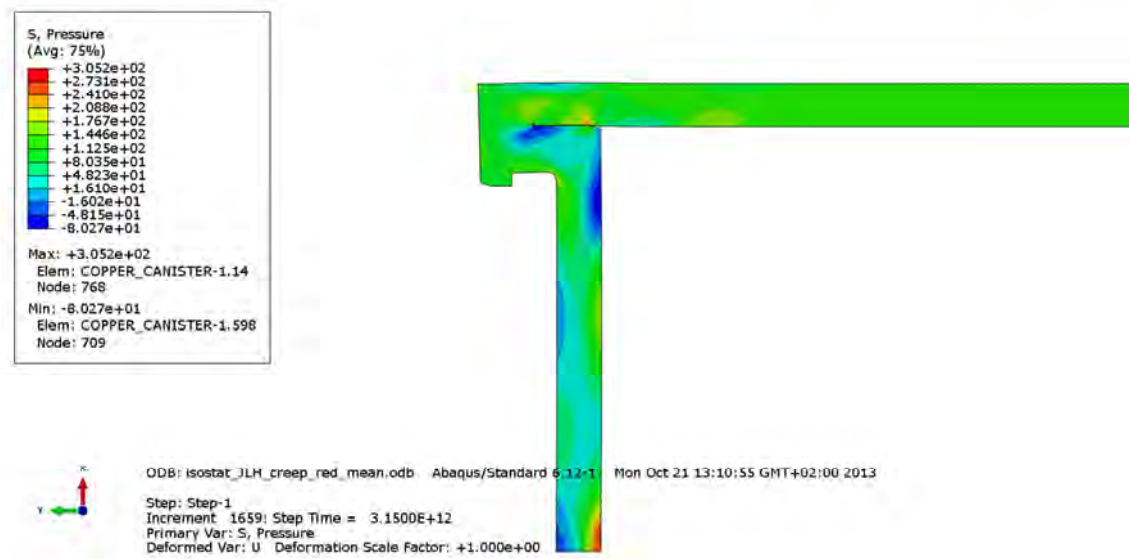


Figure A2-17. Plot showing pressure stress at the copper shell top weld after 100,000 years.

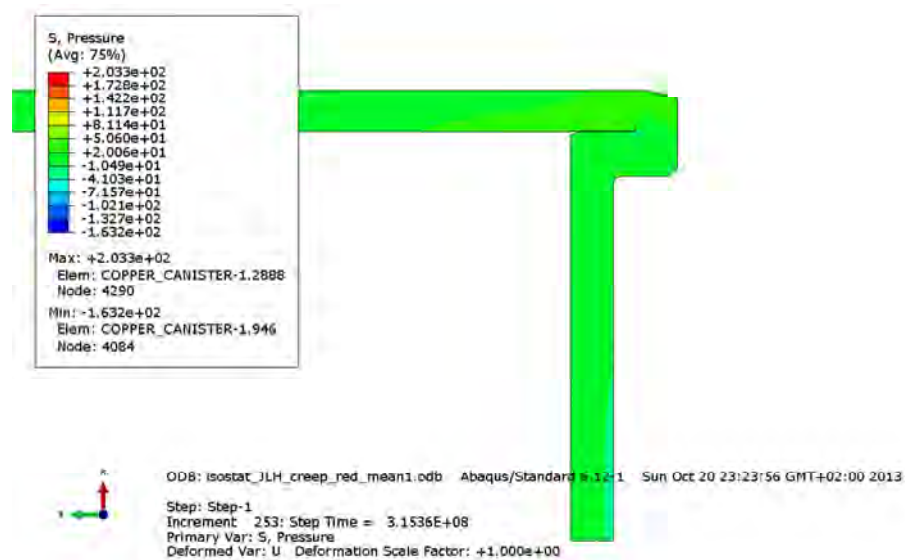


Figure A2-18. Plot showing pressure stress at the copper shell bottom weld after 10 years. Gas pressure is applied.

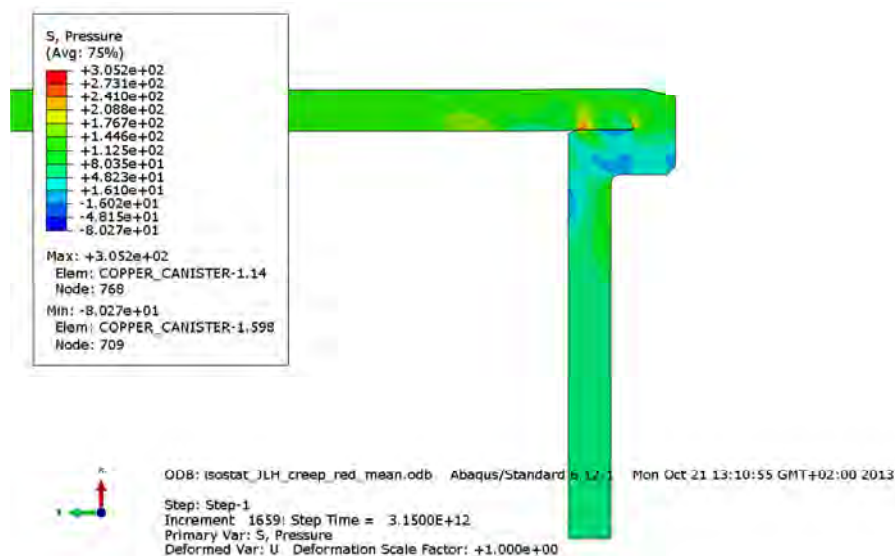


Figure A2-19. Plot showing pressure stress at the copper shell bottom weld after 100,000 years.

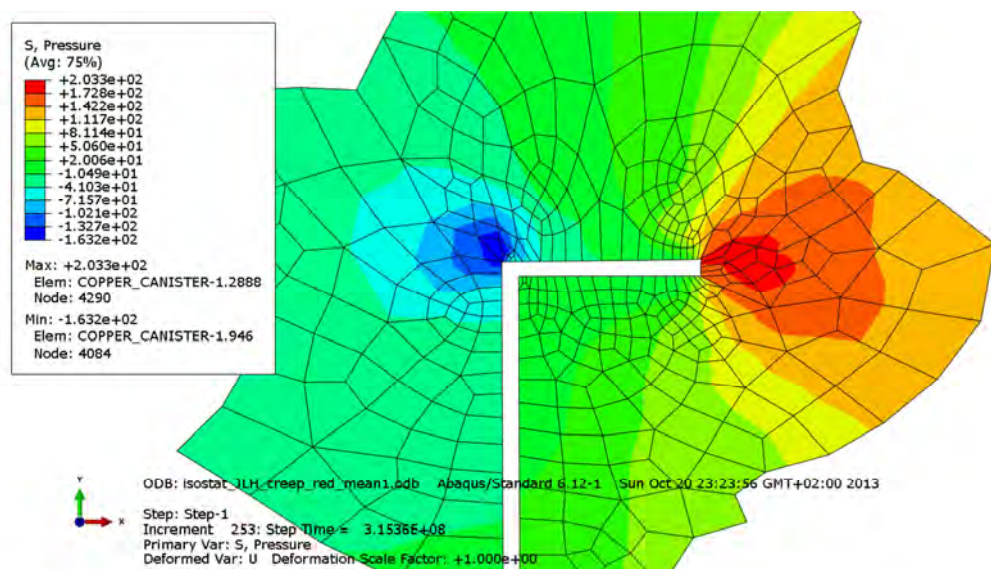


Figure A2-20. Plot showing pressure stress at the copper shell top weld after 10 years. Gas pressure is applied.

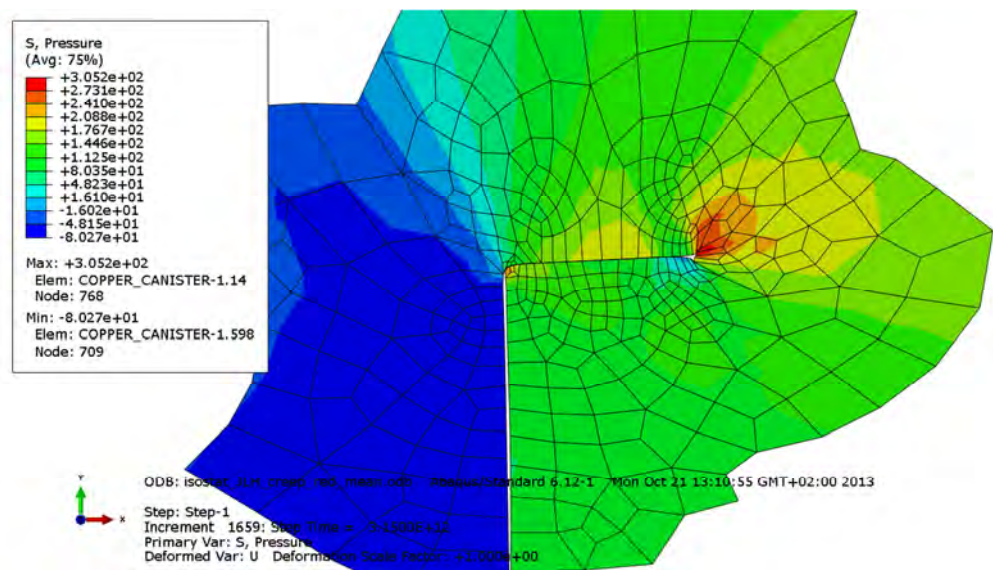


Figure A2-21. Plot showing pressure stress at the copper shell top weld after 10,000 years.

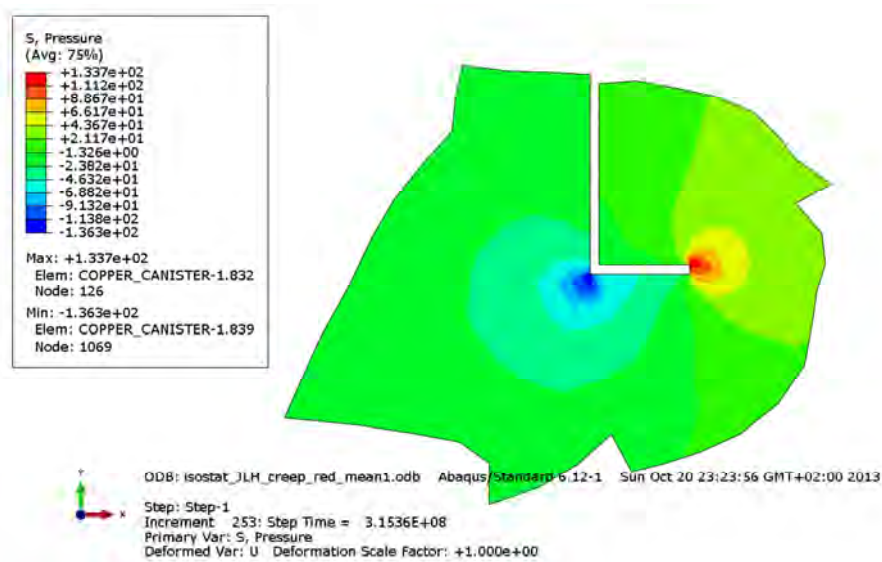


Figure A2-22. Plot showing pressure stress at the copper shell bottom weld after 10 years. Gas pressure is applied.

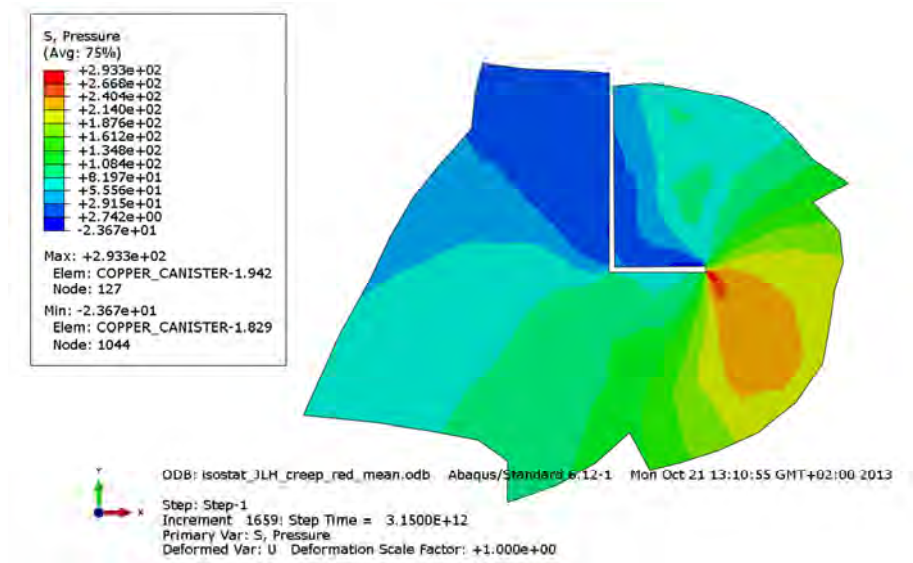


Figure A2-23. Plot showing pressure stress at the copper shell bottom weld after 100,000 years.

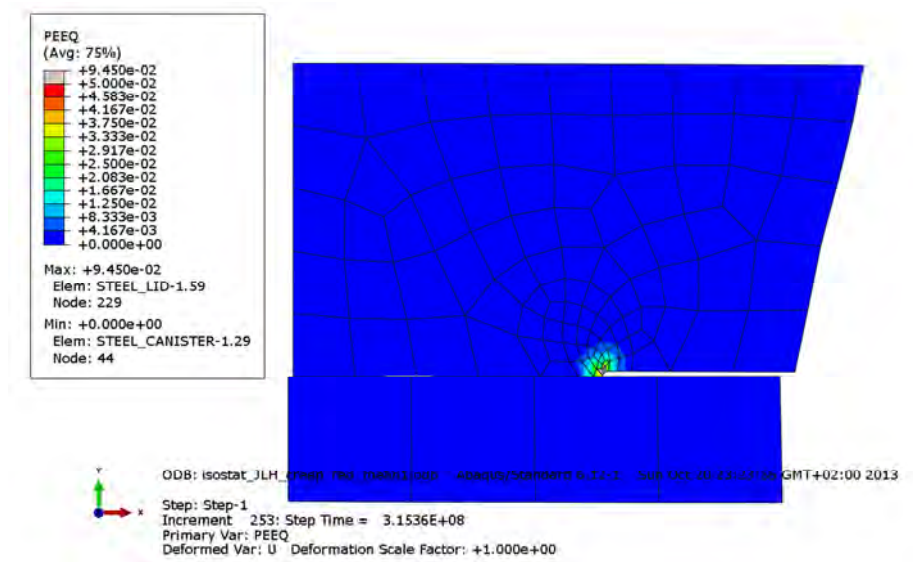


Figure A2-24. Plot showing equivalent plastic strain at the steel lid after 10 years; see also Figure 4-3 for explanation of the details. Gas pressure is applied.

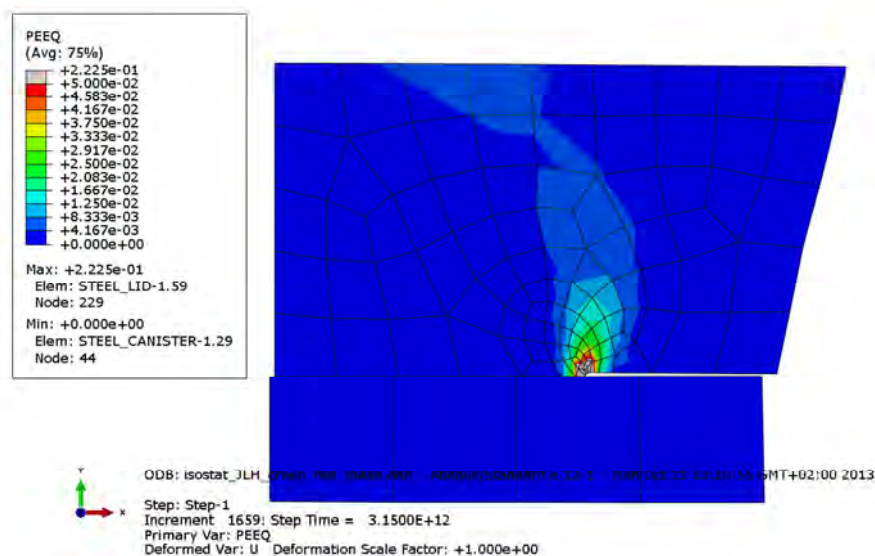


Figure A2-25. Plot showing equivalent plastic strain at the steel lid after 100,000 years; see also Figure 4-3 for explanation of the details.

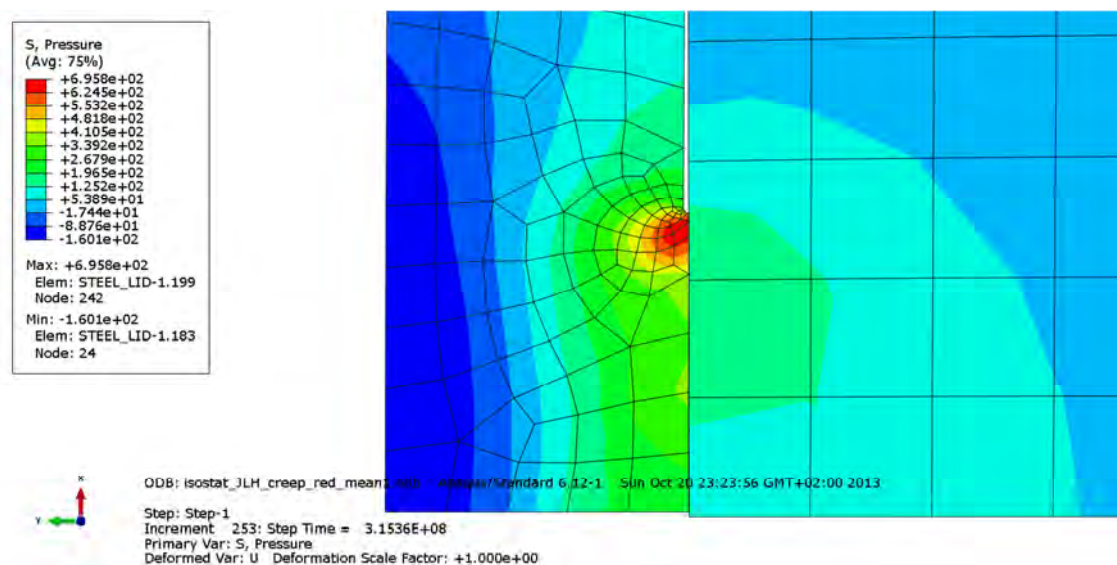


Figure A2-26. Plot showing pressure stress at the discontinuity of the insert after 10 years. Gas pressure is applied.

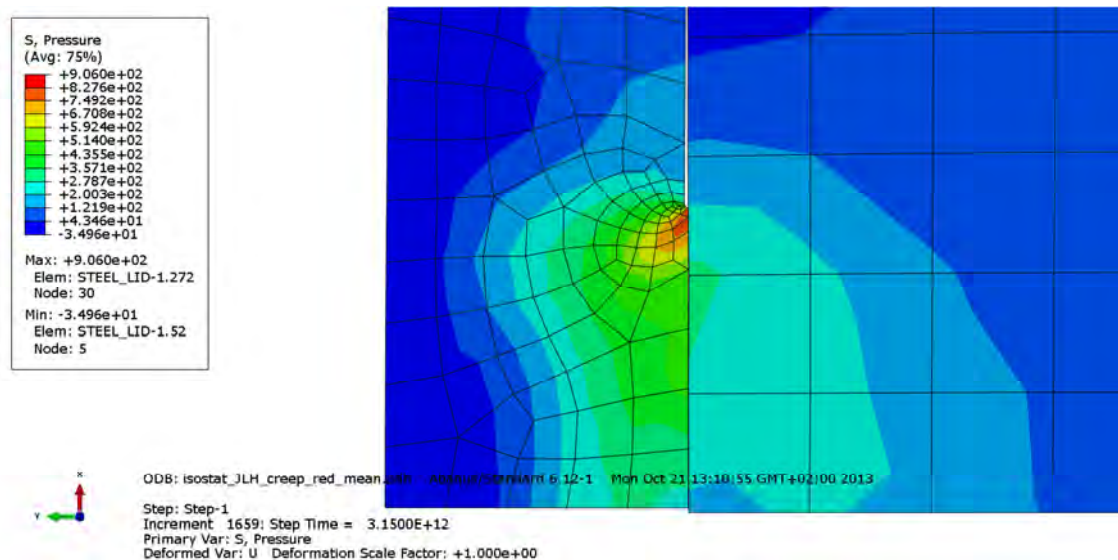


Figure A2-27. Plot showing pressure stress at the discontinuity of the insert after 100,000 years.

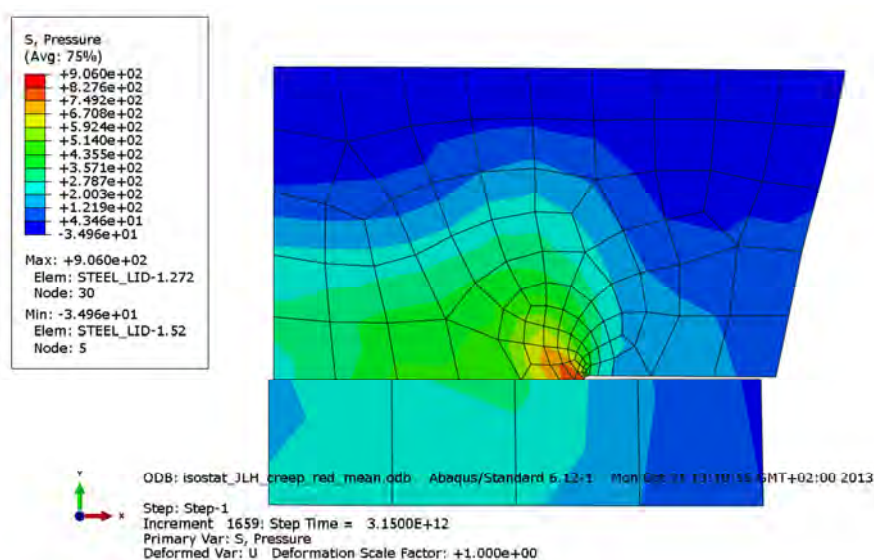


Figure A2-28. Plot showing pressure stress at the steel lid after 100,000 years; see also Figure 4-3 for explanation of the details.

Appendix 3 – Isostat_JLH_creep_blue_dim

Plots showing temperature and pressure contours and history.

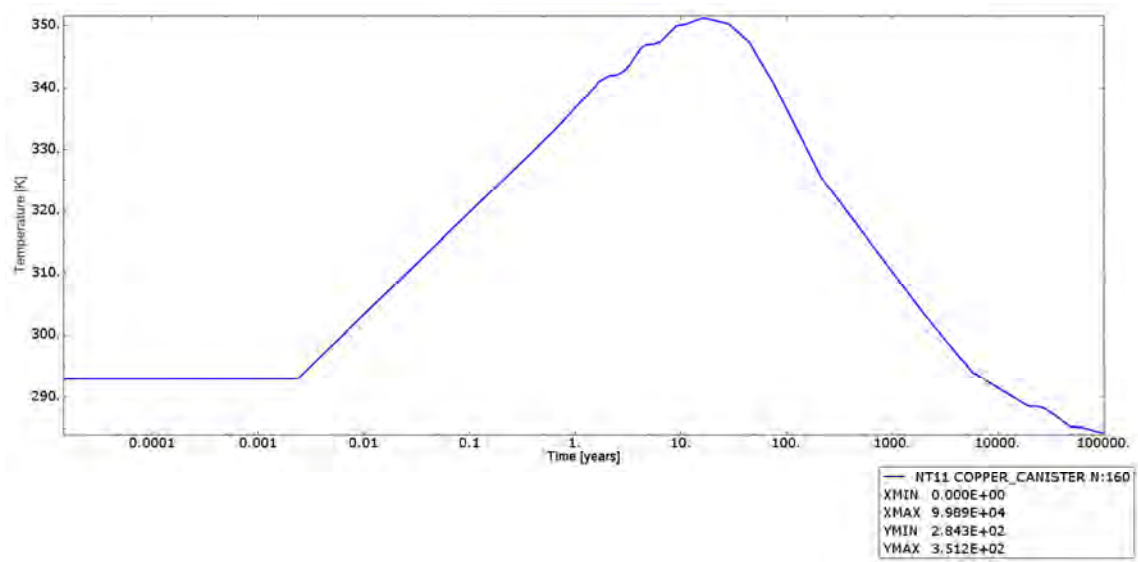


Figure A3-1. Plot showing temperature history. Time is in years, temperature is in Kelvin.

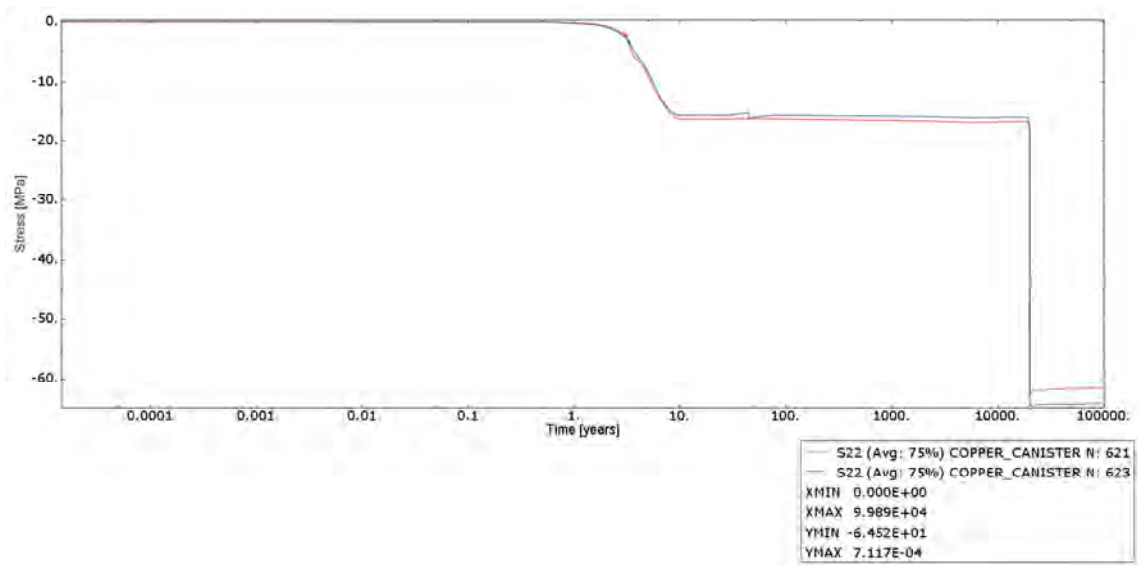


Figure A3-2. Plot showing applied pressure at the top lid of the copper shell. Time is in years and stress is in MPa.

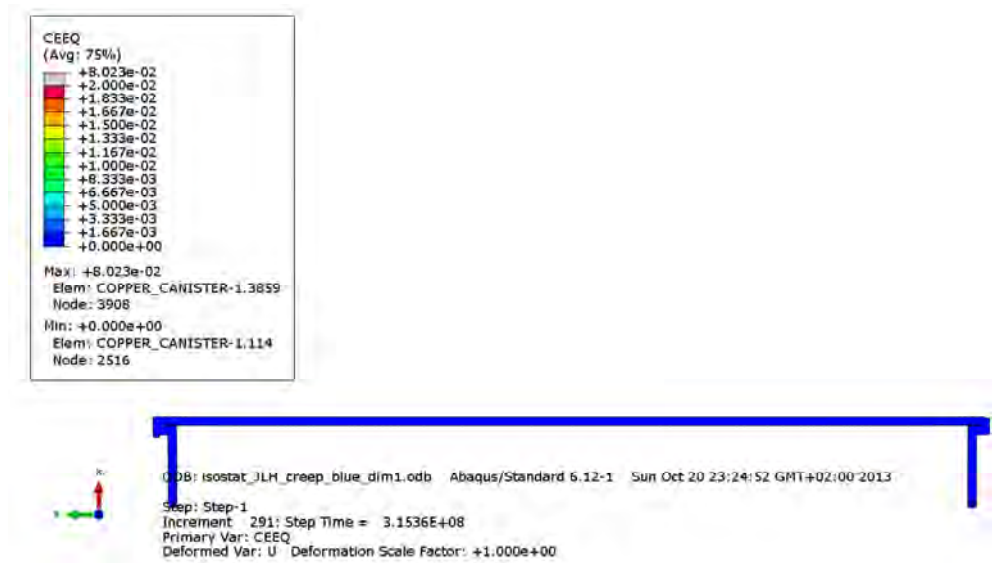


Figure A3-3. Plot showing equivalent creep strain after 10 years. Gas pressure is applied.

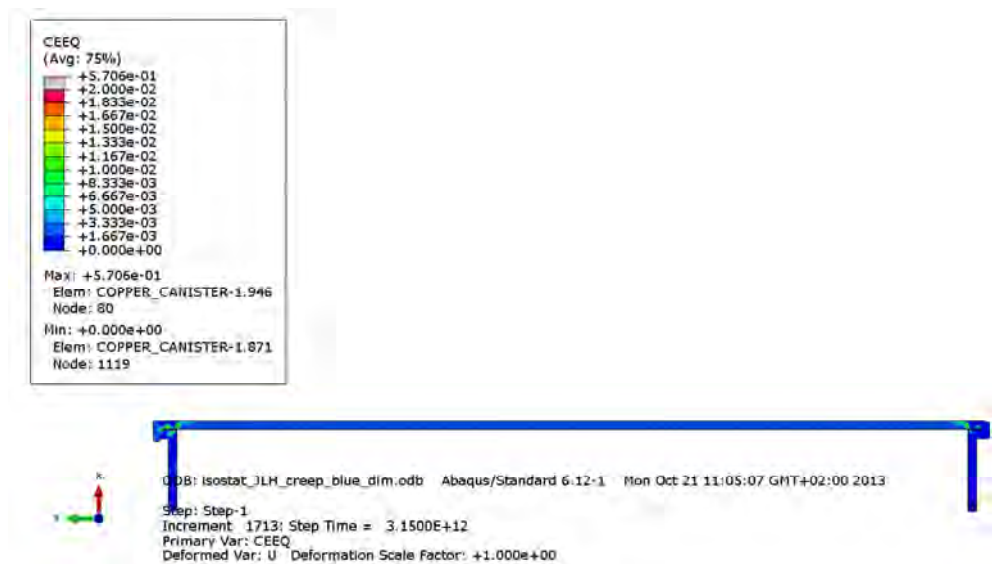


Figure A3-4. Plot showing equivalent creep strain after 100,000 years.

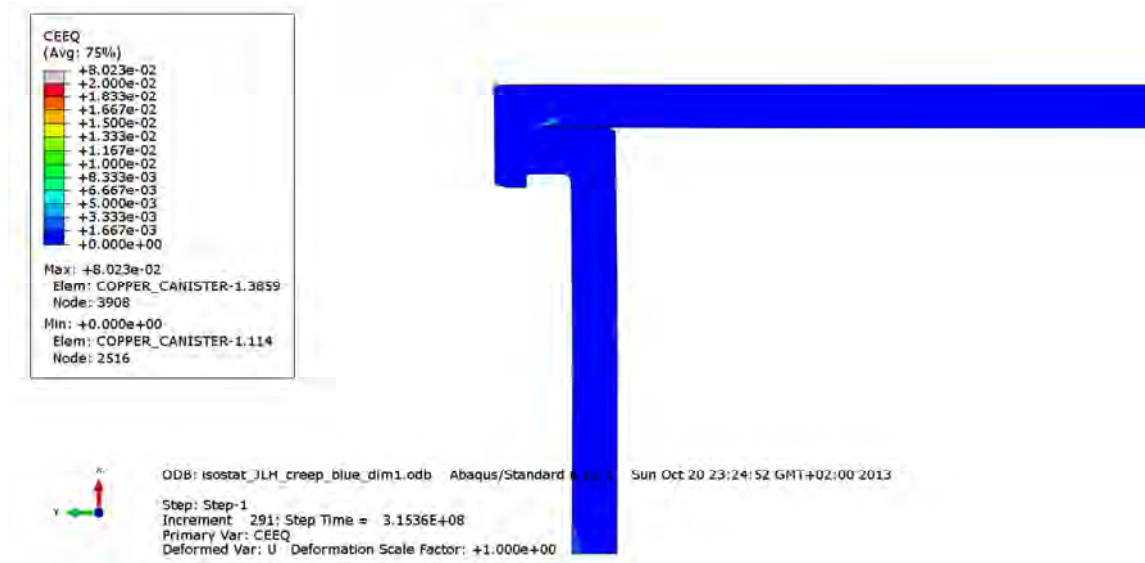


Figure A3-5. Plot showing equivalent creep strain at the top weld of the copper shell after 10 years. Gas pressure is applied.

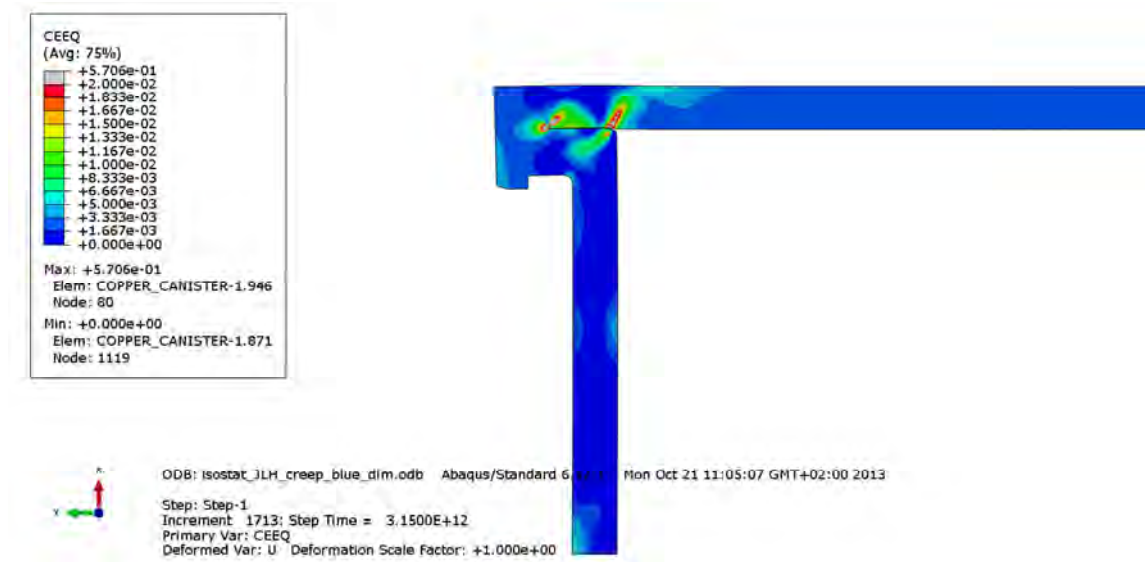


Figure A3-6. Plot showing equivalent creep strain at the top weld of the copper shell after 100,000 years.

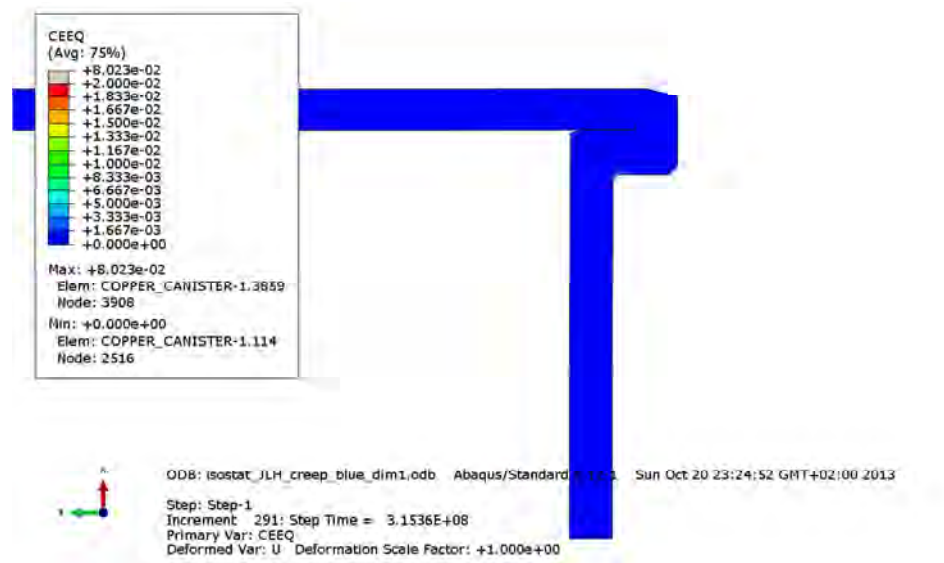


Figure A3-7. Plot showing equivalent creep strain at the bottom weld of the copper shell after 10 years. Gas pressure is applied.

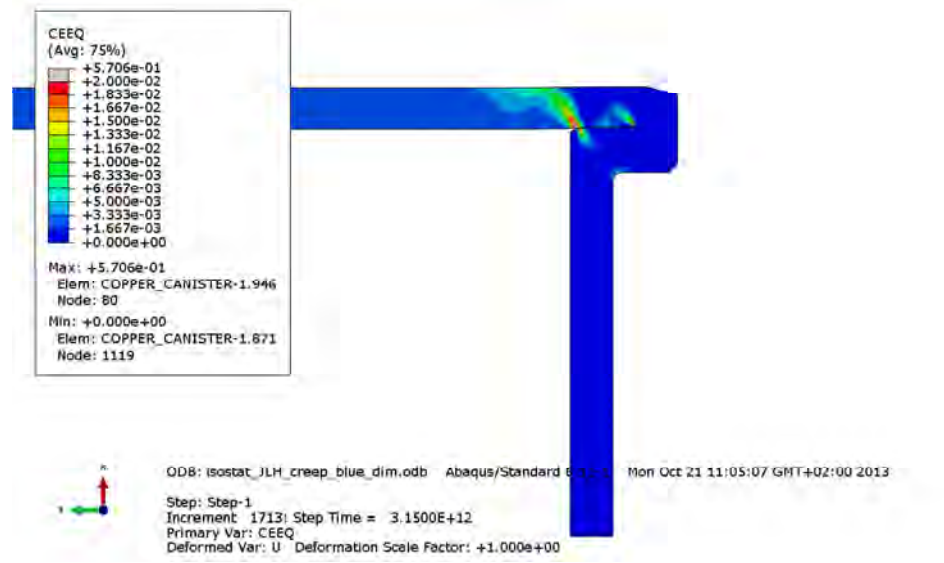


Figure A3-8. Plot showing equivalent creep strain at the bottom weld of the copper shell after 100,000 years.

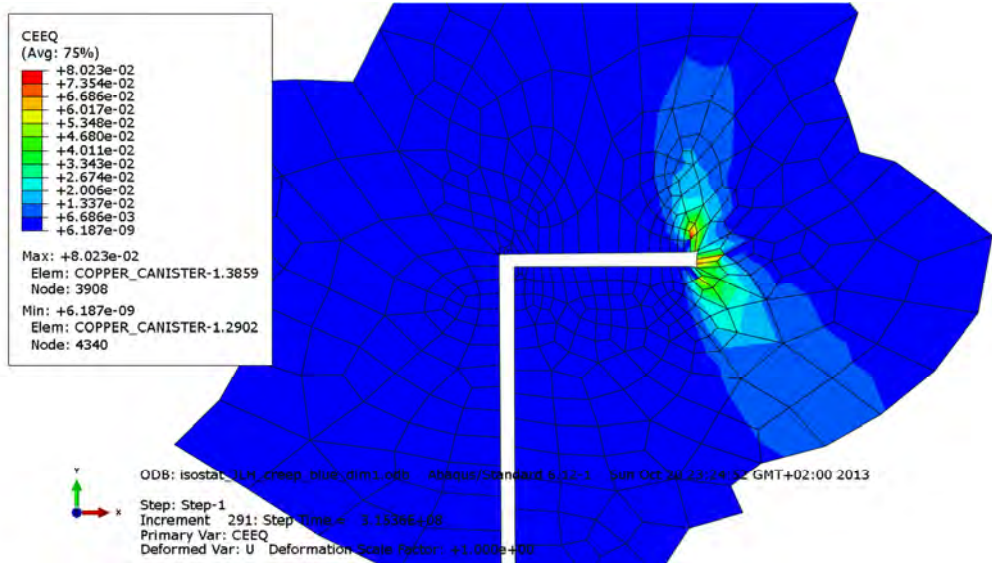


Figure A3-9. Plot showing equivalent creep strain at the copper shell top weld after 10 years. Gas pressure is applied.

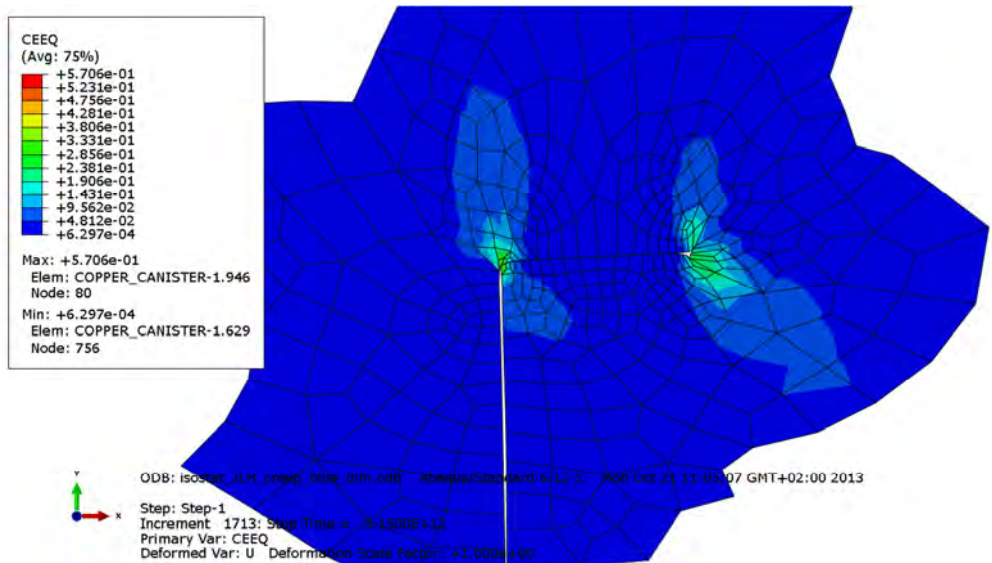


Figure A3-10. Plot showing equivalent creep strain at the copper shell top weld after 100,000 years.

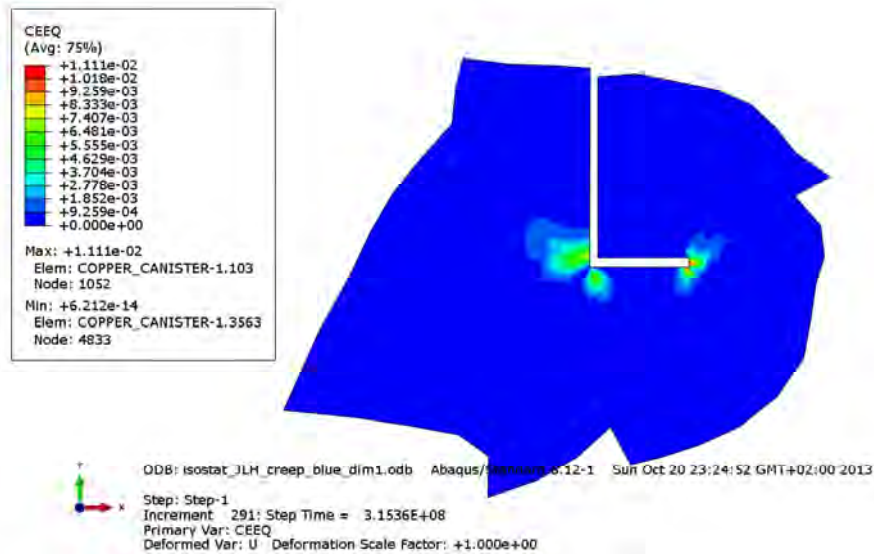


Figure A3-11. Plot showing equivalent creep strain at the copper shell bottom weld after 10 years. Gas pressure is applied.

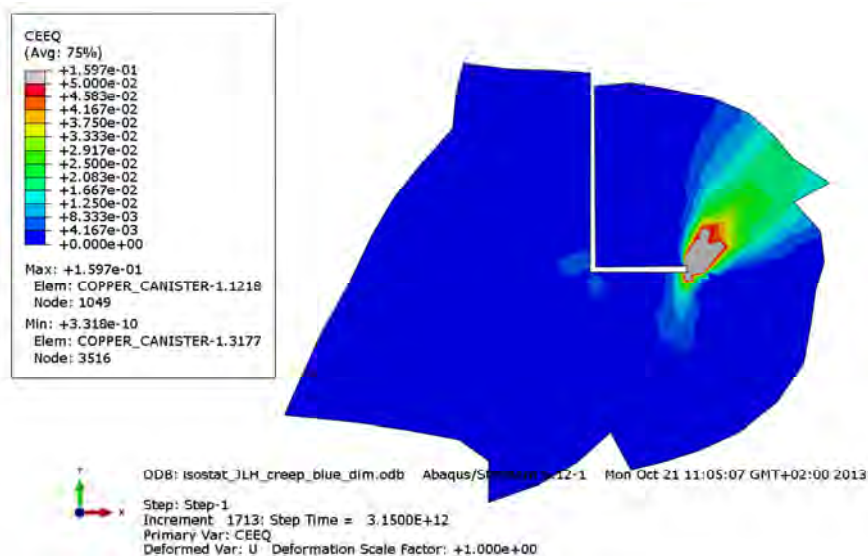


Figure A3-12. Plot showing equivalent creep strain at the copper shell bottom weld after 100,000 years.

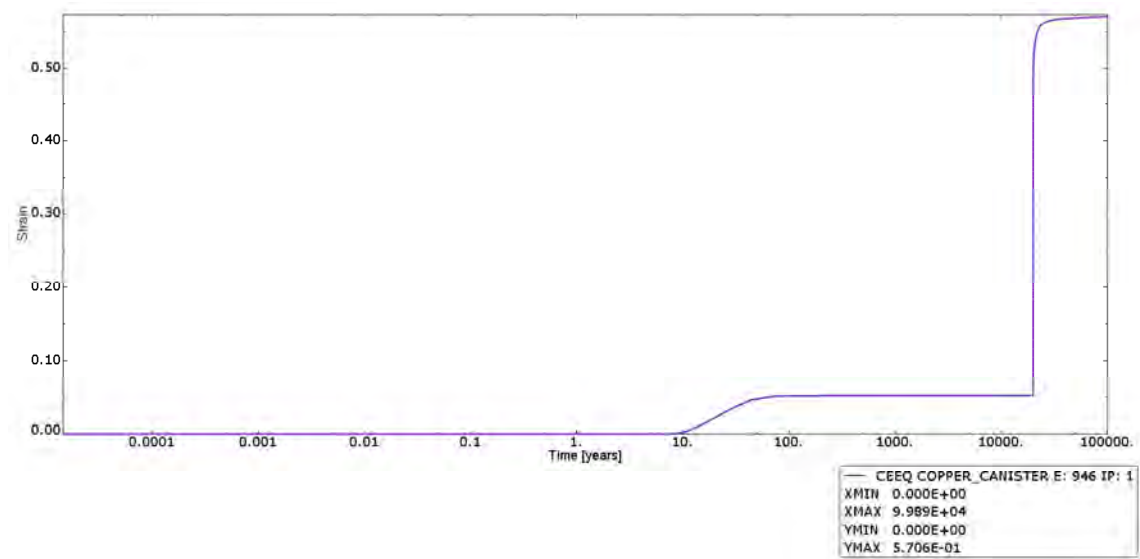


Figure A3-13. Plot showing history of equivalent creep strain in the element having the maximum magnitude. Time is in years and strain is dimensionless.

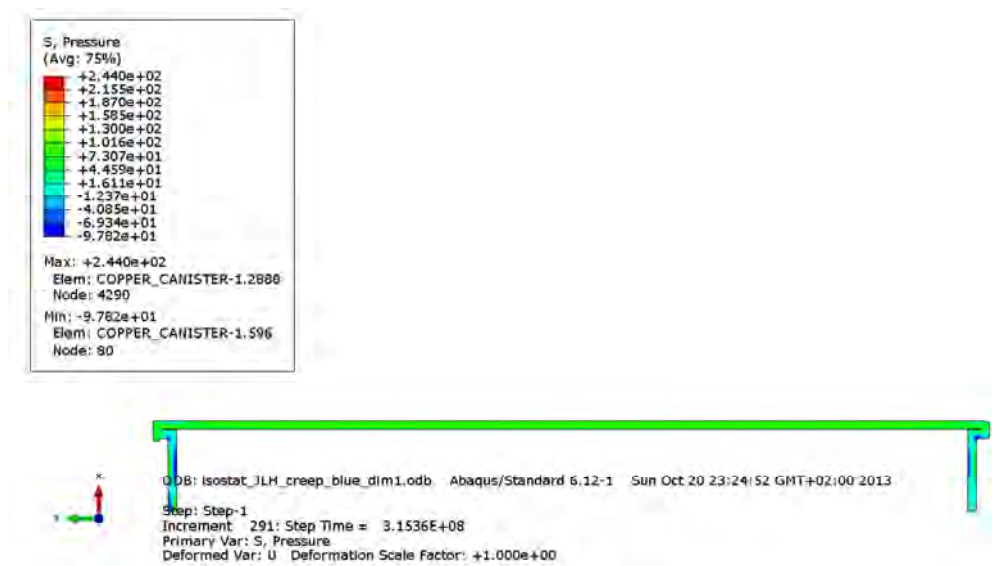


Figure A3-14. Plot showing pressure stress in the copper shell after 10 years. Gas pressure is applied.

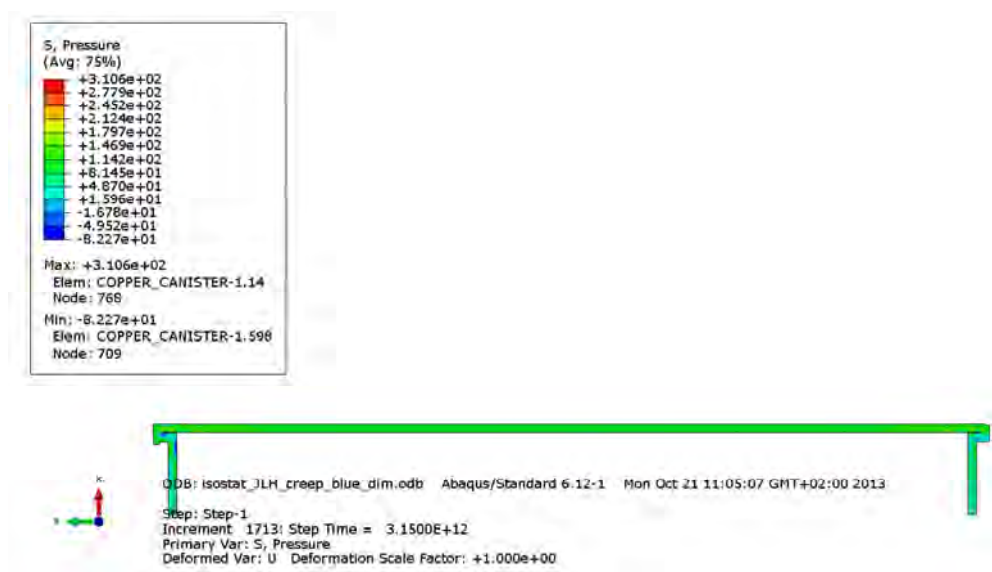


Figure A3-15. Plot showing pressure stress in the copper shell after 100,000 years.

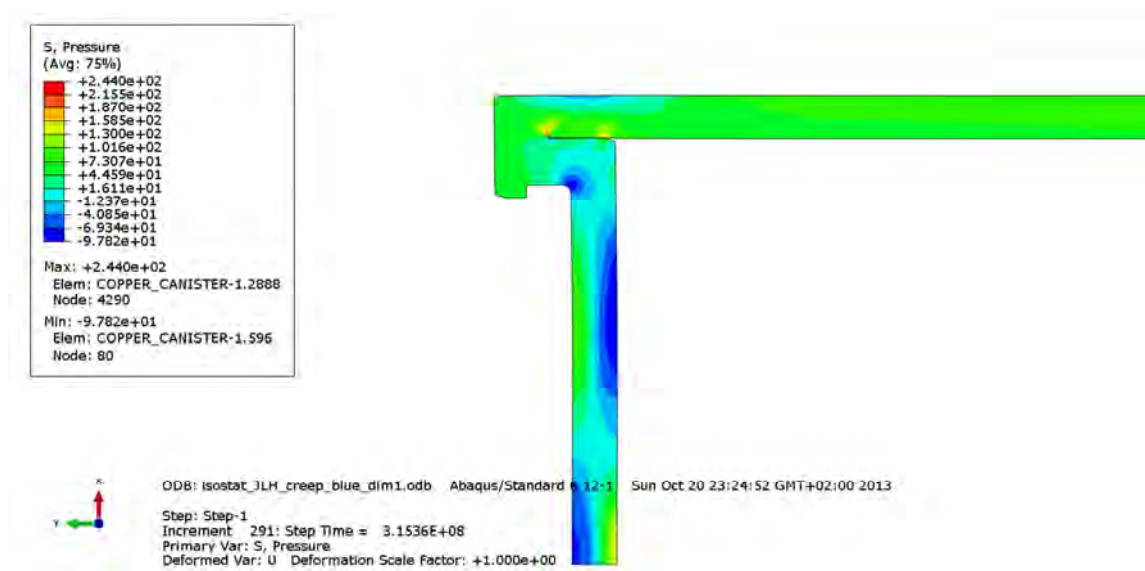


Figure A3-16. Plot showing pressure stress at the copper shell top weld after 10 years. Gas pressure is applied.

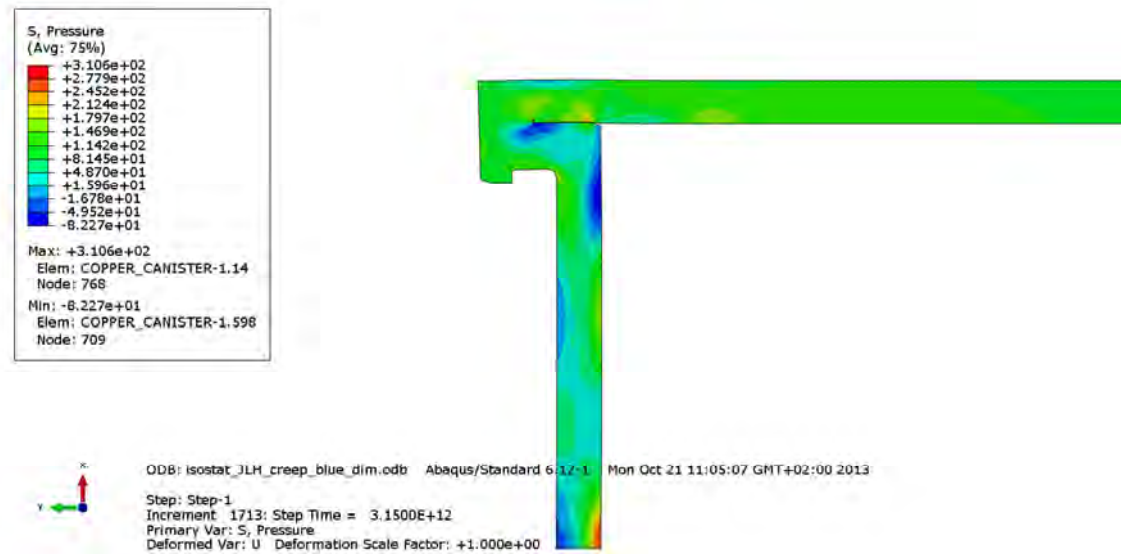


Figure A3-17. Plot showing pressure stress at the copper shell top weld after 100,000 years.

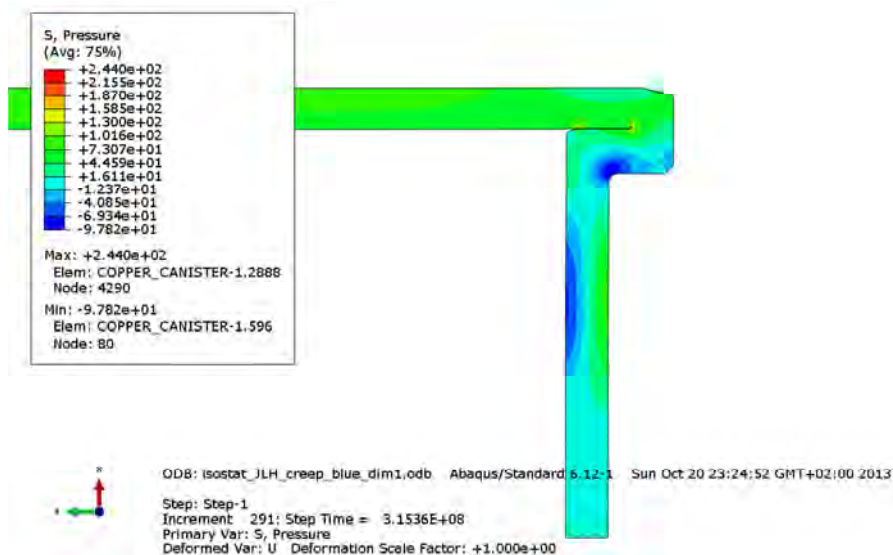


Figure A3-18. Plot showing pressure stress at the copper shell bottom weld after 10 years. Gas pressure is applied.

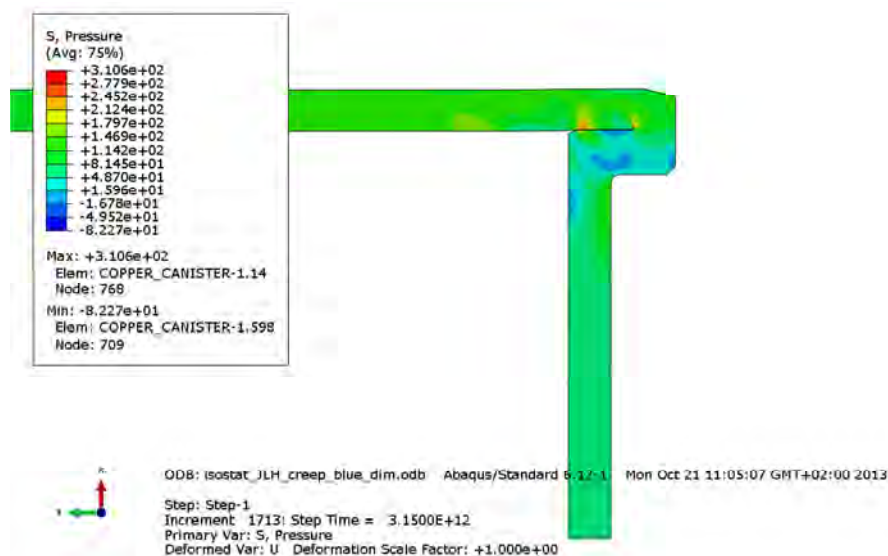


Figure A3-19. Plot showing pressure stress at the copper shell bottom weld after 100,000 years.

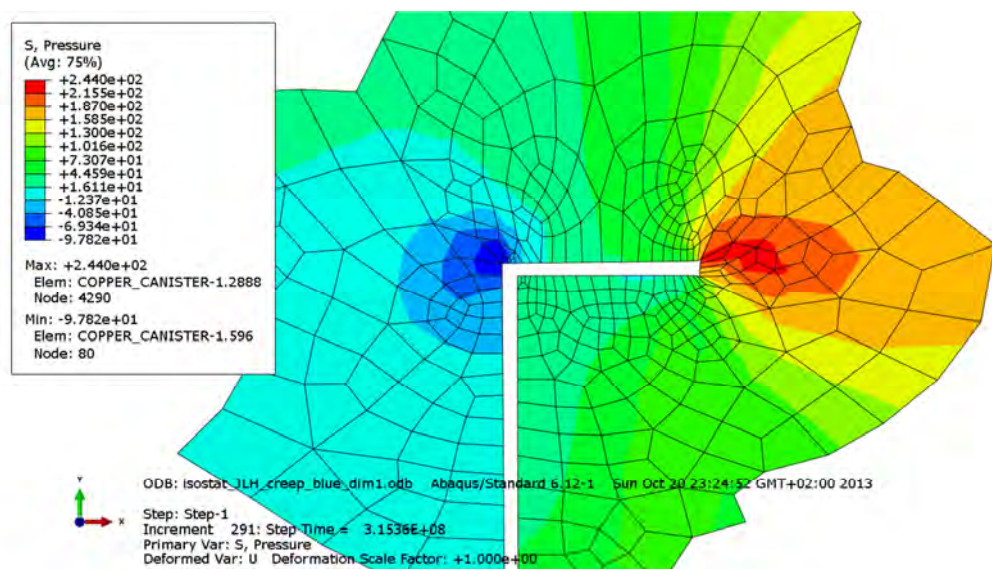


Figure A3-20. Plot showing pressure stress at the copper shell top weld after 10 years. Gas pressure is applied.

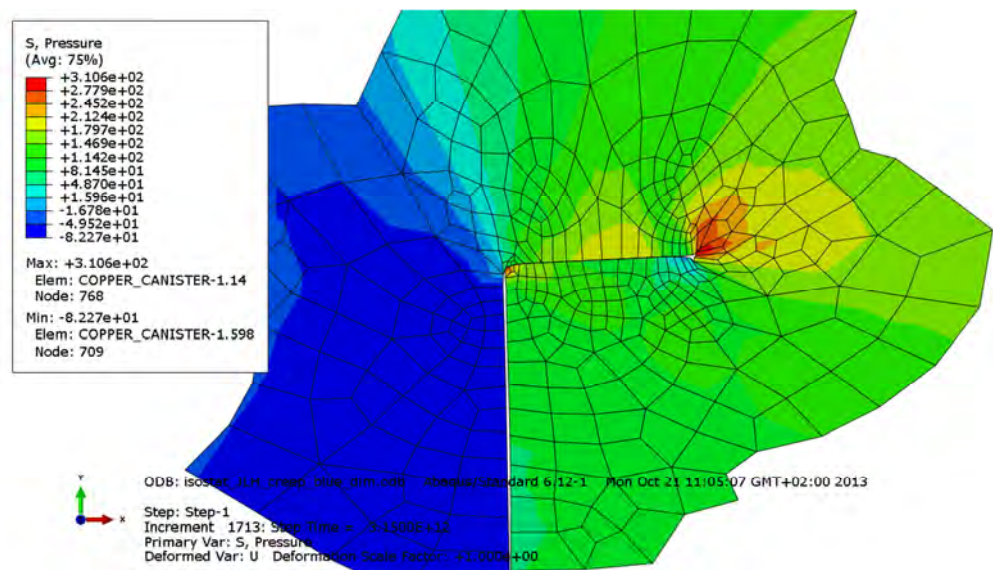


Figure A3-21. Plot showing pressure stress at the copper shell top weld after 10,000 years.

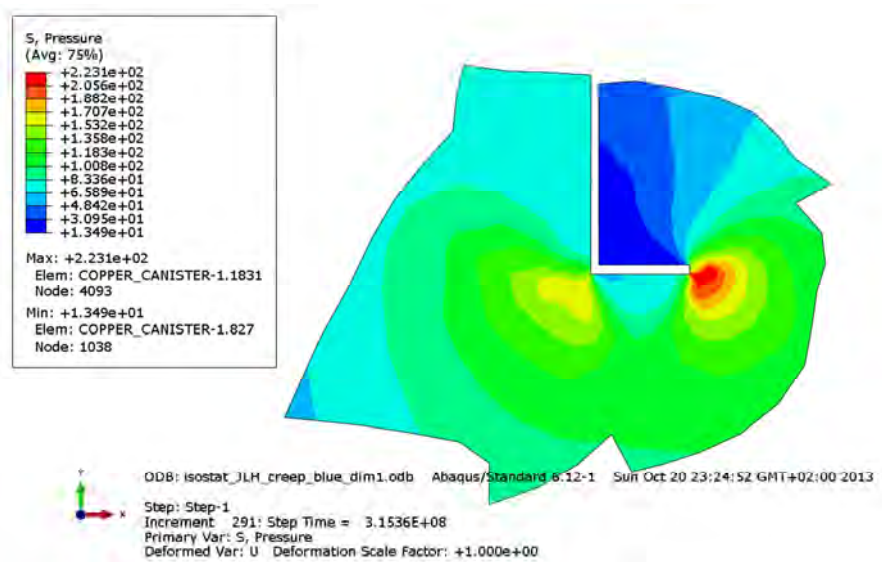


Figure A3-22. Plot showing pressure stress at the copper shell bottom weld after 10 years. Gas pressure is applied.

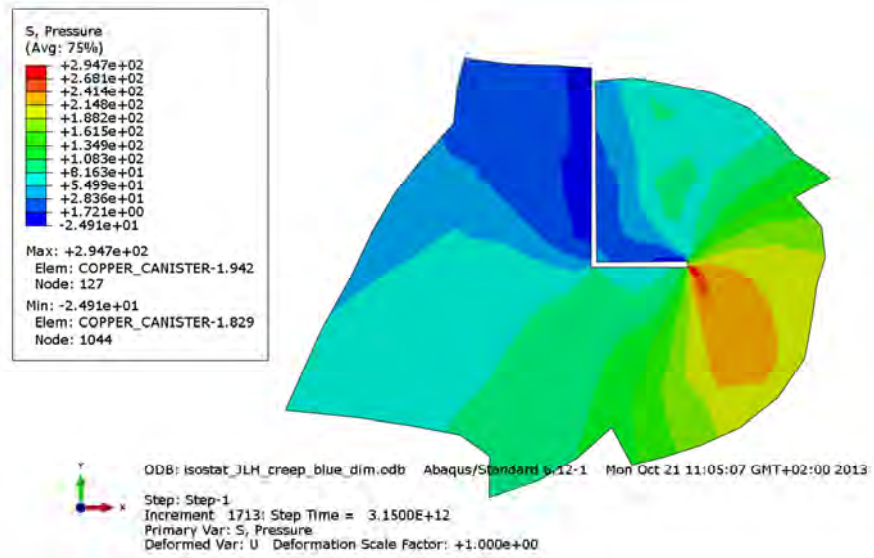


Figure A3-23. Plot showing pressure stress at the copper shell bottom weld after 100,000 years.

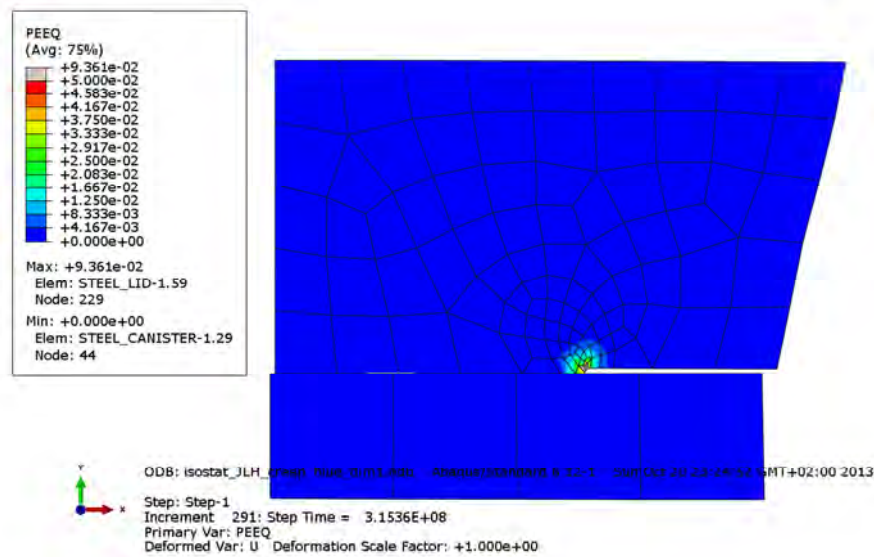


Figure A3-24. Plot showing equivalent plastic strain at the steel lid after 10 years; see also Figure 4-3 for explanation of the details. Gas pressure is applied.

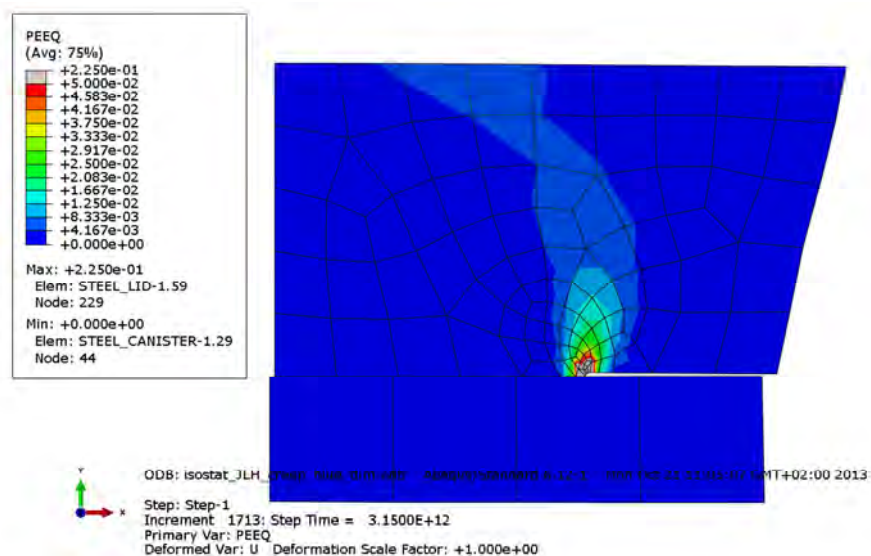


Figure A3-25. Plot showing equivalent plastic strain at the steel lid after 100,000 years; see also Figure 4-3 for explanation of the details.

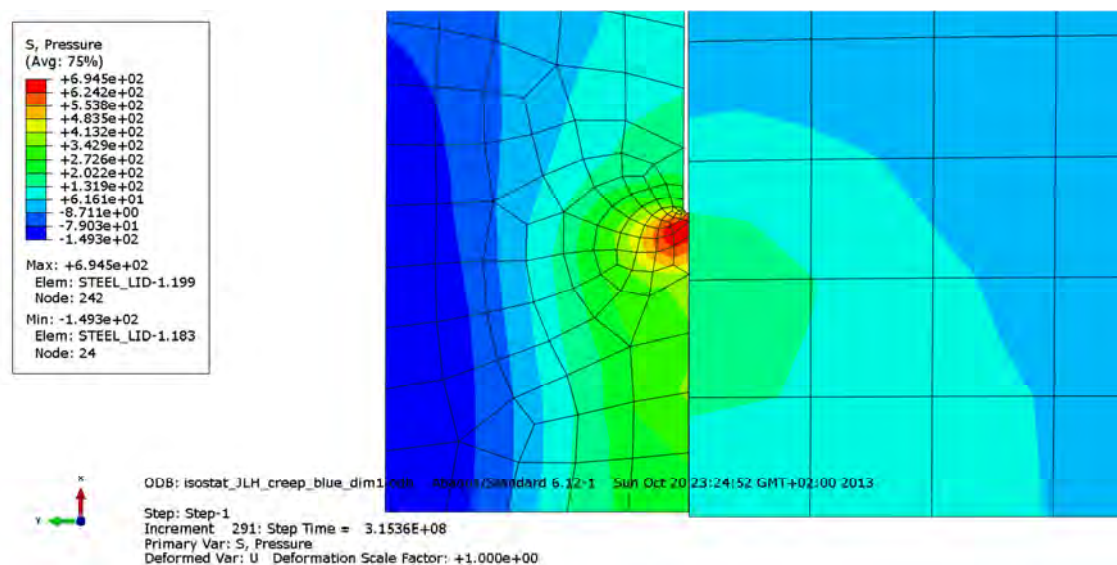


Figure A3-26. Plot showing pressure stress at the discontinuity of the insert after 10 years. Gas pressure is applied.

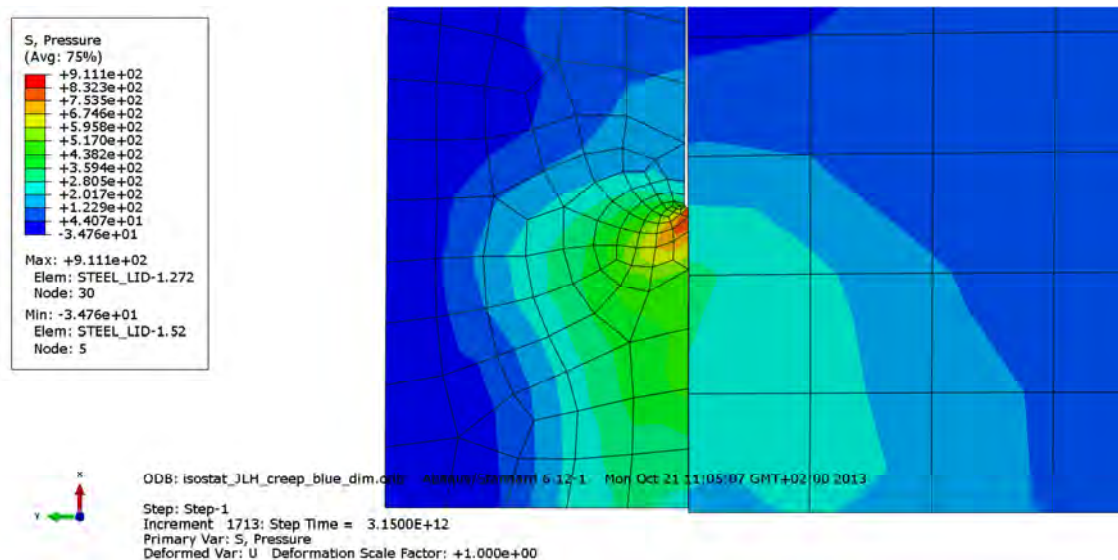


Figure A3-27. Plot showing pressure stress at the discontinuity of the insert after 100,000 years.

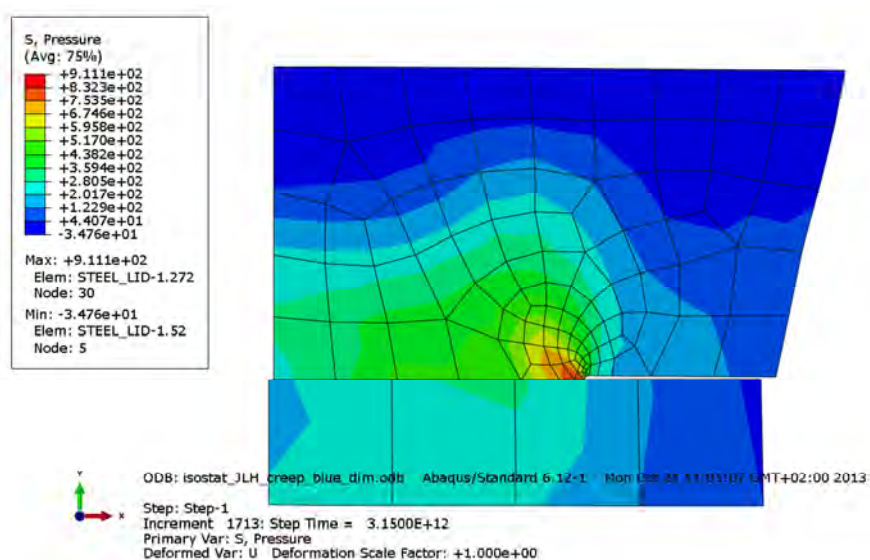


Figure A3-28. Plot showing pressure stress at the steel lid after 100,000 years; see also Figure 4-3 for explanation of the details.

Appendix 4 – Isostat_JLH_creep_blue_mean

Plots showing temperature and pressure contours and history.

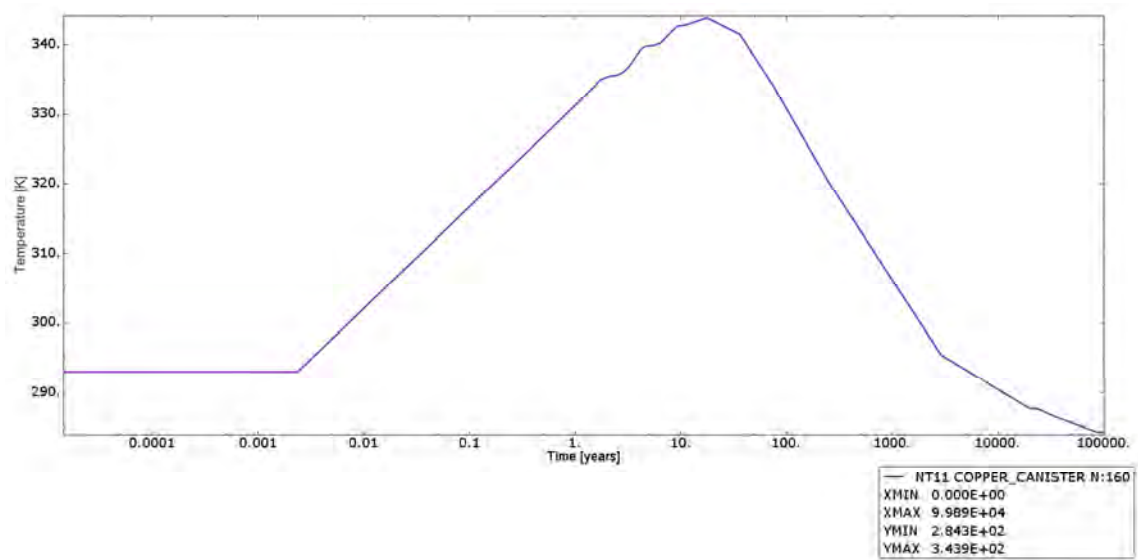


Figure A4-1. Plot showing temperature history. Time is in years, temperature is in Kelvin.

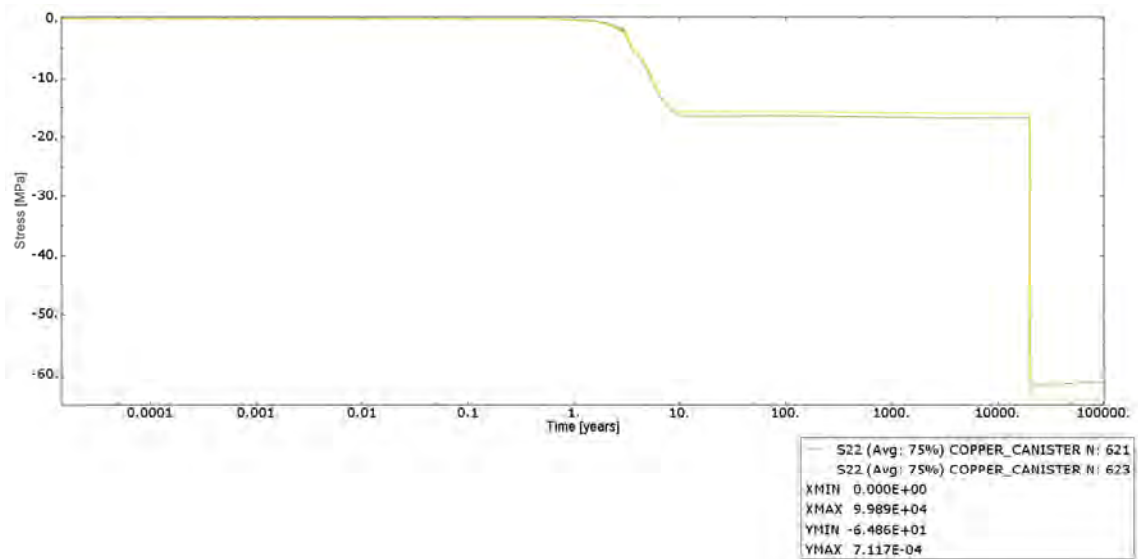


Figure A4-2. Plot showing applied pressure at the top lid of the copper shell. Time is in years and stress is in MPa.

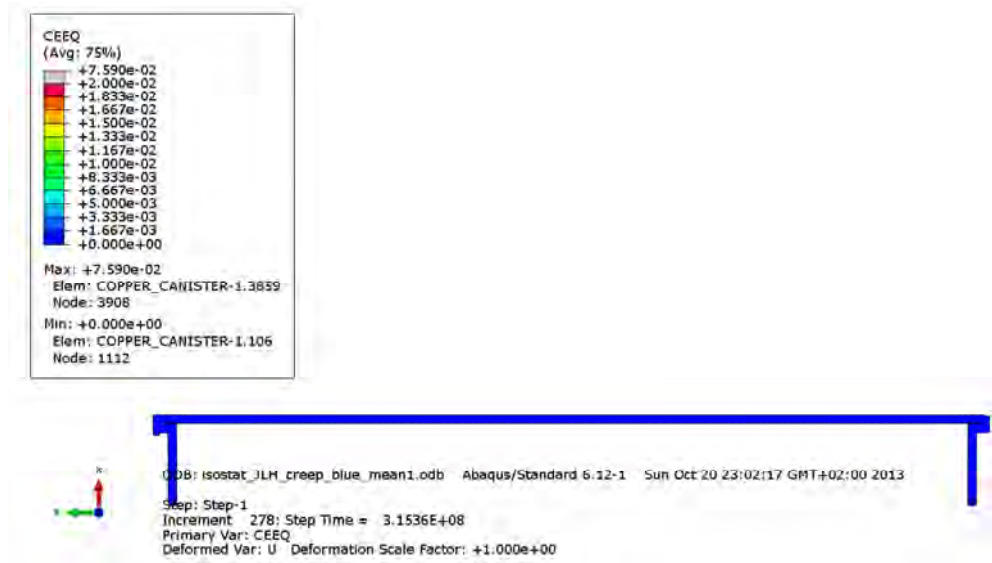


Figure A4-3. Plot showing equivalent creep strain after 10 years. Gas pressure is applied.

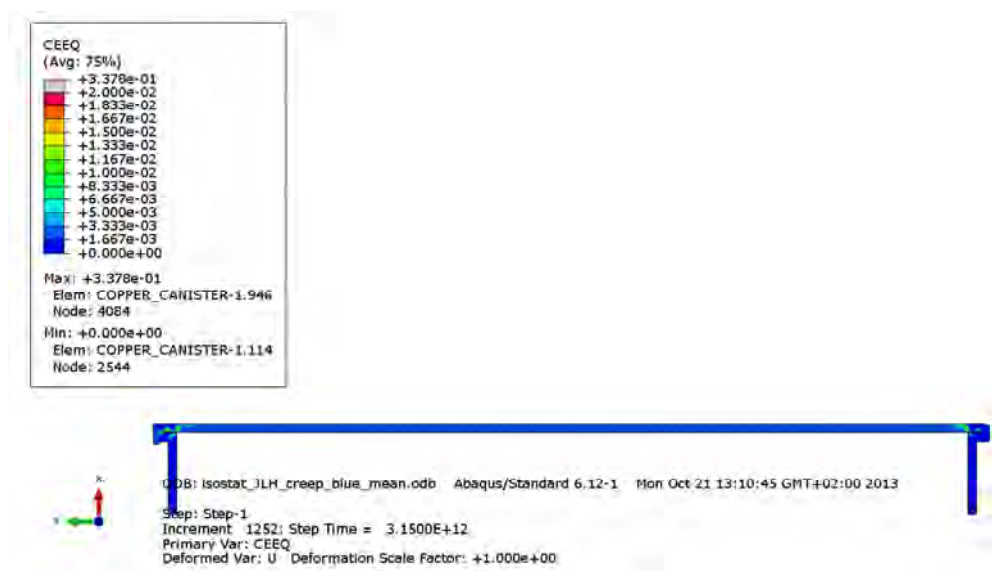


Figure A4-4. Plot showing equivalent creep strain after 100,000 years.

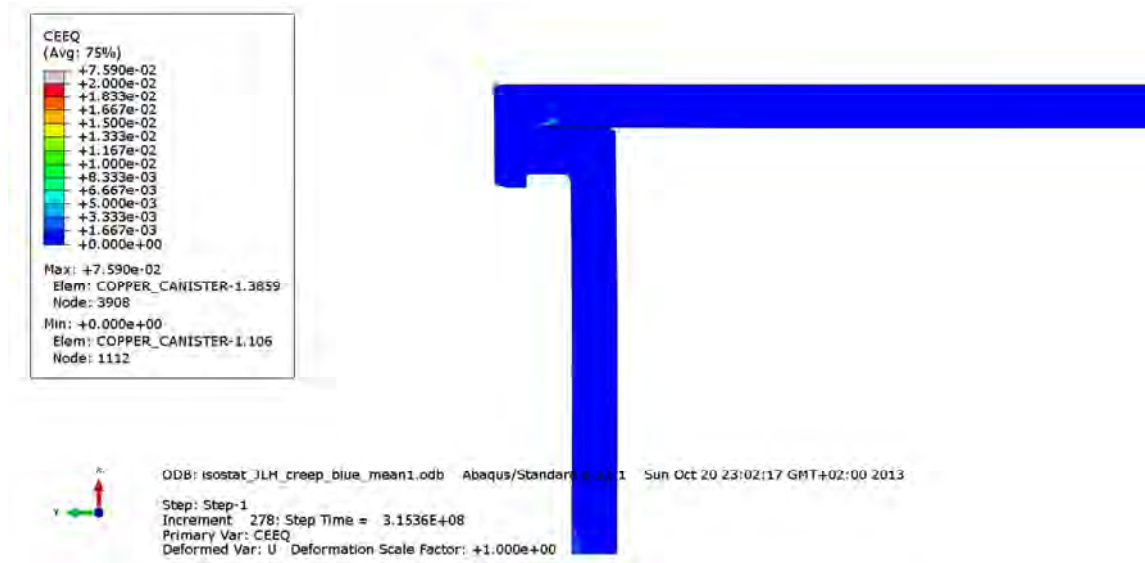


Figure A4-5. Plot showing equivalent creep strain at the top weld of the copper shell after 10 years. Gas pressure is applied.

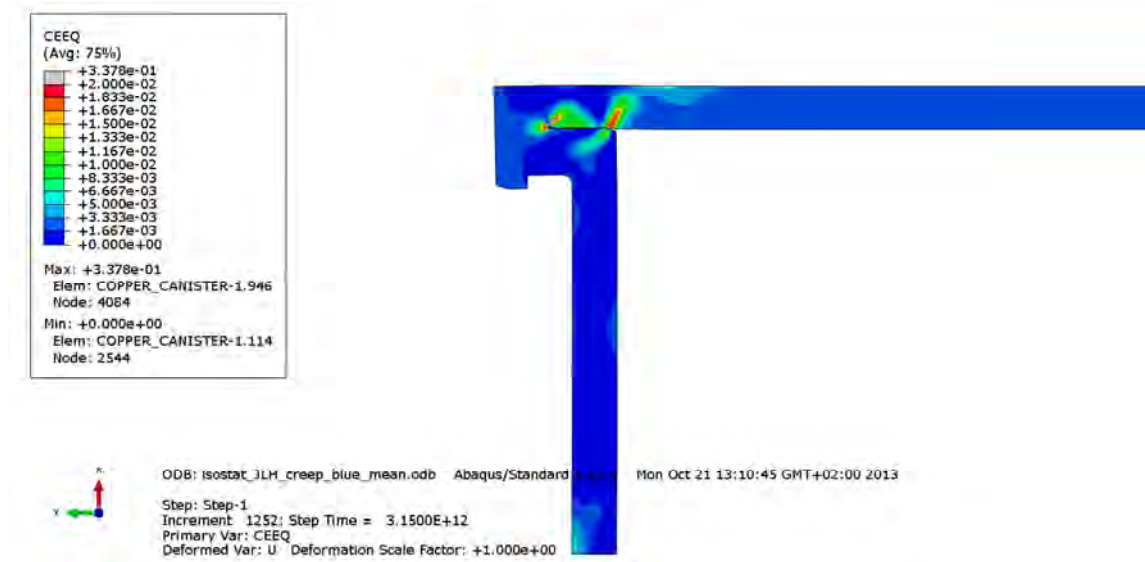


Figure A4-6. Plot showing equivalent creep strain at the top weld of the copper shell after 100,000 years.

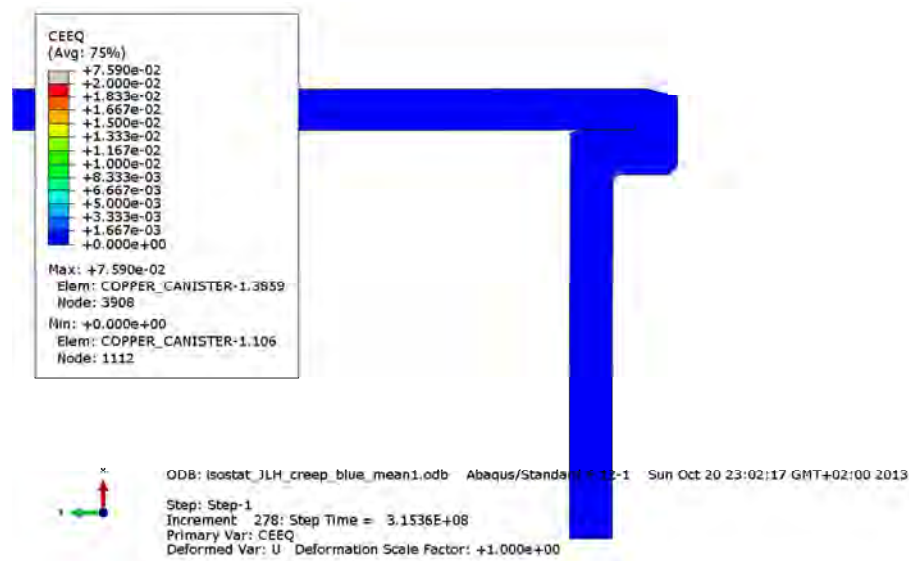


Figure A4-7. Plot showing equivalent creep strain at the bottom weld of the copper shell after 10 years. Gas pressure is applied.

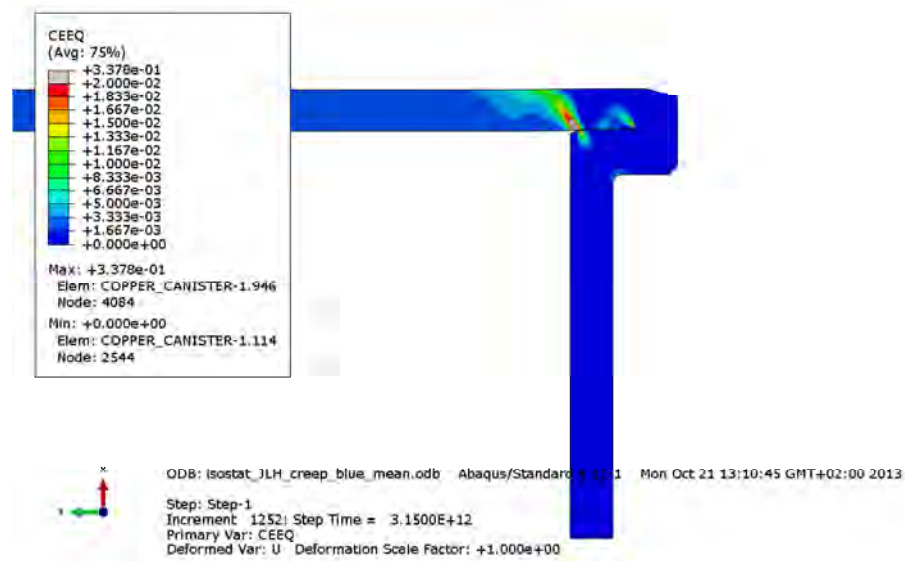


Figure A4-8. Plot showing equivalent creep strain at the bottom weld of the copper shell after 100,000 years.

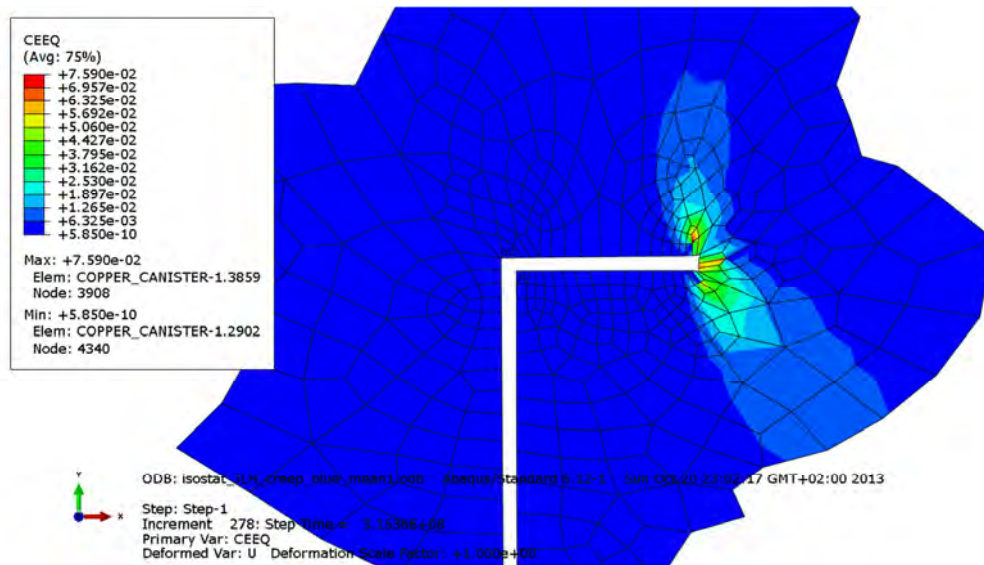


Figure A4-9. Plot showing equivalent creep strain at the copper shell top weld after 10 years. Gas pressure is applied.

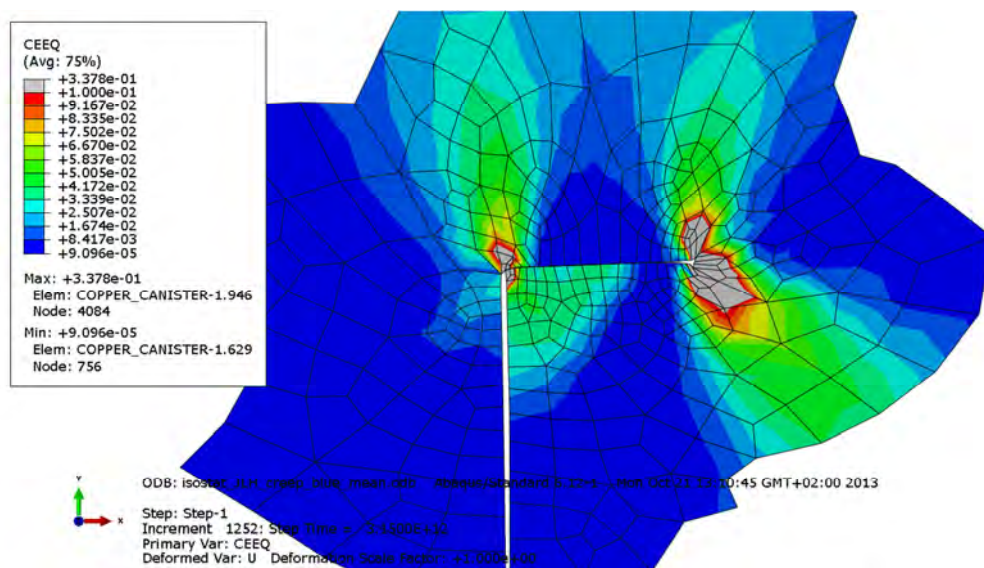


Figure A2-10. Plot showing equivalent creep strain at the copper shell top weld after 100,000 years.

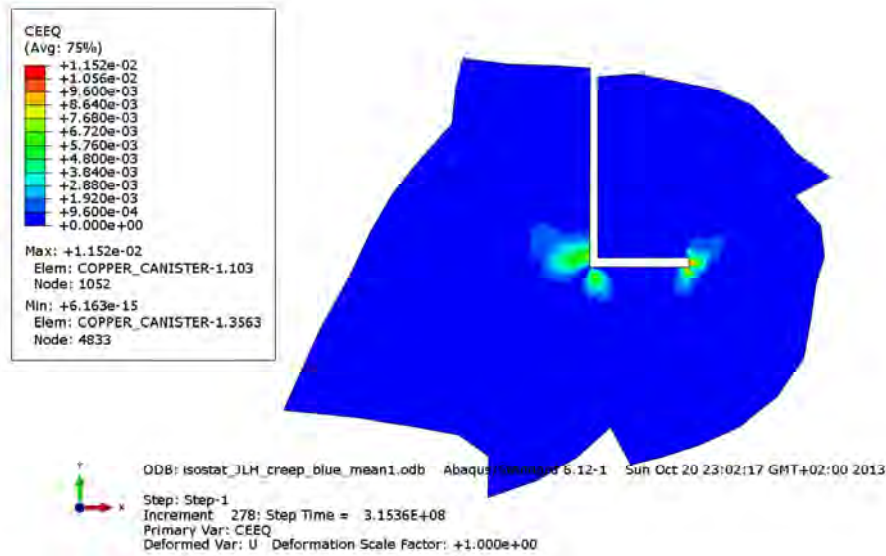


Figure A2-11. Plot showing equivalent creep strain at the copper shell bottom weld after 10 years. Gas pressure is applied.

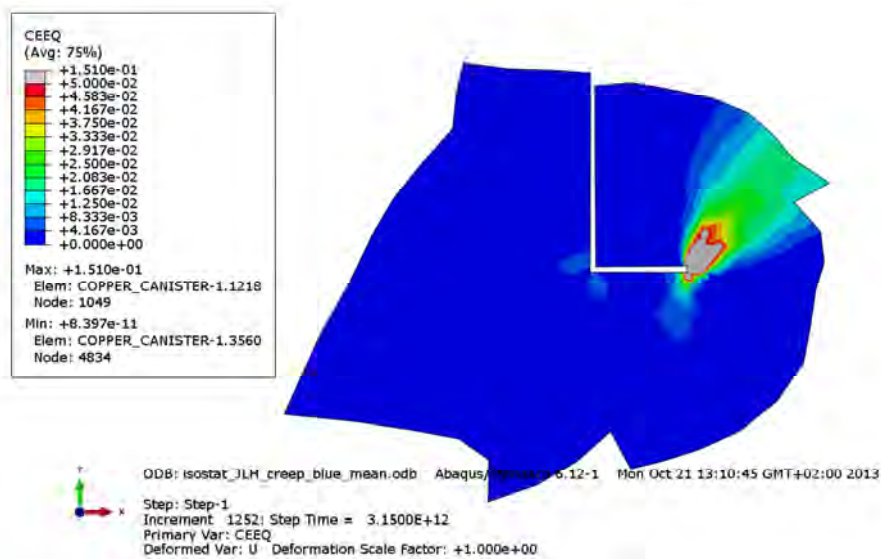


Figure A2-12. Plot showing equivalent creep strain at the copper shell bottom weld after 100,000 years.

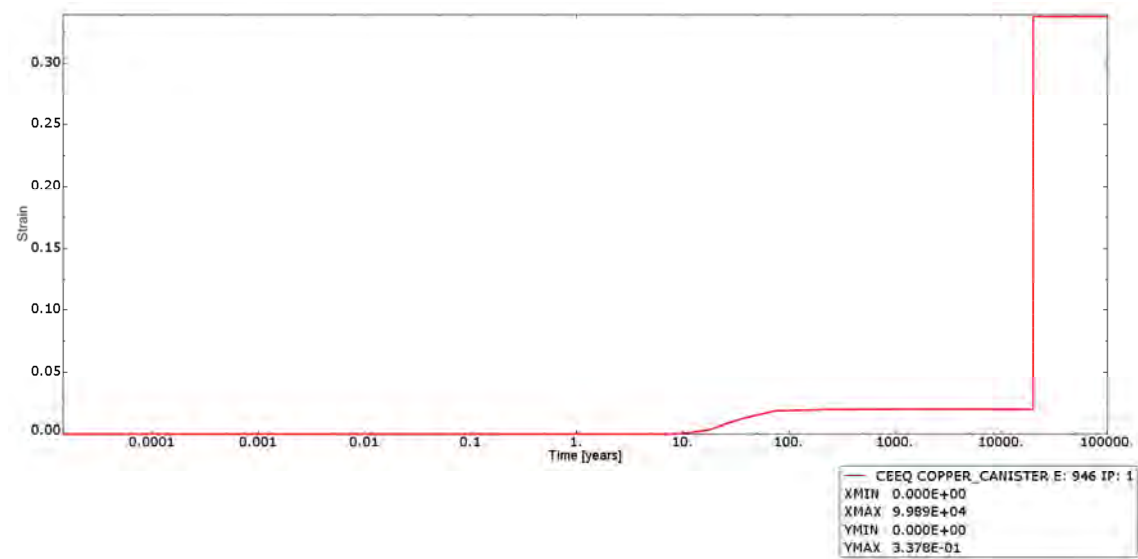


Figure A4-13. Plot showing history of equivalent creep strain in the element having the maximum magnitude. Time is in years and strain is dimensionless.

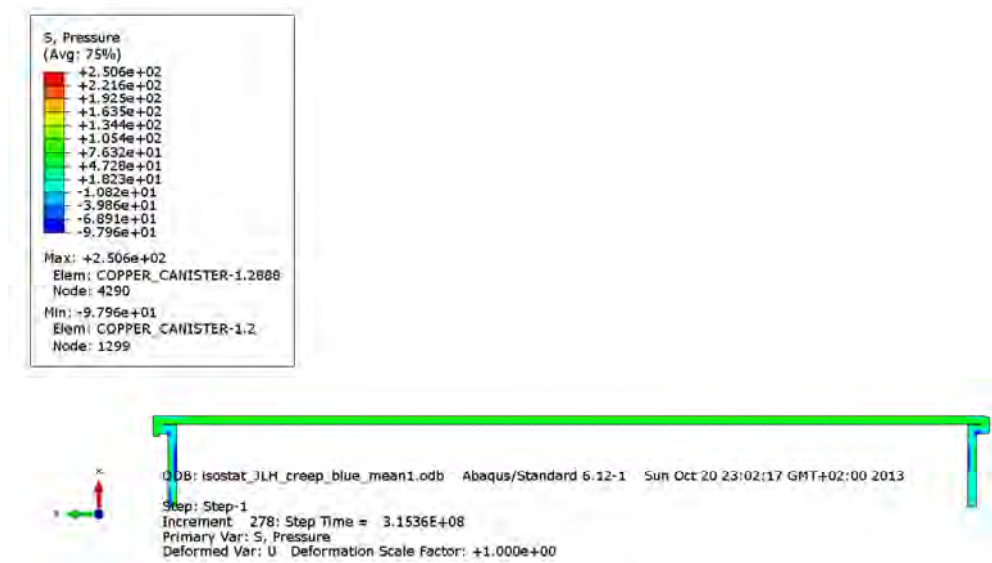


Figure A4-14. Plot showing pressure stress in the copper shell after 10 years. Gas pressure is applied.

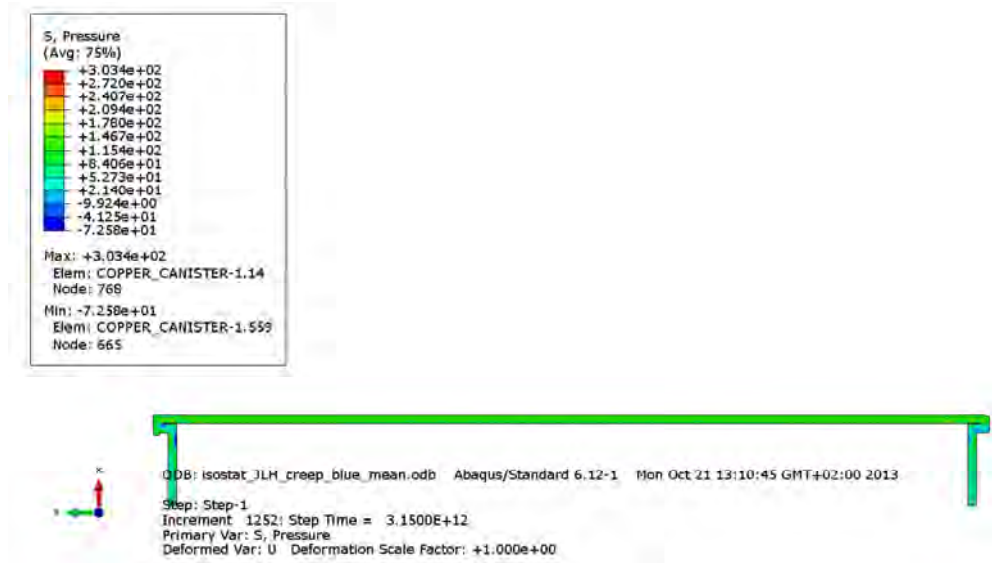


Figure A4-15. Plot showing pressure stress in the copper shell after 100,000 years.

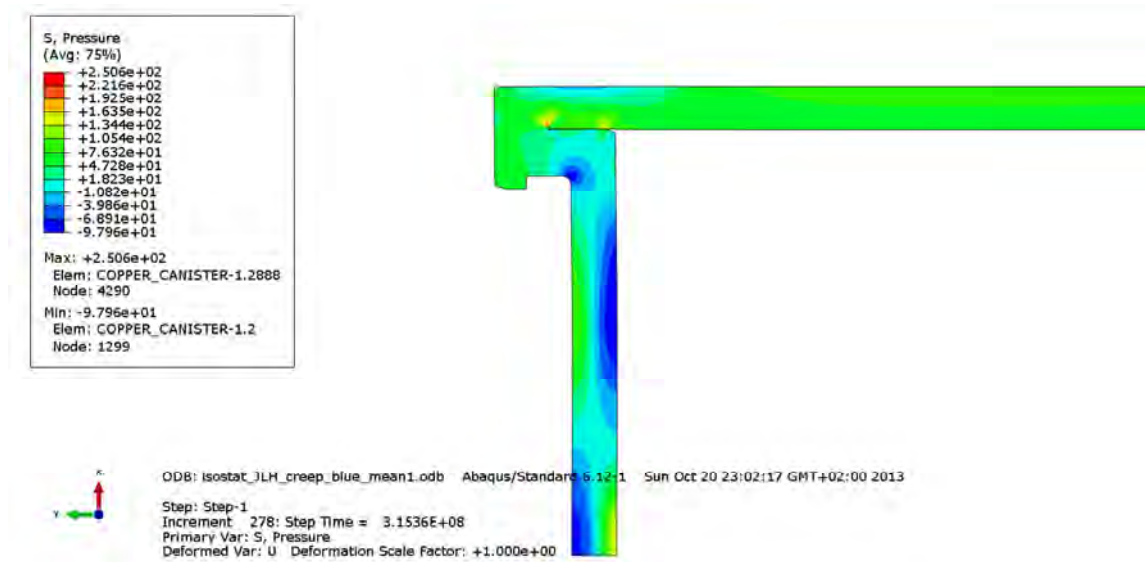


Figure A4-16. Plot showing pressure stress at the copper shell top weld after 10 years. Gas pressure is applied.

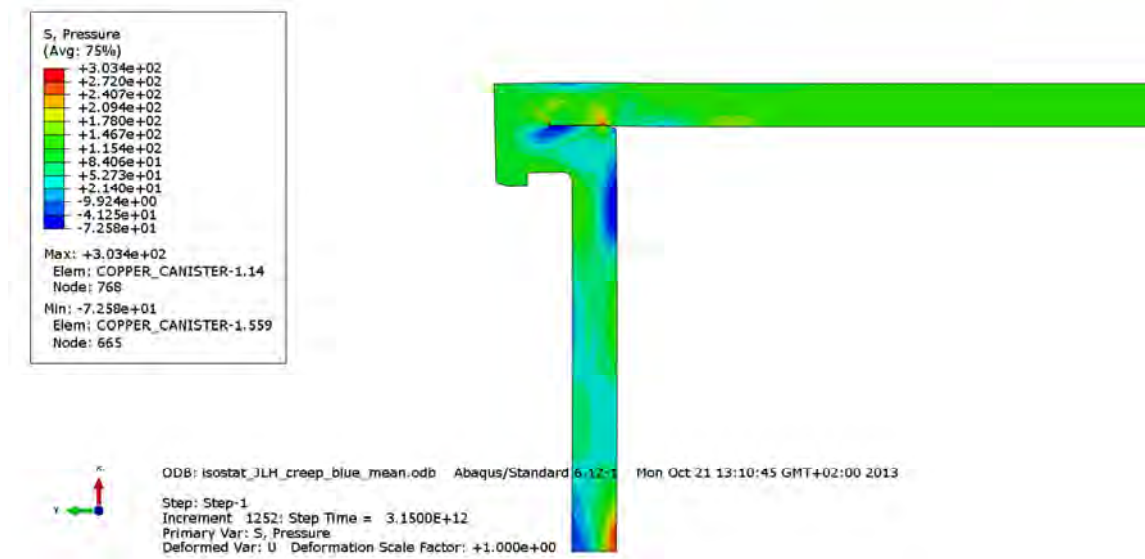


Figure A4-17. Plot showing pressure stress at the copper shell top weld after 100,000 years.

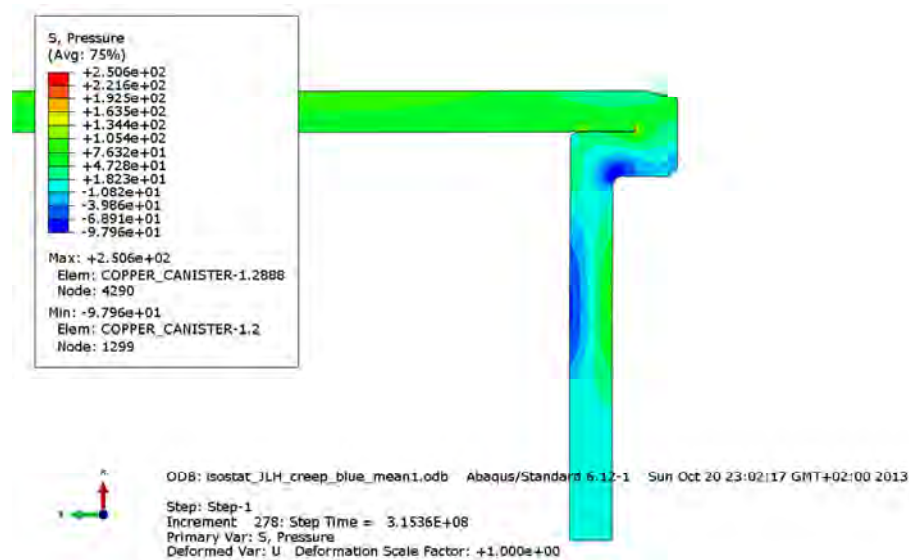


Figure A4-18. Plot showing pressure stress at the copper shell bottom weld after 10 years. Gas pressure is applied.

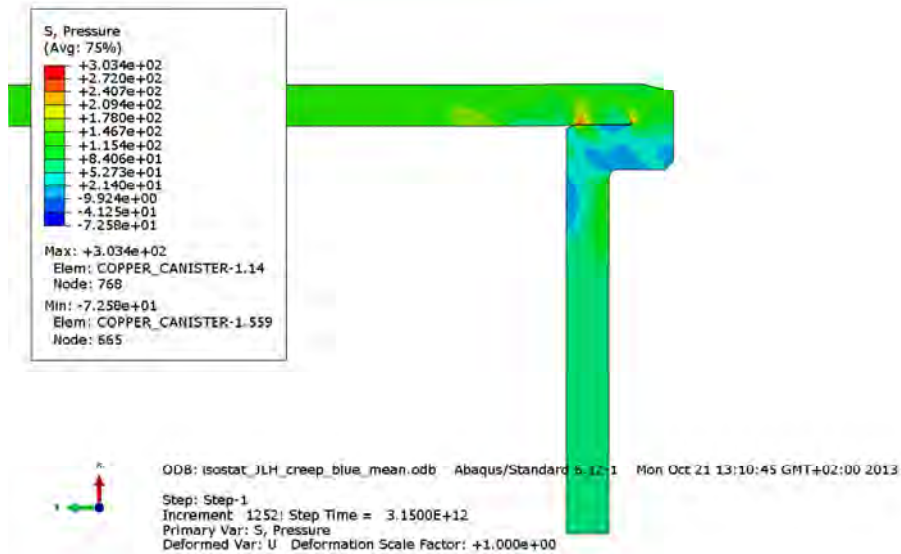


Figure A4-19. Plot showing pressure stress at the copper shell bottom weld after 100,000 years.

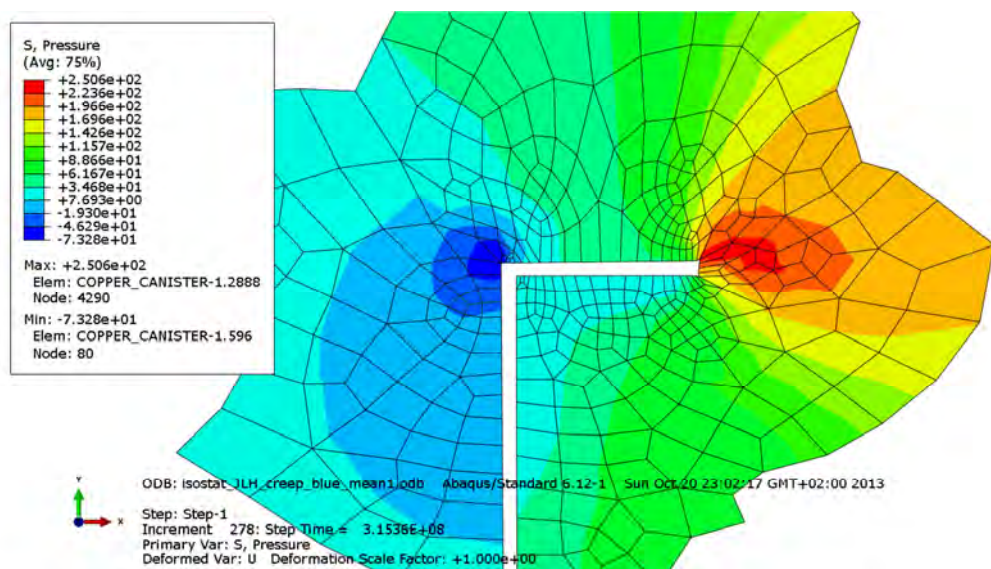


Figure A4-20. Plot showing pressure stress at the copper shell top weld after 10 years. Gas pressure is applied.

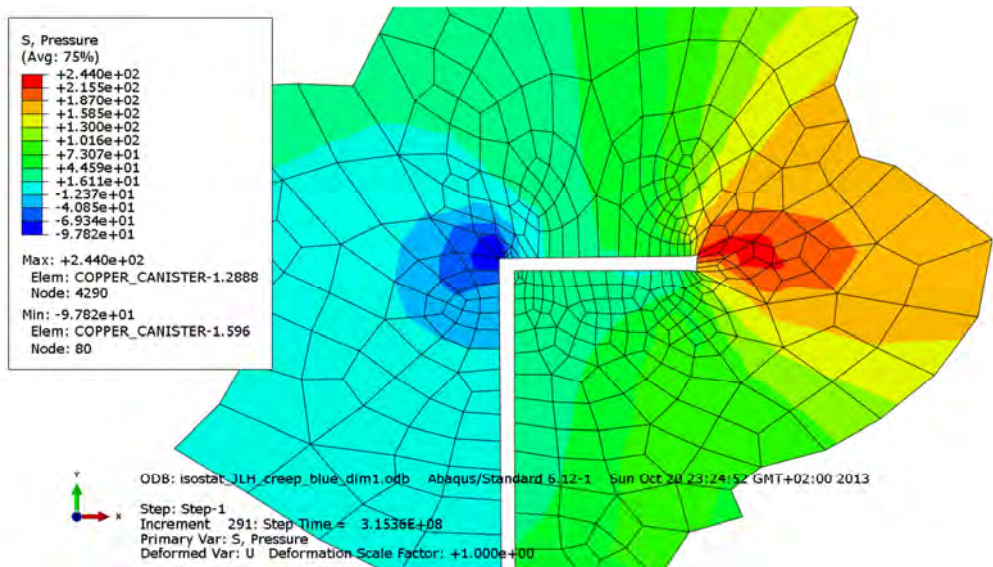


Figure A4-21. Plot showing pressure stress at the copper shell top weld after 10,000 years.

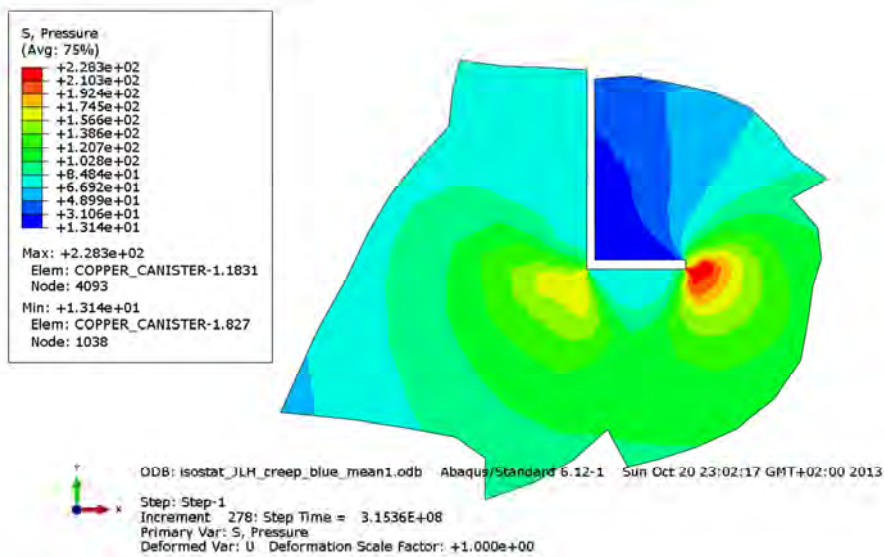


Figure A4-22. Plot showing pressure stress at the copper shell bottom weld after 10 years. Gas pressure is applied.

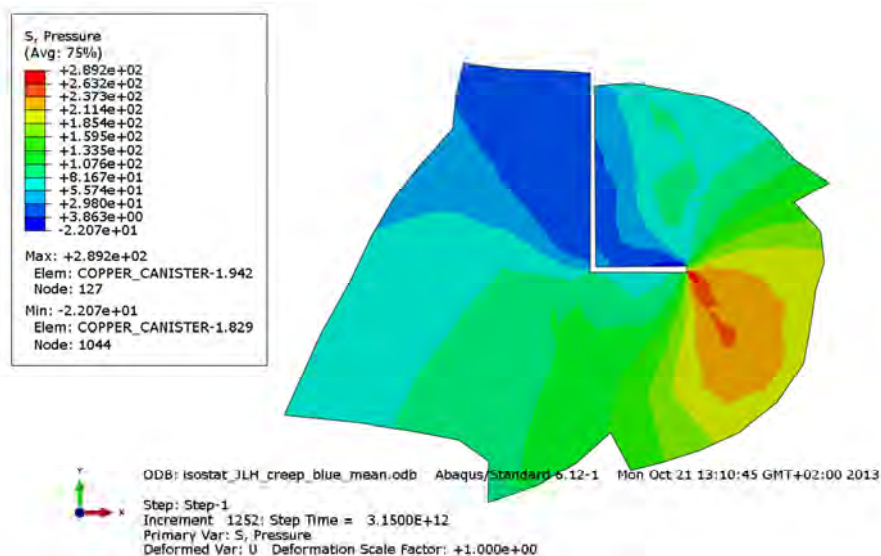


Figure A4-23. Plot showing pressure stress at the copper shell bottom weld after 100,000 years.

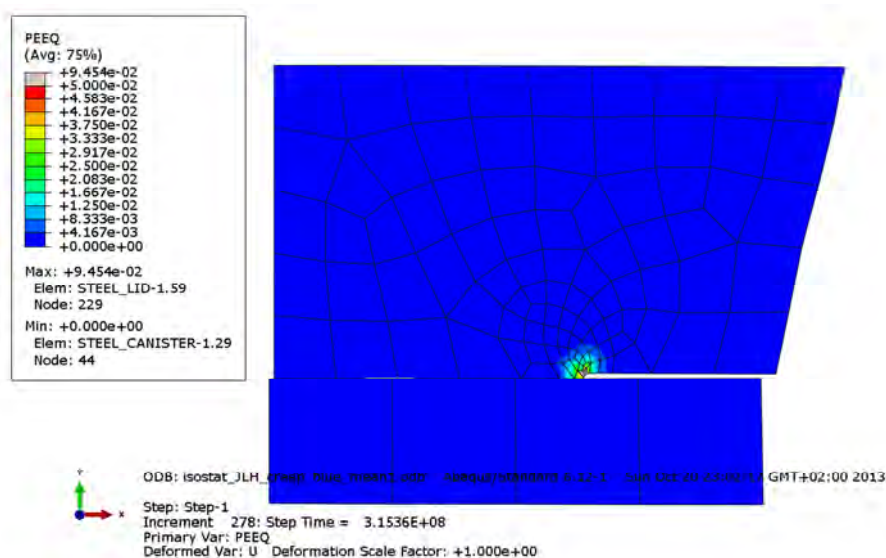


Figure A4-24. Plot showing equivalent plastic strain at the steel lid after 10 years; see also Figure 4-3 for explanation of the details. Gas pressure is applied.

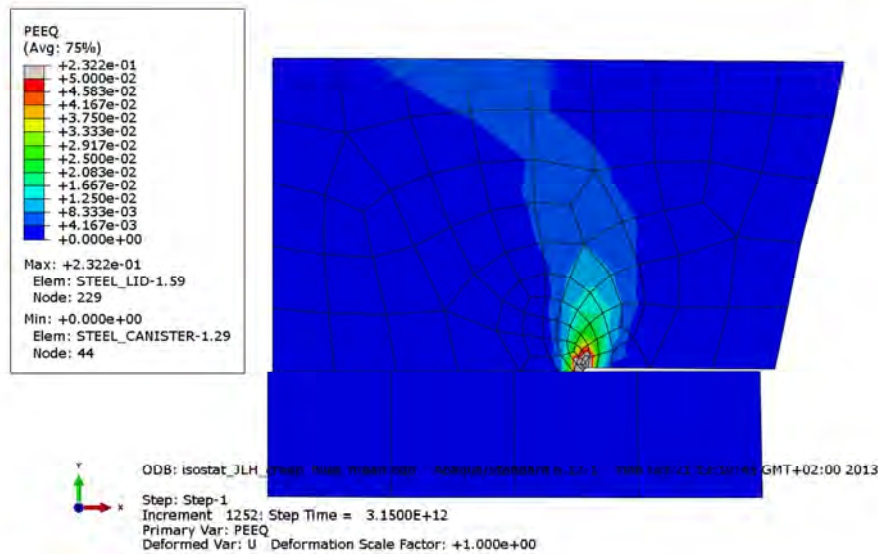


Figure A4-25. Plot showing equivalent plastic strain at the steel lid after 100,000 years; see also Figure 4-3 for explanation of the details.

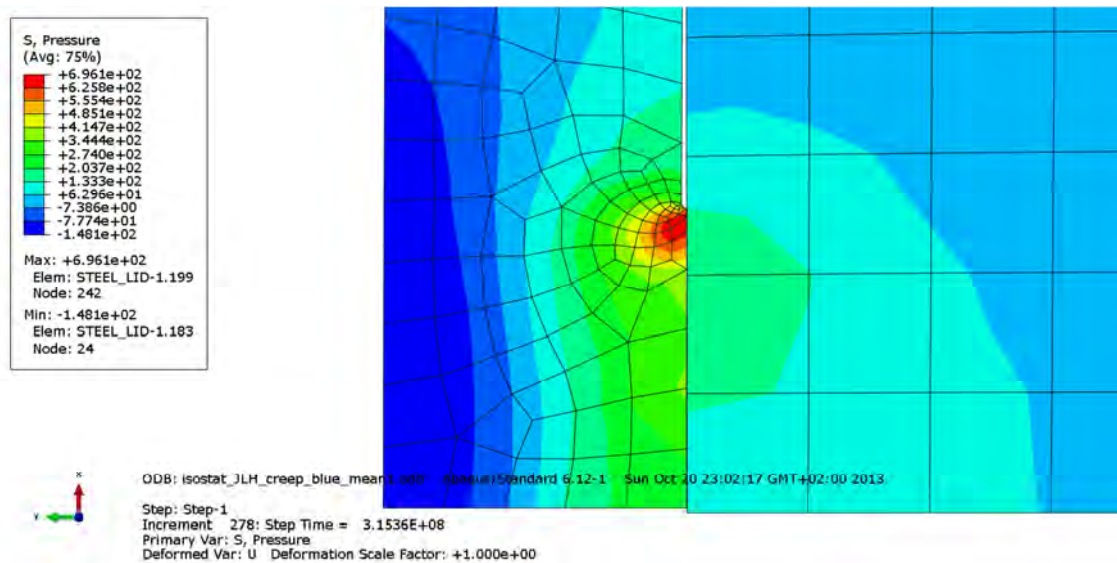


Figure A4-26. Plot showing pressure stress at the discontinuity of the insert after 10 years. Gas pressure is applied.

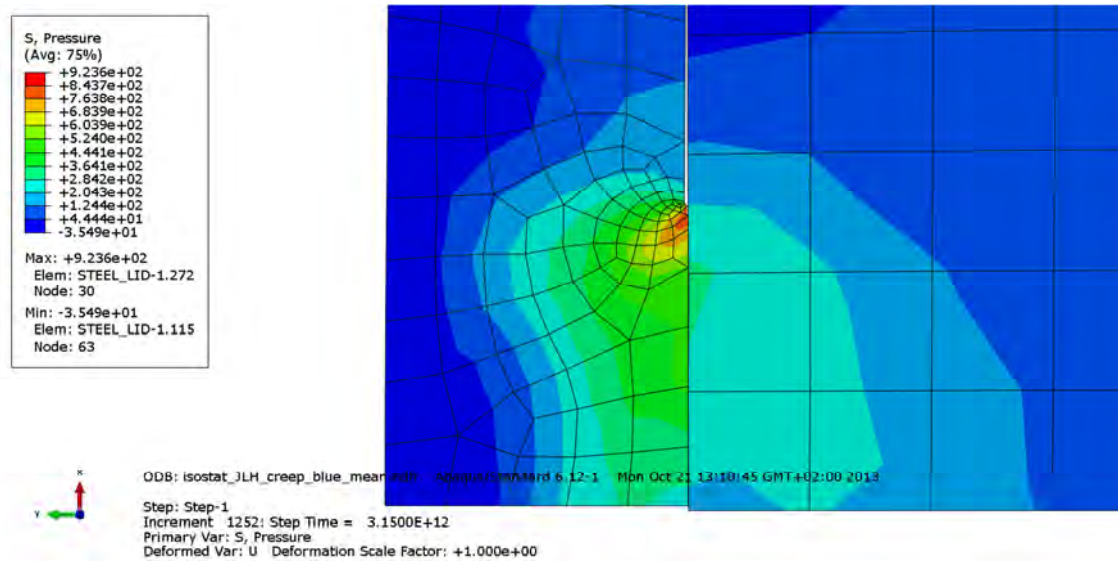


Figure A4-27. Plot showing pressure stress at the discontinuity of the insert after 100,000 years.

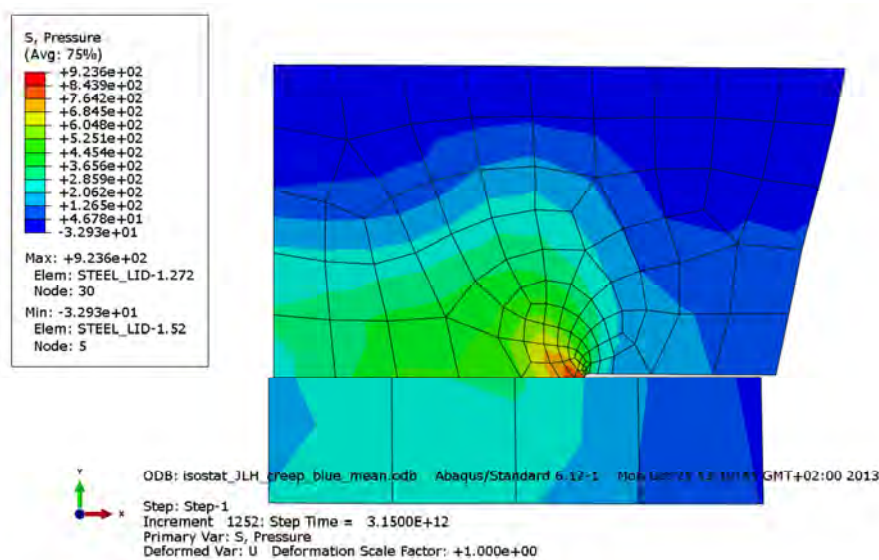


Figure A4-28. Plot showing pressure stress at the steel lid after 100,000 years; see also Figure 4-3 for explanation of the details.

Appendix 5 – Storage of files

This report is based on the results from a lot of FE-simulations using Abaqus which is a commercial available code and is thus not stored as part of the work. Below is a short description of files used in the project and directories for storage of these. These files are also stored at SKB.

The files are stored in directories as:

geometry
Inputfiles
plots
Isostat.docx - this report
scripts
subroutines

1 – Plot-files used in the report

Contents in C:\Users\jhd\mappar\skb\Isostat\plots

compare_creep_components_history.png
compare_creep_history.png
half_3d_JLH-bc.png
half_3d_JLH-mesh1.png
half_3d_JLH-mesh_copper.png
half_3d_JLH-mesh_copper_creep_red_dim-ceed.png
half_3d_JLH-mesh_insert.png
half_3d_JLH-mesh_steel_lid.png
Restart_half_3d_JLH_creep_red_dim7-ceed_10years.png
Restart_half_3d_JLH_creep_red_dim7-ceed_history.png
Restart_half_3d_JLH_creep_red_dim7-ceed_max.png
Restart_half_3d_JLH_creep_red_dim7-mises_10years.png
Restart_half_3d_JLH_creep_red_dim7-mises_channels_10years.png

Plot files used in the report

Appendix 1

isostat_JLH_creep_red_dim-ceed.png
isostat_JLH_creep_red_dim-ceed_10years.png
isostat_JLH_creep_red_dim-ceed_contour.png
isostat_JLH_creep_red_dim-ceed_contour2.png
isostat_JLH_creep_red_dim-ceed_contour3.png
isostat_JLH_creep_red_dim-ceed_contour4.png
isostat_JLH_creep_red_dim-ceed_contour4b.png
isostat_JLH_creep_red_dim-ceed_contour5.png
isostat_JLH_creep_red_dim-ceed_contour5b.png
isostat_JLH_creep_red_dim-gap_corner.png
isostat_JLH_creep_red_dim-mesh_1.png
isostat_JLH_creep_red_dim-mesh_2.png
isostat_JLH_creep_red_dim-mesh_3.png
isostat_JLH_creep_red_dim-mesh_4.png
isostat_JLH_creep_red_dim-mesh_5.png
isostat_JLH_creep_red_dim-peed_2.png
isostat_JLH_creep_red_dim-peed_contour.png
isostat_JLH_creep_red_dim-peed_contour2.png
isostat_JLH_creep_red_dim-pressure.png
isostat_JLH_creep_red_dim-pressure_canister1.png
isostat_JLH_creep_red_dim-pressure_copper1.png
isostat_JLH_creep_red_dim-pressure_copper2.png
isostat_JLH_creep_red_dim-pressure_copper3.png
isostat_JLH_creep_red_dim-pressure_copper4.png
isostat_JLH_creep_red_dim-pressure_copper4b.png
isostat_JLH_creep_red_dim-pressure_copper5b.png
isostat_JLH_creep_red_dim-s22.png
isostat_JLH_creep_red_dim-temp.png
isostat_JLH_creep_red_dim-u2.png

Appendix 2

isostat_JLH_creep_red_mean-ceed.png
isostat_JLH_creep_red_mean-ceed_10years.png
isostat_JLH_creep_red_mean-ceed_contour.png
isostat_JLH_creep_red_mean-ceed_contour2.png
isostat_JLH_creep_red_mean-ceed_contour3.png
isostat_JLH_creep_red_mean-ceed_contour4.png
isostat_JLH_creep_red_mean-ceed_contour4b.png
isostat_JLH_creep_red_mean-ceed_contour5.png
isostat_JLH_creep_red_mean-ceed_contour5b.png
isostat_JLH_creep_red_mean-peed_1.png
isostat_JLH_creep_red_mean-peed_2.png
isostat_JLH_creep_red_mean-peed_contour.png
isostat_JLH_creep_red_mean-peed_contour2.png
isostat_JLH_creep_red_mean-pressure_canister1.png
isostat_JLH_creep_red_mean-pressure_copper1.png
isostat_JLH_creep_red_mean-pressure_copper2.png
isostat_JLH_creep_red_mean-pressure_copper3.png
isostat_JLH_creep_red_mean-pressure_copper4.png
isostat_JLH_creep_red_mean-pressure_copper4b.png
isostat_JLH_creep_red_mean-pressure_copper5b.png
isostat_JLH_creep_red_mean-s22.png
isostat_JLH_creep_red_mean-temp.png
isostat_JLH_creep_red_mean-u2.png

Plot files used in the report

Appendix 3

isostat_JLH_creep_blue_dim-ceed.png
isostat_JLH_creep_blue_dim-ceed_10kyears.png
isostat_JLH_creep_blue_dim-ceed_contour.png
isostat_JLH_creep_blue_dim-ceed_contour2.png
isostat_JLH_creep_blue_dim-ceed_contour3.png
isostat_JLH_creep_blue_dim-ceed_contour4.png
isostat_JLH_creep_blue_dim-ceed_contour4b.png
isostat_JLH_creep_blue_dim-ceed_contour5.png
isostat_JLH_creep_blue_dim-ceed_contour5b.png
isostat_JLH_creep_blue_dim-peed_1.png
isostat_JLH_creep_blue_dim-peed_2.png
isostat_JLH_creep_blue_dim-peed_contour.png
isostat_JLH_creep_blue_dim-peed_contour2.png
isostat_JLH_creep_blue_dim-pressure_canister1.png
isostat_JLH_creep_blue_dim-pressure_copper1.png
isostat_JLH_creep_blue_dim-pressure_copper2.png
isostat_JLH_creep_blue_dim-pressure_copper3.png
isostat_JLH_creep_blue_dim-pressure_copper4.png
isostat_JLH_creep_blue_dim-pressure_copper4b.png
isostat_JLH_creep_blue_dim-pressure_copper5b.png
isostat_JLH_creep_blue_dim-s22.png
isostat_JLH_creep_blue_dim-temp.png
isostat_JLH_creep_blue_dim-u2.png

Appendix 4

isostat_JLH_creep_blue_mean-ceed.png
isostat_JLH_creep_blue_mean-ceed_10kyears.png
isostat_JLH_creep_blue_mean-ceed_contour.png
isostat_JLH_creep_blue_mean-ceed_contour2.png
isostat_JLH_creep_blue_mean-ceed_contour3.png
isostat_JLH_creep_blue_mean-ceed_contour4.png
isostat_JLH_creep_blue_mean-ceed_contour4b.png
isostat_JLH_creep_blue_mean-ceed_contour5.png
isostat_JLH_creep_blue_mean-ceed_contour5b.png
isostat_JLH_creep_blue_mean-peed_1.png
isostat_JLH_creep_blue_mean-peed_2.png
isostat_JLH_creep_blue_mean-peed_contour.png
isostat_JLH_creep_blue_mean-peed_contour2.png
isostat_JLH_creep_blue_mean-pressure_canister1.png
isostat_JLH_creep_blue_mean-pressure_copper1.png
isostat_JLH_creep_blue_mean-pressure_copper2.png
isostat_JLH_creep_blue_mean-pressure_copper3.png
isostat_JLH_creep_blue_mean-pressure_copper4.png
isostat_JLH_creep_blue_mean-pressure_copper4b.png
isostat_JLH_creep_blue_mean-pressure_copper5b.png
isostat_JLH_creep_blue_mean-s22.png
isostat_JLH_creep_blue_mean-temp.png
isostat_JLH_creep_blue_mean-u2.png

2 – Input files used for the simulations

Each analysis is started by abaqus job=input-file (w/o .inp) user=creep_rs_march2009.

Files with extension “incl” are referenced by some of the input-files (extension “inp”).

Contents in C:\Users\jhd\mappar\skb\Isostat\InputFiles

| | |
|------------------------------------|--|
| Isostat_JLH_creep_red_dim.inp | - temperature, dimensioning and dry buffer |
| Isostat_JLH_creep_red_mean.inp | - temperature, mean and dry buffer |
| Isostat_JLH_creep_blue_dim.inp | - temperature, dimensioning and wet buffer |
| Isostat_JLH_creep_blue_mean.inp | - temperature, mean and wet buffer |
| material_isostat.incl | - material definitions |
| half_3d_JLH_creep_red_dim7.inp | - 3D-analysis |
| half_3d_JLH_creep_red_dim7_r1b.inp | -3D-analysis, restart 1 |
| half_3d_JLH_creep_red_dim7_r2b.inp | -3D-analysis, restart 2 |

4 – Scripts used for post-processing

Used inside Abaqus/CAE or by `abaqus cae startup=script.py` after appropriate editing of job-name inside the script-file.

Contents in C:\Users\jhd\mappar\skb\Isostat\scripts

| | |
|---------------------------------------|---|
| <code>half_3d_JLH.py</code> | - post processing file 3D-analysis |
| <code>isostat_JLH.py</code> | - post processing file for axi-symmetric analyses |
| <code>postprocessing_130528.py</code> | - additional plots |

5 – Geometry definitions

Contents in C:\Users\jhd\mappar\skb\Isostat\geometry

isostat.cae - ABAQUS/CAE-database

isostat.jnl - journal file

isostat-6_11-1.jnl -journal file for previous version (Abaqus 6-11).